UNIVERSIDADE ESTADUAL PAULISTA
"JÚLIO DE MESQUITA FILHO"
Câmpus de Sorocaba

PROGRAMA DE PÓS-GRADUAÇÃO em
Ciências Ambientais

CAROL CHRISTINA DE FARIA

COMPETITIVE ADSORPTION BETWEEN NATURAL ORGANIC MATTER AND SODIUM TRIPOLYPHOSPHATE CROSS-LINKED CHITOSAN MICROSPHERES BY Cd(II) IONS IN AQUEOUS MEDIA

Sorocaba
2022

UNIVERSIDADE ESTADUAL PAULISTA
"JÚLIO DE MESQUITA FILHO"
Câmpus de Sorocaba

PROGRAMA DE PÓS-GRADUAÇÃO em
Ciências Ambientais

CAROL CHRISTINA DE FARIA

COMPETITIVE ADSORPTION BETWEEN NATURAL ORGANIC MATTER AND SODIUM TRIPOLYPHOSPHATE CROSS-LINKED CHITOSAN MICROSPHERES BY Cd(II) IONS IN AQUEOUS MEDIA

Doctoral thesis presented as a requirement for obtaining the title of Doctor in Environmental Sciences from at São Paulo State University "Júlio de Mesquita Filho" in the area of Concentration Diagnosis, Treatment and Environmental Recovery

Advisor: Prof. Dr. André Henrique Rosa
Co-advisor: Prof. Dr. Paulo Sergio Tonello

Sorocaba
2022

F224c

Faria, Carol Christina de

Competitive adsorption between natural organic matter and sodium tripolyphosphate cross-linked chitosan microspheres by Cd(II) ions in aqueous media / Carol Christina de Faria. -- Sorocaba, 2022

99 p.

Tese (doutorado) - Universidade Estadual Paulista (Unesp), Instituto de Ciência e Tecnologia, Sorocaba

Orientador: André Henrique Rosa

Coorientador: Paulo Sergio Tonello

1. Química ambiental. 2. Sorção. 3. Biopolímero. 4. Metais. I. Título.

Sistema de geração automática de fichas catalográficas da Unesp. Biblioteca do Instituto de Ciência e Tecnologia, Sorocaba. Dados fornecidos pelo autor(a).

Essa ficha não pode ser modificada.

UNIVERSIDADE ESTADUAL PAULISTA

Câmpus de Sorocaba

CERTIFICADO DE APROVAÇÃO

TÍTULO DA TESE: Competitive adsorption between natural organic matter and sodium tripolyphosphate cross-linked chitosan microspheres by Cd(II) ions in aqueous media

AUTORA: CAROL CHRISTINA DE FARIA
ORIENTADOR: ANDRÉ HENRIQUE ROSA
COORIENTADOR: PAULO SERGIO TONELLO

Aprovada como parte das exigências para obtenção do Título de Doutora em CIÊNCIAS AMBIENTAIS, área: Diagnóstico, Tratamento e Recuperação Ambiental pela Comissão Examinadora:

Prof. Dr. ANDRÉ HENRIQUE ROSA (Participaçao Virtual, assina em nome dos demais membros da Banca)
Departamento Engenharia Ambiental / Instituto de Ciencia e Tecnologia Campus de Sorocaba Unesp

Professora Associada ELIDIANE CIPRIANO RANGEL (Participaçao Virtual)
Instituto de Ciência e Tecnologia de Sorocaba / Universidade Estadual Paulista Júlio de Mesquita Filho

Profª. Drª. MARIANA BIZARI MACHADO DE CAMPOS (Participaçao Virtual)
Campus São Roque / Instituto Federal de Educação, Ciência e Tecnologia de São Paulo (IFSP)

Drª. DANIELE FRASCARELI (Participaçao Virtual)
Faculdade Anhanguera - Sorocaba

Prof. Dr. LEANDRO CARDOSO DE MORAIS (Participaçao Virtual)
Departamento de Engenharia Ambiental / Unesp Instituto de Ciencia e Tecnologia Campus de Sorocaba

Sorocaba, 26 de agosto de 2022

ACKNOWLEDGMENT

To the São Paulo State University “Júlio de Mesquita Filho” and the Postgraduate Program in Environmental Sciences. To the teachers and all technicians of the Institute of Science and Technology (ICT) – Campus of Sorocaba who, directly or indirectly, contributed to the accomplishment of this work.

To the prof. Dr. Elidiane Rangel and the Technological Plasma Laboratory technicians; to the students of the Chemistry Laboratory (ICT, Sorocaba) who helped in the analyzes carried out during my doctorate.

To my advisor Prof. Dr. André Henrique Rosa and co-advisor Prof. Dr. Paulo Sergio Tonello for all the guidance, patience and understanding in all the phases that make up the doctorate.

To my family who supported me unconditionally and always believed in my choices.

RESUMO

Níveis elevados de metais potencialmente tóxicos em ambientes aquosos têm chamado a atenção devido à sua toxicidade em seres vivos. Dentre as várias abordagens sustentáveis de tratamento / monitoramento, o método de adsorção tem se mostrado uma ferramenta atrativa, simples e poderosa para a remoção desses compostos. A quitosana (CTS) é um abundante biossorvente natural amplamente conhecido por suas propriedades de formar complexos estáveis com muitos íons metálicos. Neste trabalho, esferas de CTS reticuladas com tripolifosfato de sódio (CTS – TPP) foram produzidas para experimentos de adsorção de íons Cd(II) em batelada na presença e ausência de matéria orgânica natural (MON), um importante competidor para íons metálicos em águas naturais. Microscopia eletrônica de varredura, espectroscopia de infravermelho com transformada de Fourier, e difração de raios-X foram utilizadas para caracterizar CTS – TPP antes e depois dos experimentos de adsorção na ausência e presença de MON. As análises elementares foram feitas usando espectroscopia de energia dispersiva. Foram estudados a influência do tempo de contato, pH, quantidade de adsorbato em solução no equilíbrio adsortivo, os mecanismos da cinética e do equilíbrio de adsorção, bem como o efeito de competição com MON. O espectro de FTIR mostrou que ocorreram mudanças importantes na estrutura química da quitosana, confirmando assim o sucesso do processo de reticulação com TPP. Além disso, os espectros também mostraram o protagonismo de grupos amina no processo de adsorção de íons Cd(II) e MON. O adsorvente utilizado neste estudo apresentou boa taxa de sorção (≈ 82%) em todas as faixas de pH e concentrações iniciais em ausência de MON. Nos estudos de competição, visto que íons Cd(II) e MON estiveram em contato prévio antes de serem adicionadas à solução as esferas de CTS, cerca de 94% dos íons Cd(II) foram adsorvidos pela MON, portanto, CTS – TPP sofre grande interferência da MON devido à competição por íons cádmio. Os íons Cd(II) remanescentes em solução foram adsorvidos numa taxa de 85%. Nos estudos de tempo de contato, uma taxa de remoção de Cd(II) de 50% foi observada nas concentrações iniciais de 0,1 e 0,2 mg L^{-1} após 120 min de experimento. No entanto, para a concentração de 5,0 mg L^{-1}, é possível observar um processo cinético mais lento. A cinética do Cd(II) apresentou duas fases muito distintas; sendo a primeira bastante rápida e a segunda mais lenta. Para o estudo cinético, foram aplicados aos dados experimentais os modelos de pseudo-primeira-ordem e pseudo-segunda ordem, sendo que a cinética de pseudo-segunda-ordem descreveu melhor o processo adsortivo. O estudo do equilíbrio de adsorção foi realizado por meio dos modelos não-lineares de Langmuir e Freundlich. O dado de equilíbrio ajustou-se melhor ao modelo de Langmuir (R^2 de 0,98 – 0,99) na faixa de pH estudada. A capacidade máxima de adsorção atingida por CTS – TPP foi de 1,61 mg g^{-1} em pH 6,5. Em geral, CTS – TPP mostrou-se bastante promissora na remoção de Cd(II) de meios aquosos em diferentes concentrações iniciais e intervalo de pH em ausência de MON.

Palavras-chave: Química ambiental. Sorção. Biopolímero. Metais.

ABSTRACT

High levels of potentially toxic metals in aqueous environments have drawn attention due to their toxicity in living beings. Among the several sustainable treatment / monitoring approaches, the adsorption method has proved to be an attractive, simple and powerful tool for the removal of these compounds. Chitosan (CTS) is an abundant natural biosorbent widely known for its properties of forming stable complexes with many metal ions. In this work, sodium tripolyphosphate (CTS – TPP) crosslinked CTS spheres were produced for batch Cd(II) ion adsorption experiments in the presence and absence of natural organic matter (NOM), an important competitor of metallic ions in natural water. Scanning electron microscopy, Fourier transform infrared spectroscopy, and X-ray diffraction were used to characterize CTS – TPP before and after adsorption experiments in the absence and presence of NOM. Elemental analyzes were performed using Energy dispersive spectroscopy. The influence of contact time, pH, amount of adsorbate in solution on the adsorptive equilibrium, the mecanisms of kinetics and adsorption equilibrium, as well as the effect of competition with NOM were studied. The FTIR spectrum showed that there were important changes in the chemical structure of CTS, thus confirming the success of the crosslinking process with TPP. In addition, the spectra also showed the role of amine groups in the adsorption process of Cd(II) and NOM ions. The adsorbent used in this study showed good sorption rate (≈ 82%) in all pH ranges and initial concentrations in the absence of NOM. In competition studies, since Cd(II) and NOM ions were in previous contact before the CTS beads were added to the solution, about 94% of the Cd(II) ions were adsorbed by NOM, therefore, CTS – TPP undergoes high NOM interference due to competition for cadmium ions. The remaining Cd(II) ions in solution were adsorbed at a rate of 85%. In the contact time studies, a Cd(II) removal rate of 50% was observed at initial concentrations of 0.1 and 0.2 mg L^{-1} after 120 min of experiment. However, for the concentration of 5.0 mg L^{-1}, it is possible to observe a slower kinetic process. The kinetics of Cd(II) showed two very distinct phases; the first being quite fast and the second being slower. For the kinetic study, pseudo-first-order and pseudo-second-order models were applied to the experimental data and the pseudo-second-order kinetics better described the adsorptive process. The study of the adsorption equilibrium was carried out using non-linear models of Langmuir and Freundlich. The equilibrium data fitted better to the Langmuir model (R^2 of 0.98 – 0.99) in the studied pH range. The maximum adsorption capacity achieved by CTS – TPP was 1.61 mg g^{-1} at pH 6.5. In general, CTS – TPP showed to be quite promising in removing Cd(II) from aqueous media at different initial concentrations and pH range in the absence of NOM.

Key-words: Environmental chemistry. Sorption. Biopolymer. Metals.

ILLUSTRATION LIST

FIGURES

TABLE LIST

ABBREVIATION AND ACRONYMS LIST

Ag	= Silver
Ar	= Argonium
As	= Arsenic
ATR	= Attenuated total reflectance
Au	= Gold
C	= Carbon
C_0	= Initial concentration of an analyte in the solution
Cd	= Cadmium
Cd(II)	= Cadmium ion
C_e	= Final concentration of the analyte in the solution
cm^{-1}	= per centimeter
Cr	= Chromium
CTS	= Chitosan
CTS–TPP	= Chitosan microspheres cross-linked with Sodium Tripolyphosphate
Cu	= Copper
Cu(II)	= Copper ion
DA	= Degree of acetylation
DD	= Degree of deacetylation
EDS	= Energy dispersive spectrometry
FA	= Fulvic acid
FT–IR	= Fourier transform infrared spectroscopy
g	= Gram
GlcN	= D-glucosamine units
GlcNAc	= N-acetylglucosamine units
H^+	= Hydrogen ion
HA	= Humic acid
HCl	= Hydrochloric acid
Hg	= Mercury
Hg(II)	= Mercury ion
HNO_3	= Nitric acid

HS = Humic substances

ICP–OES = Inductively coupled plasma - optical emission spectrometry

IR = Infrared

kDA = Kilodalton

keV = One thousand electron volts

kPa = Kilopascal

kV = Kilovolt

L = Liter

mA = Milliamp

mg / g = Quantity (mg) of adsorbate/contaminant can adhere to per g of the adsorbent material

mg L^{-1} = Milligram per liter

mg = Milligram

MHz = Mega HertZ

min = Minute

min^{-1} = per minute

mL = Millilitre

mm = Milimeter

MW = Molecular weight

MΩ cm = Megaohm-centimeter

N = Nitrogen

Na = Sodium

$Na_5P_3O_{10}$ = Sodium tripolyphosphate

$NaNO_3$ = Sodium nitrate

NaOH = Sodium hydroxide

–NH = Amide group

– NH_3^+ = Protonated amine group

Ni = Nickel

Ni(II) = Nickel ion

nm = Nanometer

NOM = Natural organic matter

^{o} C = Celsius degree

O = Oxygen

OH^- = Hydroxyl

–OH	= Hydroxyl group
P	= Phosphorus
Pb	= Lead
Pb(II)	= Lead ion
pH	= Potential of hydrogen
pKa	= Strength of the acid
PO_4^{3-}	= Phosphoric ions
PTM	= Potentially toxic metals
q_{max}	= Maximum adsoption capacity of a material
$R–NH_2$	= Amine group
$R–NHCOCH_3$	= Acetamine group
rpm	= Revolutions per minute
Se	= Selenium
sec	= Second
SEM	= Scanning electron microscopy
T	= Temperature
TOC	= Total organic carbon
TPP	= Sodium tripolyphosphate
v / v	= Volume per volumen
w / v	= Weight per volume
W	= Weight of the dry adsorbent
XRD	= X-ray Diffraction
Zn	= Zinc
%	= Percent
θ	= Theta

SUMMARY

1. INTRODUCTION

Since the Industrial Revolution in the 18th Century, the impacts on the environment have been increasing exponentially, culminating in a serious threat to life on Earth (MANISALIDIS et al., 2020). The deterioration of aquatic environmental matrices has been a long-standing global concern because water-dependent biota and human being easily might suffer with substantial health effects or even die (KANMANI et al., 2017; SCHWARZENBACH et al., 2010). Consequently, aquatic environment pollution has emerged as a core issue due to the scarcity of water resulting from the increase in its demand around the world (DYBERN, 1974; SALEHI, 2022). We can cite as a direct and indirect source of contaminated wastewater: textile dyeing, dyes and dyes intermediates, fertilizer industries, smelting processes, pharmaceutical industries, mining industries, agricultural and livestock activities, domestic sewage, among other activities (SHETH et al., 2021).

A class of elements that has been one of the biggest global concerns is denoted as inorganic pollutants, which includes the potentially toxic metals (PTM), e.g., copper (Cu), zinc (Zn), nickel (Ni), cadmium (Cd), lead (Pb), mercury (Hg), chromium (Cr), and metalloids, e.g., selenium (Se) and arsenic (As) (REHMAN et al., 2021). However, some of these metals (the essential elements) have a certain duality, that is, they are fundamental to maintain the metabolism of many living beings, but they are toxic at higher concentrations such as Cu, Zn and Se (BRYAN, 1971). In contrast, Cd even at low concentrations is highly toxic and carcinogenic to biota (HAYAT et al., 2019). This metal and its compounds have been classified as known human carcinogens (group I) by the International Agency for research on Cancer (IARC, 1993). This metal has been widely applied in batteries, pigments, textiles, insecticides, metallurgical industries, metal-finishing industries, synthetic chemicals, among other applications (QIU et al., 2018; RANI et al., 2014).

PTM are considered an environmental threat due to their non-biodegradability, bioaccumulation, environmental stability, persistence and biotoxicity characteristics (ALI et al., 2021). Besides that, the presence of large amounts of these elements may negatively influence the physical and chemical homeostasis of sediment, soils, and water (OMWENE et al., 2018). In the aquatic environment, the PTM are generally distributed as water-soluble species, colloids,

suspended matter, and sedimentary phases (RAHMAN; SAHA; MOLLA, 2014). Many studies have demonstrated that sediments often act simultaneously as a carrier and as secondary source of pollutants in the aquatic system (MA et al., 2016). Thus, they are regarded as sensitive indicators for monitoring of these pollutants in both spatial (LI et al., 2015) and temporal (ZHAO et al., 2018) trends.

In order to estimate the effects and potential risks associated with elevated amount of PTM in waters, the total concentration do not necessary correspond all the elements that are actually bioavailable to the aquatic biota. Therefore, to understand and predict the bioavailability of a metal in an environment it is necessary to be able to understand and measure its chemical speciation (ZHANG; DAVISON, 2015). It has been shown that the bioavailable fraction generally corresponds to free metal ions and the most kinetically labile forms (usually weakly bound) (BAEYENS et al., 2018), and generally this fraction occurs in trace quantities in the environment. According to Morel and Hering (1993), the PTM free forms can be easily assimilated, absorbed or accumulated by organisms, which directly or indirectly, interfere with their metabolic processes. Trace metals may be present in a wide range of chemical species, e.g. hydrated ions, simple inorganic and organic complexes in a truly dissolved fraction, species associated with heterogeneous colloidal dispersions and particulate trace elements with associations ranging from weak physical adsorption to chemical binding (LIU; LEAD; ZHANG, 2013; URE; DAVIDSON, 1995). The trace elements in waters have their dynamics governed by different factors such as pH, temperature (T), ionic strength, etc, which induce transfers from one chemical form into another one, so that the relative importance of each of these chemical forms changes with time (GALCERAN et al., 2021).

It is often suggested that humic substances (HS) play a crucial role in controlling the behavior and mobility of metals in the dissolved and particulate phases of waters, whether these are essential trace elements or metals derived from pollution (LIVENS, 1991; TIPPING et al., 1995). These substances include humin, fulvic acid (FA) and humic acid (HA), which represent a large portion of the natural organic matter (NOM), which, in turn, it is distributed in soils, sediments and waters (MORALES et al., 2012). The great physicochemical complexity of HS, which culminates in the great affinity of these components to metallic ions and, consequently, governing the bioavailability of metals in water, justifies the vast number of articles published on the subject (LIU et al., 2022; LODEIRO et al., 2020;

REY-CASTRO et al., 2009; YANG; TANG; ANTONIETTI, 2021). Thus, the studies focused on the interference of HS in water is fundamental to understand chemical speciation.

HS are formed through aerobic and anaerobic decomposition of (mostly) plant detritus (ZAVARZINA et al., 2021), as well as secondary microbial synthesis (KLEBER; LEHMANN, 2019). Due to their multiple origins, age, and genesis the degree of chemical and morphological complexity is high in these substances which makes their characterization difficult (VON WANDRUSZKA, 2000). The content of aromatic and phenolic groups is very abundant in HS which allows the complexation and ionic exchange of these compounds with metallic ions in the environment (REY-CASTRO et al., 2009). The main groups found in HS are carboxylic, phenolic, quinone, ketone, alcohol, amino and sulfhydryl (MEINELT et al., 2007) (Figure 1).

Figure 1 – Structural concept of a humic acid

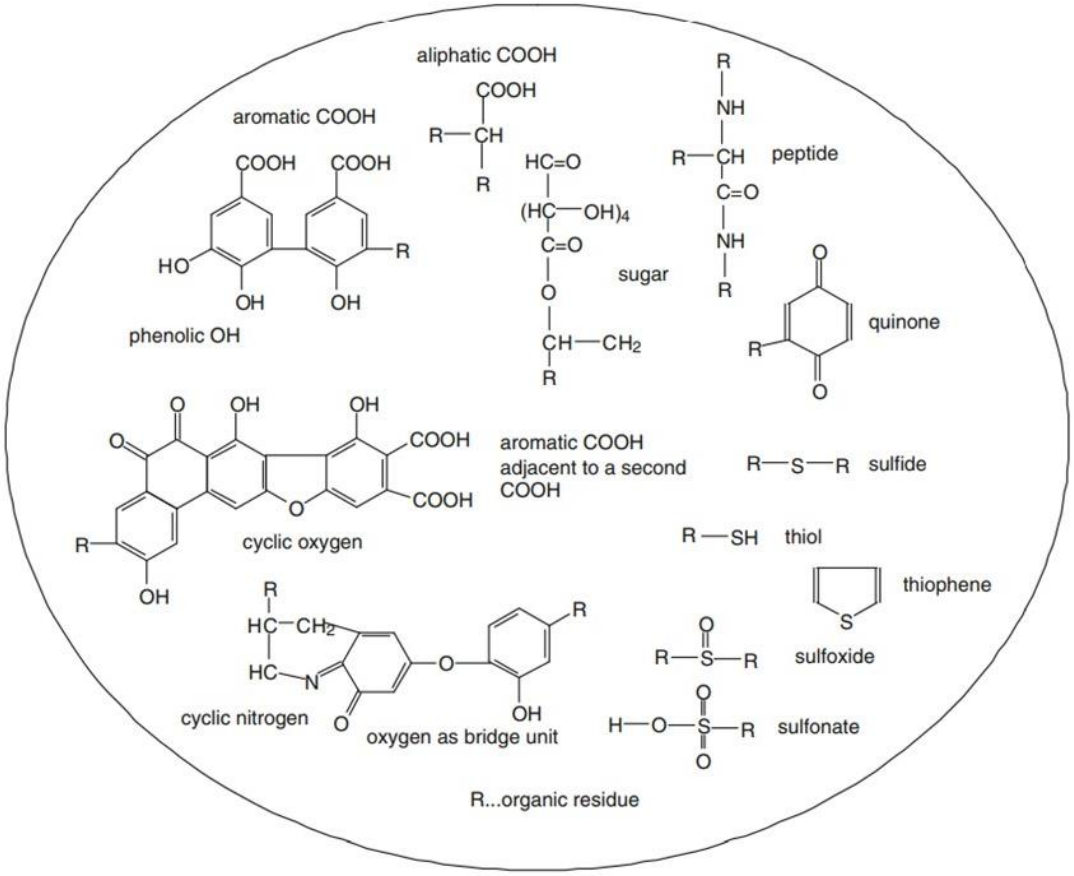

Source: Stevenson (1994) and Xia et al. (1998).

2. APPLICATION OF BIOPOLYMERS AS AN IMPORTANT TOOL FOR AQUATIC POLLUTION

Due to their multiple favorable characteristics such as the non-toxicity, biocompatibility, renewability, higher efficacy, flexibility, low-cost production, availability and generally produce no secondary pollution, many types of biopolymers have been applied to remove pollutants from water (BILAL; IQBAL, 2019; GODAGE; GIONFRIDDO, 2020). Biopolymers such as alginate (SUTIRMAN; SANAGI; WAN AINI, 2021), chitosan (DE FARIA et al., 2020), cellulose (PEI et al., 2021), pectin (ZHANG et al., 2020), agarose (MAI; HOANG; PHAN, 2021), carrageenan (PALANISAMY et al., 2019), dextran (GHIMICI; NICHIFOR, 2018) have been attracting wide interest of researchers over the past several years because these materials play a significant role to minimize the chemical pollution caused by PTM that are released into the environmental compartments (PALANISAMY et al., 2019). Besides that, the elemental composition of these natural polymers, most of time, has similarity with biological structures that, in this way, makes them more easily recognized by the bioenvironment and, thus, metabolized to non-toxic residues and eliminated naturally (LI; ELANGO; WU, 2020).

Biopolymers are formed under natural conditions during the growth cycles of all organisms, and they are basically a chain of molecules made up of blocks (monomers) linked together (KANMANI et al., 2017). They possess a great number of available reactive sites that offer significant functionalities with multi-purpose applications (BILAL; IQBAL, 2019). For this reason, many derived biopolymers have been developed to enhance their properties to remove a broad range of PTM from aqueous media (KRSTIĆ; UROŠEVIĆ; PEŠOVSKI, 2018; RAHIM; MAS HARIS, 2015). Often biosorption is the key process behind most work on removing trace metals by biopolymers and this process has been shown to be quite effective, sustainable and economically viable in monitoring or treating water (BASHIR et al., 2019; DE FREITAS; DA SILVA; VIEIRA, 2019). In general, this process basically consists of the passive mass transfer of a substance from the liquid phase to the surface of a solid of biological origin, where connections will be established through physical and / or chemical interactions that will culminate in reducing contaminants concentration in solution (KURNIAWAN; BABEL, 2003; VIJAYARAGHAVAN; YUN,

2008). Figures 2 and 3 summarized the main mechanisms that can be established in a biosorption process.

Figure 2 − Different mechanisms involved in biosorption phenomenon

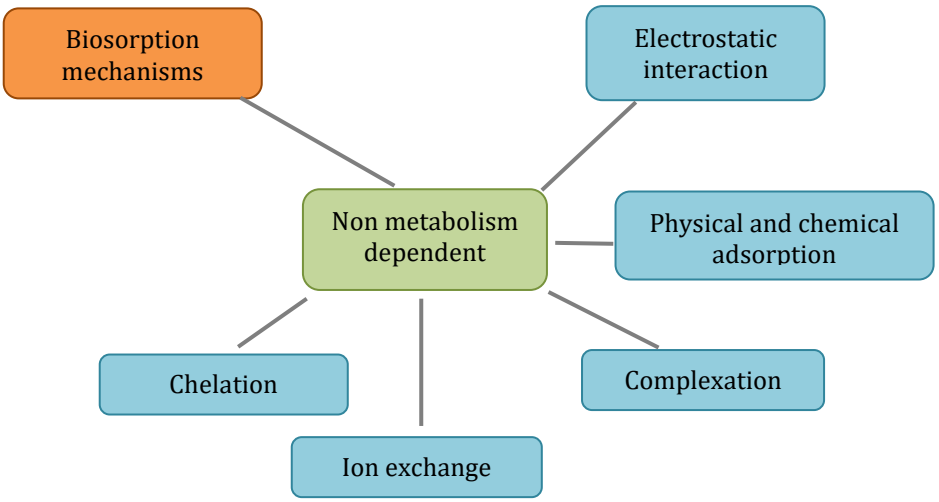

Source: Volesky et al. (1993), Asgher (2012) and Torres (2020).

Figure 3 – Schematic representation of the mechanisms involved in the biosorption of PTM

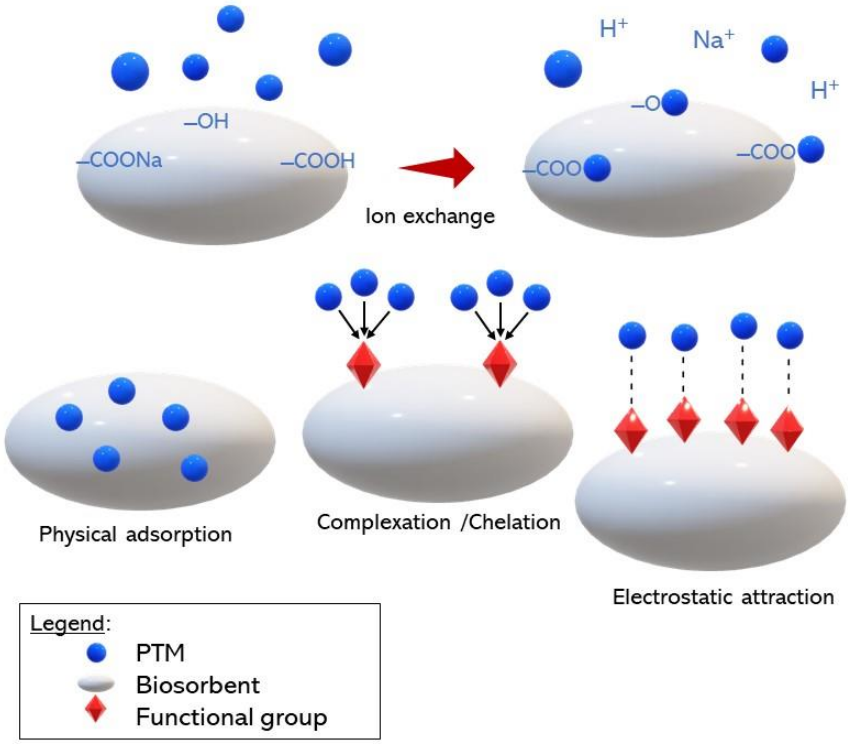

Source: Adapted from Bilal et al., (2018).

2.1. CHITIN

For a better understanding of the main historical aspects of chitin and chitosan, a thorough review was published by Crini (2019). Chitin is a semi-crystalline homopolymer of (β-(1 → 4)-N-acetyl-D-glucosamine) and it is one of the most abundant biopolymer on Earth (BAKSHI et al., 2020) (~ 100 billion tons are naturally produced / year) after cellulose (MUXIKA et al., 2017). Chitin is a structural biopolymer, widely found in the exoskeleton of arthropods such as insects (KAYA; ASAN-OZUSAGLAM; ERDOGAN, 2016), crustaceans (ZHU et al., 2016) and arachnids (ELIEH-ALI-KOMI; HAMBLIN, 2016), annelids (DUTTA, 2015), mollusks such as gastropods (JOTHI; NACHIYAR, 2012), bivalves (SHARP, 2013) and cephalopods (HAMED; ÖZOGUL; REGENSTEIN, 2016), coelenterates (STAINLOSS; SANKARAN, 2016), algae such as diatoms (RINAUDO, 2006), brown and green algae (SHARP, 2013) and fungi (ERDOGAN; KAYA; AKATA, 2017). Generally, the commercial source of chitin is crab, shrimp, krill bark, and fungi that are discarded or wasted from the food industry (BAKSHI et al., 2020). Chitin is obtained up to 14 – 27% and 13 – 15% of the dry weight of shrimp and crab processing wastes respectively (VARUN et al., 2017).

Chitin is highly nitrogenous, hydrophobic and insoluble in water and most organic solvents (KUMAR, 2000). This insolubility may be due to the strong intra and intermolecular bonding of the hydrogens with adjacent – NH or – OH functions groups formed by the oxygen of acetamido group and due to the degree of N-acetylation (PHILIBERT; LEE; FABIEN, 2017). Besides that, this chemical configuration provides chitin a crystalline structure with great rigidity (WILSON; OMOKANWAYE, 2013) and, particularly, its high percentage of nitrogen (6.89%) gives it a great chelating power when compared to cellulose (1.25% of nitrogen) (ELIEH-ALI-KOMI; HAMBLIN, 2016). Through the chitin deacetylation reaction, that is, the partial transformation of its acetamine groups ($R - NHCOCH_3$) into amine groups ($R - NH_2$) it is possible to obtain a highly chelating polysaccharide called chitosan (CTS) (AZUMA et al., 2015) (Figure 4). However, more than 50% of chitin monomers need to be deacetylated to obtain CTS (ROBERTS, 2008).

Figure 4 – Overview of production of chitin and chitosan

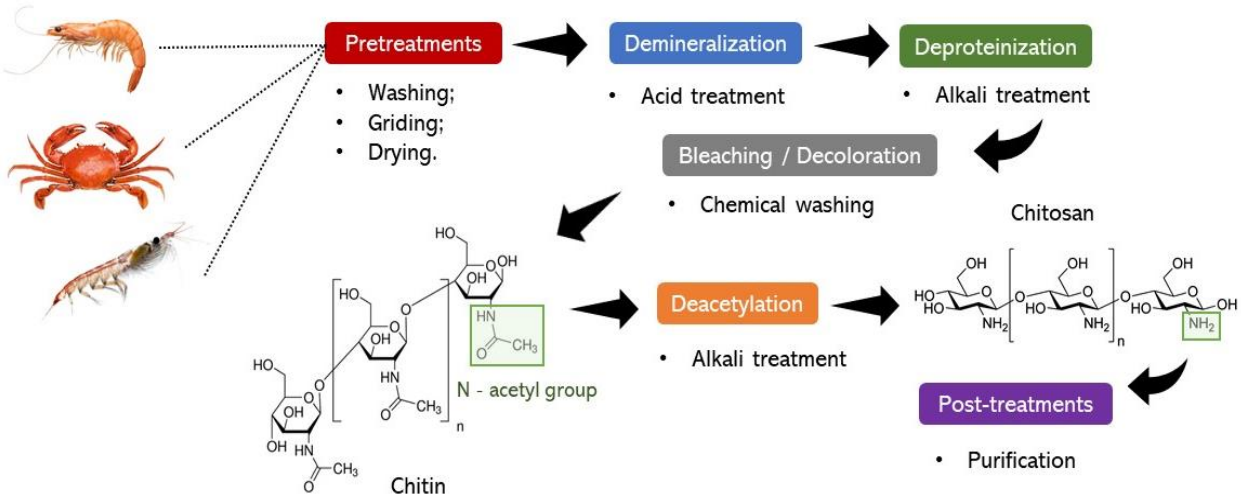

Source: The author.

2.1.1. Chitosan

The history of the main derivative of chitin dates back to 1859 when Charles Rouget boiled this biopolymer in concentrated potassium hidroxide solution under reflux and found that it became soluble in organic acids leading to the discovery of CTS (BAKSHI et al., 2020; CRINI, 2019). The denomination of CTS was introduced by Hoppe-Seyler (1894). This biopolymer is obtained through biological or chemical methods; however, the second process is the most used on an industrial scale (RINAUDO, 2006). CTS has poor or negligible solubility in water as the hydroxyl groups confer hydrophilicity (DOSHI et al., 2017), on the other hand, it has solubility under acidic conditions (SHETH et al., 2021). In recent decades, many researchers have focused on CTS as an important agent for monitoring or removing pollutants from water and soil (UPADHYAY et al., 2021; VARMA; DESHPANDE; KENNEDY, 2004). Nevertheless, CTS may have poor affinity for some trace metals (AZAROVA; PESTOV; BRATSKAYA, 2016; GEROMEL-COSTA et al., 2018) and to overcome these difficulties, many efforts have been made to derivatize CTS by chemical modifications (BAKSHI et al., 2020).

CTS is a high charge density (one positive charge per glucosamine residue) cationic and hydrophilic heteropolysaccharide. This biopolymer has important

properties such as: biocompatibility (MENG et al., 2022), bioadhesivity (ANISIEI et al., 2022), bioactivity (KOU; PETERS; MUCALO, 2022), nontoxicity (MENG et al., 2022), biodegradable (JI et al., 2022), antimicrobial activity (DEVLIEGHERE; VERMEULEN; DEBEVERE, 2004), antiacid (NGUYEN; NGUYEN, 2022), antiulcer, antitumoral properties (CERAMELLA et al., 2022), blood anticoagulants (POPOVICH et al., 2022), hypolipidemic activity (ALFURAYDI; ALMINDEREJ; MOHAMED, 2022), forms salts with organic and inorganic acids, chelating and complexing properties, ionic conductivity, flocculating agent, entrapment and adsorption properties, filtration ability, etc (ZARGAR; ASGHARI; DASHTI, 2015). These characteristics are mainly correlated to the reactive – NH_2 and – OH present in their backbone that act as coordination sites (WU; TSENG; JUANG, 2000). Moreover, these groups also allow immense structural possibilities for chemical and mechanical modifications (e.g., cross-linking, acylation, hydroxylation, nitration, alkylation, sulphonation, phosphorylation, xanthation blending, graft co-polymerization, curing, etc) to generate special desired properties and functions in different fields (SHUKLA et al., 2013).

The basic CTS structure is composed of N-*acetylglucosamine* units (*GlcNAc*) and D-*glucosamine* units (*GlcN*) (Figure 5). The degree of deacetylation (DD), the molar fraction of *GlcN* units in the chain, will be directly influenced by the type of technique and by the conditions used during the conversion reaction of the R − $NHCOCH_3$ groups. The active primary amino group in CTS is reactive and provides a specific platform for side group attachment under mild reaction conditions (SHUKLA et al., 2013).

Figure 5 – Chemical structure of chitosan composed of β(1→4) linked units

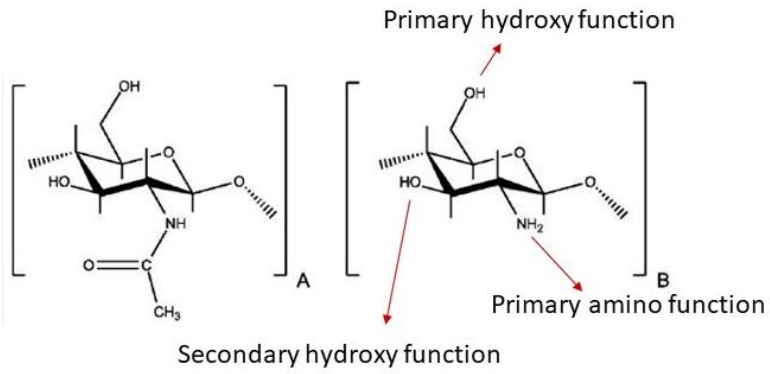

Source: The author.
Legend: N-acetyl-d-glucosamine (A) and d-glucosamine (B).

Molar fraction of *GlcN* units in the chain is defined as shown in Equation 1:

$$DD = 100 \times (n_{GlcN} / n_{GlcN} + n_{GlcNac}) \quad (1)$$

where

n_{GlcN}: average number of D-*glucosamine* units;
n_{GlcNAc}: average number of N-*acetylglucosamine* units.

Degree of acetylation (DA) is defined as shown in Equation 2:

$$DA = 100 - DD \quad (2)$$

Previous studies suggest that DD, molecular weight (MW) and charge density of this polymer have strong influence on its physical-chemical and biological properties (VARMA; DESHPANDE; KENNEDY, 2004). On the other hand, environmental conditions such as pH, ionic strength, temperature, etc. can also affect these properties (PAL et al., 2021). Therefore, the intrinsic characteristics of CTS and the environmental conditions need to be considered to predict the effectiveness of this biopolymer in its most different applications.

CTS acts as a weak base and has pKa varying between 6.3−6.7 (SHUKLA et al., 2013). The large number of free $–NH_2$ groups, that can be protonated in the presence of H^+ ions in the solution, acquire a cationic behavior, culminating in the sorption of metallic anions by CTS in acidic medium, as protons and metallic anions compete for interaction with the $–NH_2$ groups (RAHANGDALE; KUMAR, 2017). While the pH increases (pH > 5.0), the deprotonation of the CTS coordination groups occurs and this contributes to enhancing the sorption of metallic cations due to progressive reduction of repulsion between the cationic species and N and O donor reactive groups (HAMZA et al., 2020). Depending on the electrostatic properties of the metal ions and the conditions of the medium (GUIBAL, 2004), the binding mechanism may vary. The interaction between CTS and a metallic anion is attributed to electrostatic attraction or ion exchange or coordinative complexation in the case with a metallic cation (KAN et al., 2020). However, –OH groups (mainly at the C–3 position) can also contribute to the sorption process. The free electron

doublet on nitrogen can coordinate with metal cations at neutral pH (or weak acidity) (GUIBAL, 2004).

Moreover, the protonation of $–NH_2$ groups allows this biopolymer to be soluble in weak acids (e.g., acetic acid, formic acid, succinic acid, lactic and malic acid) and insoluble in neutral or alkaline solutions

Thus, when a $–NH_2$ group accepts a proton (protonated amine group form), consequently the positively charged CTS particles are separated through repulsive force and become suspended in aqueous acidic solution (SANNAN; KURITA; IWAKURA, 1976). The solubility of CTS increases with an increase in $–NH_2$ groups, however, this is not a convenient property for the adsorption-desorption cycle, for instance. In that manner, it is important to enhance its chemical / physical properties through different techniques, such as cross-linking (GUIBAL, 2004).

Cross-linking is a chemical modification that aims to promote improvements in the intrinsic properties of CTS, such as: adsorptive capacity, increase in mechanical strength / chemical stability, and resistance against acidic environments (GUIBAL, 2004; LAUS et al., 2010). This modification can be performed by chemical cross-linkers or physical procedures (BABAKHANI; SARTAJ, 2020). Cross-linking occurs through the application of mono or bifunctional chemical agents that present reactive groups capable of promoting the formation of bonds between or within polymeric chains (BERGER et al., 2004). There is a wide variety of cross-linkers, such as Epichlorohydrin, Glutaraldehyde, Ethylene Glycol Diglycidyl Ether, Glyoxal, to improve CTS properties, however, these chemicals can be toxic and cause negative effects on the environment (WANG; ZHUANG, 2017).

As an alternative to that, Sodium tripolyphosphate (TPP) ($Na_5P_3O_{10}$) is a low-cost, environmentally friendly multivalent polyanion that induces a reversibly reaction called ionic cross-linking in CTS (LEE et al., 2001). When TPP is dissolved in water, dissociates to hydroxyl (OH^-) and phosphoric ions (PO_4^{3-}), both presenting negative charges. Thus, the cross-linking occurs between TPP PO_4^{3-} groups and CTS – NH_3^+ groups through ionic reaction (KAŠPAR; JAKUBEC; ŠTĚPÁNEK, 2013) (Figure 6).

Figure 6 – Crosslinking reaction of chitosan with sodium tripolyphosphate

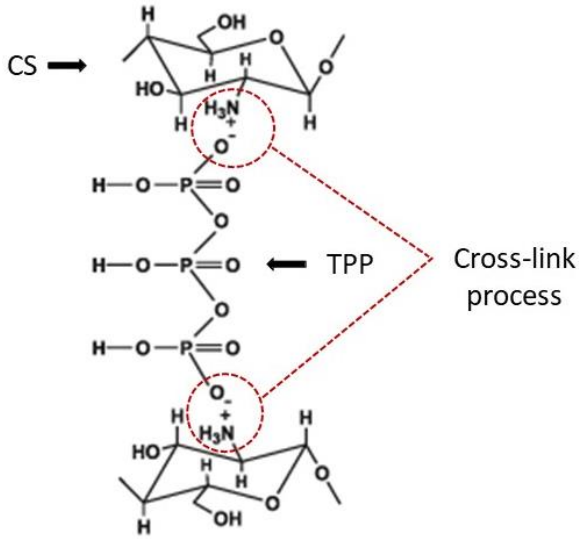

Source: Adapted from Madni et al. (2017).
Legend: CS = CTS.

The protonation of $–NH_2$ groups is also useful because, after dissolution, CTS can be subjected to a range of different chemical processes and take on distinct physical forms. CTS and its derivatives have high functionalities for a wide range of applications in the form of solutions, gels / hydrogels, films, fibers, membranes, suspensions, particles, beads, microspheres, nanoparticles and sponges, and scaffolds (MORIN-CRINI et al., 2019b). In recent years, CTS derivatives have received increasing interest due to their chemical, biological, and functional advantages in many fields, such as: medicine, veterinary, hygiene and personal care, pharmacy, cosmetology, biotechnology, agriculture and agrochemistry, food industry and nutrition, enology, nanotechnology and environmental chemistry (MORIN-CRINI et al., 2019b).

a) CTS microspheres

CTS microspheres (50 nm – 2 mm) (JAYAN et al., 2009) can be prepared by many methods, such as: cross-link of CTS with anions (sulphate, phosphate, hydroxides) (SHU, 2001), spray drying (ZHONG et al., 2020), precipitation, solvent evaporation, complex-coacervation, modified emulsification and ionotropic gelation, cross-link induced by chemical-precipitation, glutaraldehyde cross-linking, thermal

cross-linking (SINHA et al., 2004). The purpose of using each microsphere will define which method is the most suitable, as these processes can produce spheres with different sphericities, size, mechanical strength, and chemical-physical characteristics.

Ionic gelation using TPP can form biocompatible, cross-linked microspheres through inter and intramolecular linkages by electrostatic interactions between TPP phosphate groups and CTS amino groups (CHO et al., 2014). This simple technique has advantages over other methods, such as: the microspheres are spontaneously obtained under mild control conditions without involving high temperatures, organic solvents or sonication (CALVO et al., 1997). After dissolving CTS in acidic aqueous solution (pH 4 – 6), it is added dropwise to the TPP solution (pH 7 – 9). Due to the complexation between oppositely charged species, CTS undergoes ionic gelation and precipitates to form immediately spherical particles (MITRA; DEY, 2011) with good morphology (WULANDARI et al., 2018) (Figure 7).

Figure 7 – Ionic gelation using sodium tripolyphosphate

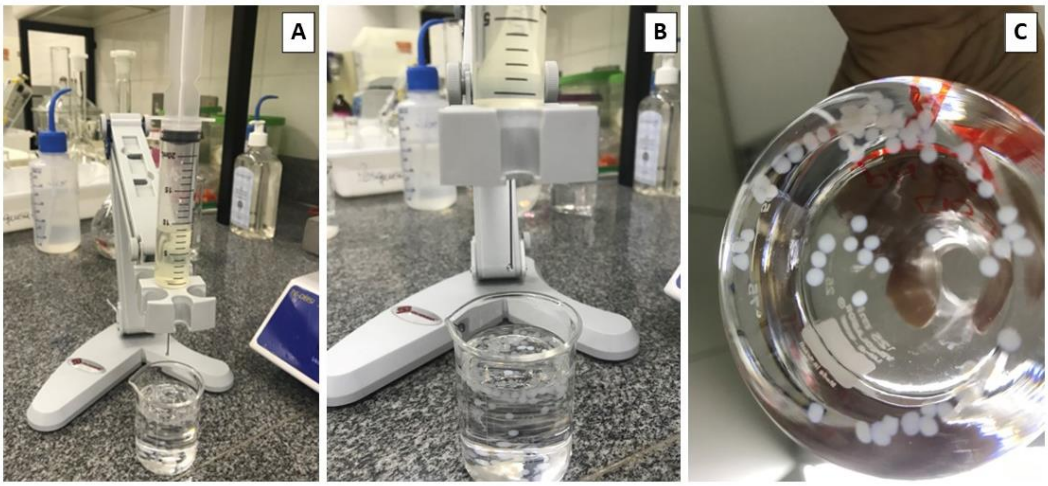

Source: Personal collection.

Legend: Ionic gelation process overview (A), chitosan drop formation in detail (B), microspheres in detail (C).

a.1. CTS microspheres application fields

a.1.1. General application

Many scientific works have been carried out to explore the use of CTS microspheres as matrix to immobilize active components for many purposes (RAZA et al., 2020). The advantages of encapsulating active agents in a biopolymer matrix include their protection from the surrounding medium or processing conditions and their controlled release (HARRIS et al., 2011). CTS microspheres have been applied to provide controlled release of different types of drugs and to improve the bioavailability of degradable substances such as protein or improve the uptake of hydrophilic substances across the epithelial layers (BANSAL et al., 2011; SINHA et al., 2004). CTS microspheres have been successfully used for bone repairing (MENG et al., 2015) and to solve oral health problems (BAKSHI et al., 2020). Besides that, CTS microspheres can be applied in many other areas such as food field (BODAKOWSKA-BOCZNIEWICZ; GARNCAREK, 2019) or agriculture (DOS SANTOS PEREIRA et al., 2020).

a.1.1.1 Environmental application

CTS has been studied as adsorbent for monitoring and decontamination of water for over three decades. Due to the easy availability of free $–NH_2$ groups in CTS, it spontaneously reacts with many pollutants like metals, pesticides, herbicides, phenolic compounds, herbicides, dyes, drug, phosphate, etc (BAKSHI et al., 2020). This biopolymer can be directly applied in solid form for the removal of pollutants (e.g., cations or organic molecules) from the aqueous media by filtration or adsorption processes or in liquid state (dissolved in acidic media), to neutralize charges, for coagulation-flocculation (dissolved matter, colloids and particles in suspension), and membrane filtration (polymer-assisted ultrafiltration) (DESBRIÈRES; GUIBAL, 2018).

Compared to the other physical forms, microspheres provide a larger surface area and huge binding position, and have good rate of diffusion, adsorption, dispersion, mass transfer and attachment behavior (JONGPAIBOONKIT; FRANKLIN-FORD; MURPHY, 2009; RAZA et al., 2021). Besides that, microspheres can pose better physical-chemical and mechanical properties due to its desired constitution (RAZA et al., 2021). There is also the possibility of improving the adsorption properties of the microspheres through the addition of chemical groups (e.g., amino group, carboxyl group, sulfur group, phenolic group, among others)

during its making process (JEYASEELAN; MEZNI; VISWANATHAN, 2022; RANJBARI et al., 2022).

Removal of PTM ions from aqueous media by CTS microsphere and its derivatives has been extensively studied in recent decades (Table 1), and the chelation mechanism develop an important role in this process since the amino group acts as an electron rich donor (BAKSHI et al., 2020).

Table 1 – Some reported works on metal ions adsorption on modified chitosan beads

Adsorbent	Adsorbate	qmax (mg g^{-1})	Ref.
Magnetic glycine-grafted chitosan bead	Cd(II)	171.06	Nina et al., 2022
Chitosan-pectin gel beads	Cu(II), Cd(II), Hg(II), Pb(II)	169.4, 177.6, 208.5, 266.5	Shao et al., 2021
Magnetic kaolinite immobilized chitosan beads	Pb(II), Cd(II)	90.0, 88.5	Elanchezhiyan et al., 2021
Chitosan immobilised in alginate beads	Cu(II), Cd(II),	527.3, 207.0	Kuczajowska-Zadrożna; et al., 2020
Tripolyphosphate cross-linked chitosan beads	Cd(II)	99.87	Babakhani et al., 2020
Magnetic chitosan beads	Hg(II), Cd(II)	0.4, 3.04	Purnamawati et al., 2019
Arginine cross-linked chitosan–carboxymethyl cellulose beads	Pb(II), Cd(II)	182.5, 168.5	Manzoor et al., 2019
Crosslinked chitosan beads grafted poly(methacrylamide)	Cu(II), Cd(II)	140.9, 178.6	Sutirman et al., 2018
Cross-linked chitosan microspheres poly(maleic acid)-grafted cross-linked	Cd(II)	14.5	Yu et al., 2017
Chitosan microspheres		39.2	
Chitosan Microsphere Surface Successively Grafted by Methyl Acrylate and Diethylenetriamine	Pb(II), Cd(II)	239.2, 201.6	Zhang et al., 2017
Surfactant-modified chitosan beads	Cd(II)	125.0	Pal et al., 2017
Carboxymethyl-β-cyclodextrin functionalized chitosan impregnated with water-insoluble epichlorohydrin cross-linked β-cyclodextrin polymer composite beads	Cd(II)	378.0	Sikder et al., 2017
Cross-linking chitosan/rectorite nano-hybrid composite microsphere	Cu(II), Cd(II), Ni(II)	20.49, 16.23, 13.32	Zeng et al., 2015

Source: The author.

2.2. JUSTIFY

Since potentially toxic metals can induce great damage to the biota and cause imbalance in the chemical homeostasis of aquatic systems, monitoring and/or removing these compounds from these environments becomes increasingly urgent. Among the several sustainable approaches to this end, the adsorption method has proved to be an attractive, simple and powerful tool for the removal of numerous inorganic pollutants. In this sense, chitosan appears as a good alternative, since it is a very abundant, non-toxic biosorbent, widely known for its properties of forming stable complexes with many metal ions. However, the scientific literature still does not have much information about the performance of this biopolymer for the removal of metallic ions in the presence of natural competitors. Natural organic matter is a complex matrix of organic compounds that is extremely common in natural waters and has a known affinity for metallic ions. Thus, studying how this matrix can interfere in the adsorptive process of chitosan is essential to develop the best strategies in the use of this biopolymer for the target purpose.

2.3. GENERAL OBJECTIVE

The present research aimed to evaluate the performance of chitosan microspheres cross-linked with Sodium Tripolyphosphate for removal / recovery of low concentrations of Cd(II) from aqueous solutions in the presence and absence of NOM.

2.3.1. Especific objectives

In order to reach the general objective, were studied:

- The morphological and structural features of chitosan beads before and after contact with Cd(II) ions and NOM;
- The influence of the contact time, the amount of adsorbate in solution in the adsorptive equilibrium, as well as the isothermal and kinetic parameters of the adsorption.

3. MATERIALS AND METHODS

3.1. MATERIALS AND INSTRUMENTS

All reagents were of analytical grade and were used as received without further purification. Low MW chitosan was purchased from Sigma-Aldrich (St. Louis, USA) with 75–85% DD and with average MW of 122.74 kDa (based on viscosity), nitric acid, TPP, sodium nitrate and sodium hydroxide (Synth, São Paulo, Brazil), acetic acid (glacial) (NEON, Suzano, Brazil). Aqueous solutions were prepared with 18.2 MΩ cm purified water produced using deionized water (Gehaka − MS 2000, São Paulo, Brazil). A stock solution containing 1000 mg L^{-1} of Cd(II) supplied by SpeCSol (Quimlab, Jacareí-SP, Brazil) was used to prepare the working test standard solutions. The dissolution of the reagents was made with the aid of a magnetic stirrer (Quimis®-Q221M). The pH of the test standard solutions was adjusted using pH meter (Quimis −Q400AS, São Paulo, Brazil). For the batch adsorption experiments was used a floor standing shaking incubator (AMERICAN LAB) and an orbital table shaker (Quimis−Q225M). The total organic carbon (TOC) content of the NOM applied in the competition experiment was determined using a TOCN Multi N/C 3100 Analityk Jena (Germany).

3.1.1. Scanning Electron Microscopy (SEM) and Energy Dispersive Spectrometry (EDS)

The surface morphology analysis of CTS−TPP before and after NOM contact and Cd(II) uptake was analyzed by SEM. SEM analyzes were performed using a JEOL JSM – 6010LA (Tokyo, Japan) with an acceleration voltage of 3 kV, at the Technological Plasma Laboratory of the São Paulo State University – Sorocaba campus. In the same sample, three different regions were analyzed and in each region six magnifications were made, namely: 70, 100, 150, 300, 550 1000 and 3000 times. The EDS with accelerating voltage of 10 kV was performed in three regions at 70x, 100x and 550x magnification. The analyzed elements were: C, O, N, Na, P and Cd and the images were produced by a scan time of 80 seconds. The metallization process applied on CTS−TPP surface was gold-palladium.

3.1.2. Fourier Transform Infrared Spectroscopy (FTIR)

The functional groups of CTS−TPP before and after NOM contact and Cd(II) uptake were characterized by FTIR (Model 660 – IR, Varian) in conjunction with a attenuated total reflectance (ATR) accessory with diamond crystal (Pike Technologies Glade). A total of 64 scans were conducted on samples with wavenumber range of 400 to 4000 cm^{-1} (YONG et al., 2013) at the Technological Plasma Laboratory of the São Paulo State University – Sorocaba campus.

3.1.3. X-Ray Diffraction (XRD)

The XRD patterns of pristine CTS, CTS−TPP (without and with adsorbed Cd(II)) were recorded on an X-ray Diffractometer (Panalytical X'Pert Powder) at room temperature at the Technological Plasma Laboratory of the São Paulo State University – Sorocaba campus. The voltage and current used were 40 kV and 44 mA, respectively, and the angle range scanned (2θ) from 10 to 60º with a step of 0.02º taken at 1.2 sec/step (Adapted from MIRDA et al., 2021).

3.1.4. Optical Emission Spectrometry (ICP–OES)

All determination of metal ion concentrations was carried out using Inductively coupled plasma – optical emission spectrometry (ICP–OES) (Agilent Technologies–720, Santa Clara, USA) with the following instrumental parameters, as shown in Table 2:

Table 2 − Instrumental parameters for ICP–OES analyses

(continued)

ICP-OES parameter	Type or value
Spray chamber	Cyclonic
Nebulizer	Concentric
RF generator	40 MHz
RF power	1.1 kW

Coolant gas flow rate (Ar)	15.0 L min^{-1}
Auxiliary gas flow rate (Ar)	1.5 L min^{-1}
Nebulization flow rate (Ar)	200 kPa
Wavelengh for Cd^{2+}	226.502 nm
Torch mode	Axial

Source: The author.

3.2. EXPERIMENTAL

3.2.1. Preparation of CTS–TPP

CTS–TPP was made by adapting, the methodology proposed by Laus et al. (2006). Two grams of CTS was dissolved with the aid of a magnetic stirrer at 140 rpm in 100 mL of acetic acid at 1% (v / v). Then, the TPP solution was prepared at pH 8.5 with 5% (w / v) concentration. The viscous solution obtained was dropped using a syringe (Needle: 30 x 7 mm) coupled to a TPP solution bath. Then, the microspheres were filtered, and deionized water was used continuously to rinse them. The microspheres were stored at room temperature in the laboratory cabinet. A digital micrometer (150 x 0.02 mm) was used to measure the microspheres, as shown in Figure 8.

Figure 8 – Measurement of chitosan microspheres cross-linked with sodium tripolyphosphate

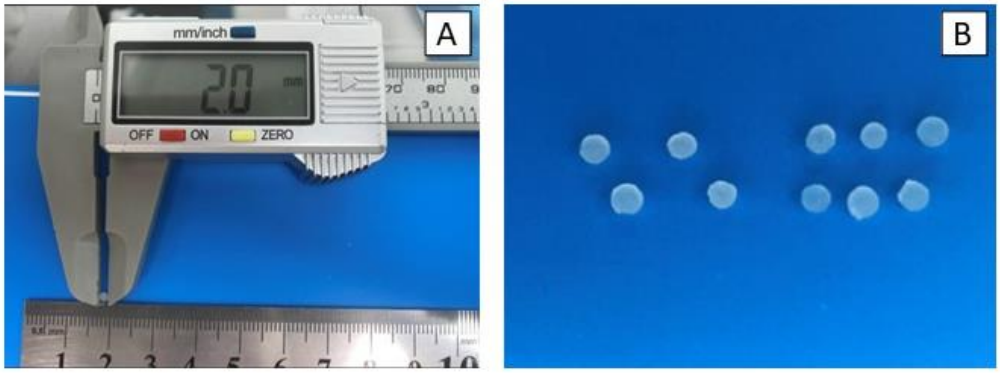

Source: The author.

Legend: Measurement of microspheres using a micrometer (A); appearance of chitosan microspheres (B).

3.2.2. Adsorption capacity

Cd(II) adsorption experiments on CTS–TPP were performed by batch equilibrium. Standard stock solution of Cd (1000 mg L^{-1}) was diluted using deionized water to obtain solutions with different initial concentrations. For each experiment, a certain amount of adsorbent was placed in 125 mL Erlenmeyer flask and the contents were shaken thoroughly to avoid mass transfer resistance using an orbital table shaker or shake incubator at a speed of 140 rpm at 25 °C (Figure 9) (WANG et al., 2014). The experiments were conducted in triplicates and average of the determinations was used for calculations. A summary of the experimental conditions used is given in Table 3.

Table 3 – Experimental conditions for determination of adsorption capacity

CTS–TPP added (g)	Sol. vol. (mL)	Ionic strength ($NaNO_3$) (mg L^{-1})	pH	Temp. (° C)	Cd(II) initial conc.(mg . L^{-1})
0.5	100	0.01	5.5	25	0.1, 0.2, 0.5, 1.5, 2.5, 5.0, 8.0
			6.5		0.1, 0.2, 0.5, 1.5, 2.5, 5.0, 8.0
			7.0		0.1, 0.2, 0.5, 1.5, 2.5, 5.0, 8.0

Source: The author.

Figure 9 – Batch adsorption with chitosan microspheres cross-linked with sodium tripolyphosphate

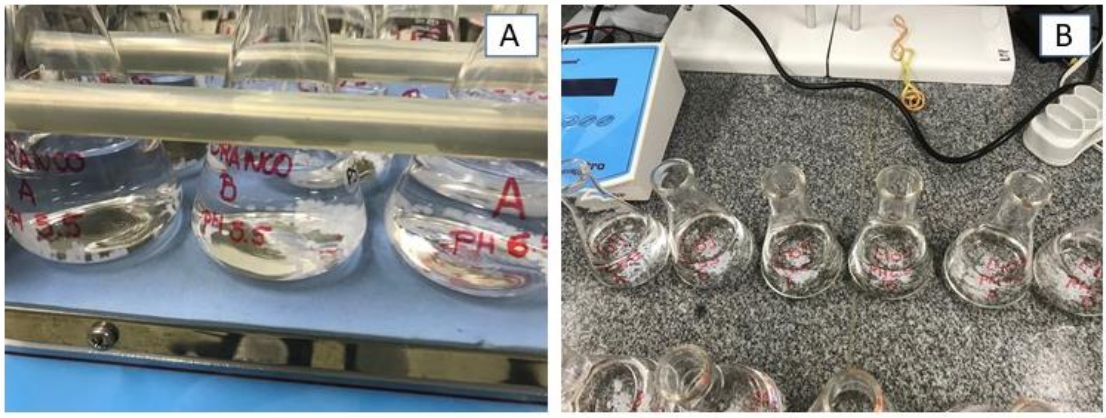

Source: The author.

Legend: Erlenmeyers with chitosan microspheres cross-linked with sodium tripolyphosphate during the experiment (A), Erlenmeyers overview (B).

After giving enough time to the adsorption system, the amount adsorbed per unit mass of adsorbent at equilibrium, q (mg g^{-1}), was calculated by using the following Equation 3:

$$q = \frac{(C_0 - C_e)}{W} V \quad (3)$$

where

C_0 and C_e (mg L^{-1}) are the initial and final concentration of a metal ion in the solution, V (L) is the volume of the solution, and W (g) is the mass of the adsorbent.

The percentage of metal removed due to biosorption was calculated according to Equation 4.

$$\%\, removal = \frac{(C_0 - C_e)}{C_0} x100 \quad (4)$$

3.2.3. The effect of pH on adsorption capacity

This test was performed to determine the pH of adsorption at which maximum uptake of Cd(II) occurs. The pH studied was 5.5; 6.5 and 7.0 and the adjustment was made by adding a few drops of either NaOH 0.1 mol L^{-1} or HCl 0.1 mol L^{-1}. The pH of the solution in the flask was not controlled during the adsorption process to avoid introduction of additional ions into the solution. A summary of the experimental conditions used is given in Table 3.

3.2.4 Time of equilibrium and kinetic studies

These studies were conducted by adding CTS–TPP to each series of Erlenmeyer (V = 125 mL) flasks with different initial metal ion concentrations. The flasks were shaken thoroughly at 140 rpm and 25 ^oC under different pH values. Two and half mL of samples solution were removed at different intervals (0; 15; 30; 60; 120; 240; 480 and 1440 min) and acidified in a 2% HNO_3 solution to determine the metal ion concentration by ICP–OES. All experiments were performed in triplicate. A summary of the experimental conditions used is given in Table 4.

Table 4 – Experimental conditions for determination of equilibrium time and kinetics

CTS–TPP added (g)	Sol. vol. (mL)	Ionic strength ($NaNO_3$) (mg L^{-1})	pH	Temp. (° C)	Cd(II) initial conc.(mg . L^{-1})
0.5	100	0.01	5.5	25	0.1, 0.2, 5.0
			6.5		0.1, 0.2, 5.0
			7.0		0.1, 0.2, 5.0

Source: The author.

3.2.5. Equilibrium adsorption isotherm

Isotherm models are used to plot the graph to express the distribution of the adsorbate between the adsorbent and the liquid phase which gives the equilibrium measure. The Langmuir and Freundlich model were used to determine the appropriate isotherm for Cd(II) onto CTS–TPP. The parameters of these isoterms are summarized in the Table 5. In the equations, C_e (mg L^{-1}) is the concentration of Cd(II) in equilibrium and q_e (mg g^{-1}) is the amount of adsorbate adsorbed per unit mass of adsorbent at equilibrium. Theoretical monolayer capacity is expressed as q_m (mg g^{-1}) and K_L (L mg^{-1}) is the Langmuir isotherm constant related to energy of the adsorption system. K_F ((mg g^{-1}) (L mg) $^{(1/n)}$) and n (dimensionless) are Freundlich constants that incorporate all the factors that affect the adsorption process, that is, they represent the capacity and adsorption intensity, respectively.

Table 5 – Linear and nonlinear forms of equilibrium isotherm models

Isotherm model	Non-linear equation	Linear form	Graph plotted
Langmuir	$q_e = \frac{q_m K_L C_e}{1 + K_L C_e}$	${C_e}/{q_e} = {1}/{q_m K_L} + {C_e}/{q_m}$	${1}/{q_e}\ vs. C_e$
Freundlich	$q_e = K_F C_e^{1/n}$	$lnq_e = lnK_F + {1}/{n}\ ln$	$ln\ q_e vs. lnC_e$

Source: The author.

3.2.6. The competitive effect of NOM on adsorption

The influence on the Cd(II) adsorption process by CTS–TPP in the presence of NOM was performed applying the experimental conditions that are summarized in Table 6.

The flasks were shaken thoroughly at 140 rpm and 25 ^{o}C for 1 hour before the CTS spheres were introduced. Two and half mL of samples extracted at times 0, 60, 120 and 1440 min were acidified with 2% HNO_3 for later ICP–OES readings.

Table 6 – Experimental conditions for competition study

CTS–TPP added (g)	Sol. vol. (mL)	Ionic strength ($NaNO_3$) (mg L^{-1})	pH	Temp. (^{o}C)	Cd(II) initial conc.(mg L^{-1})	NOM conc. (mg L^{-1})
0.5	100	0.01	6.5	25	0.2	10.0

Source: The author.

4. RESULTS AND DISCUSSION

4.1. CTS–TPP

The microspheres formed by the application of ionic gelation were formed instantly after mixing of TPP (5%, w/v) and CTS solutions as molecular linkages were formed between the phosphate groups of TPP and the amine groups of CTS. The large size of wet beads suggests high swelling and water retention ability of the beads (SRINATHA; PANDIT; SINGH, 2008). The CTS spheres had a pale white color and an average size of 1.75 ± 0.12 mm, as shown in Figure 10:

Figure 10 – Chitosan beads resulting from ionic gelation using sodium tripolyphosphate

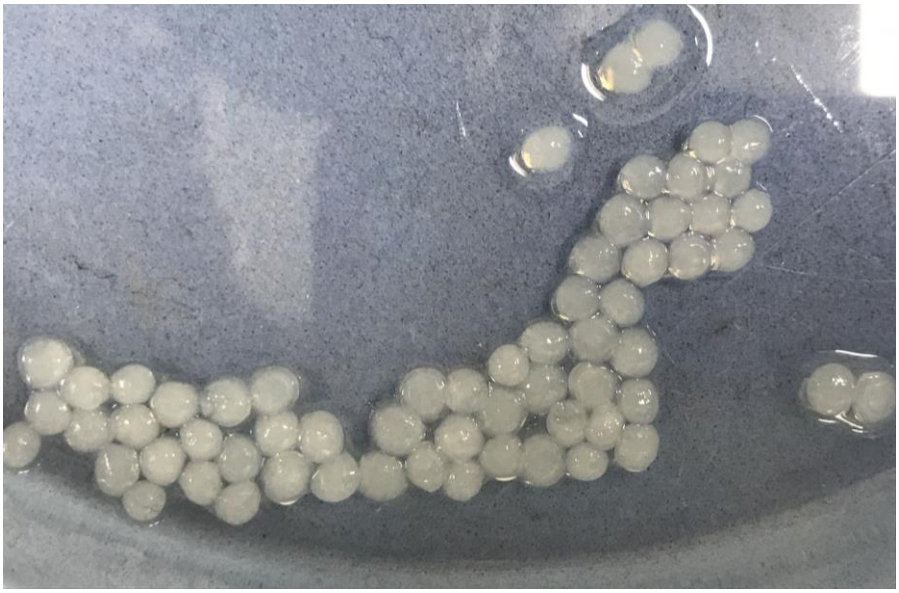

Source: The author.

After contact with NOM, the color of the CTS–TPP changed from pale white to brown color (Figure 11). A similar result was obtained in the work of Ngah and Musa (1998).

Figure 11 – Chitosan beads resulting after natural organic matter contact

Source: The author.

4.2. CARACTERIZATION

4.2.1. SEM

The shape and surface features of CTS–TPP after Cd(II) uptake are shown in Figure 12 ((A) – (C)). SEM imaging revealed that TPP facilitated the formation of non-uniform shape beads, with a porous structure, leading to a less smooth surface (JIANG et al., 2020), however, without many cracks and / or stratifications. Some microspheres were not completely spherical in shape.

Figure 12 – SEM micrograph images of chitosan microspheres cross-linked with sodium tripolyphosphate after Cd(II) uptake

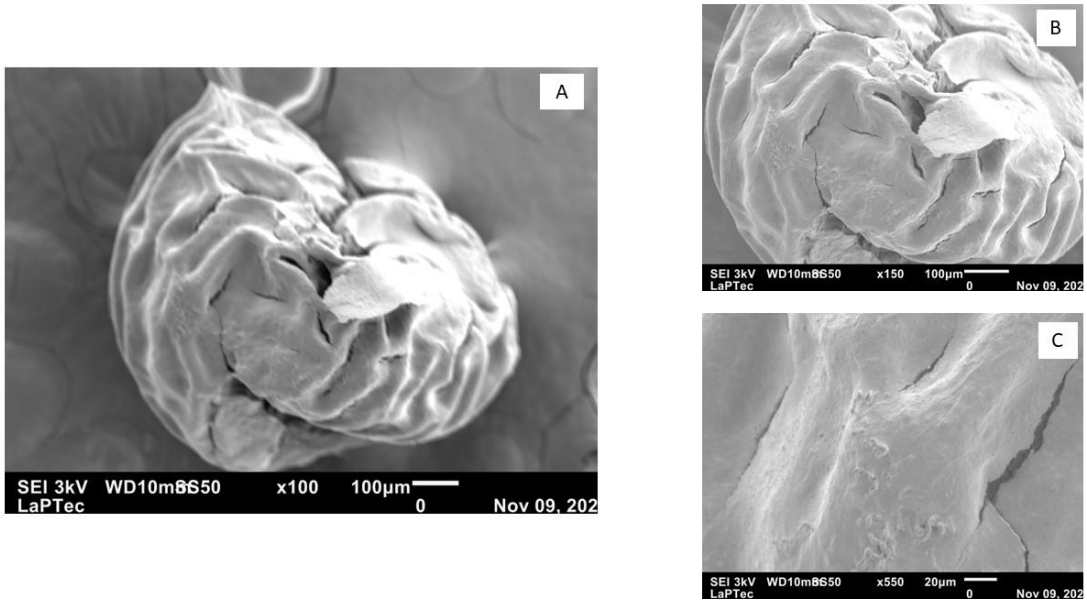

Source: The author.

Legend: Chitosan microspheres cross-linked with sodium tripolyphosphate morphology after Cd(II) uptake at x 100 magnification (A), at x 150 magnification (B) and at x 550 magnification (C).

In Figure 13 (A) and (B) shows, respectively, the existence of many regularly shaped pores evenly distributed on the CTS–TPP rough surface and a zoom-in of a pore before the Cd(II) uptake. The existence of a large pore density is beneficial for the mass transfer during the adsorption of metals in CTS–TPP (SAKAI; NAKAMURA; KISHI, 2014). Regarding the SEM images after adsorption of Cd(II) (Figure 13 (C) and (D)), it can be clearly observed that the sample exhibited a “sponge” aspect (high density of intercommunicating pores) with some accumulation of material on its surface.

Figure 13 – SEM micrograph images of chitosan microspheres cross-linked with sodium tripolyphosphate before and after Cd(II) uptake

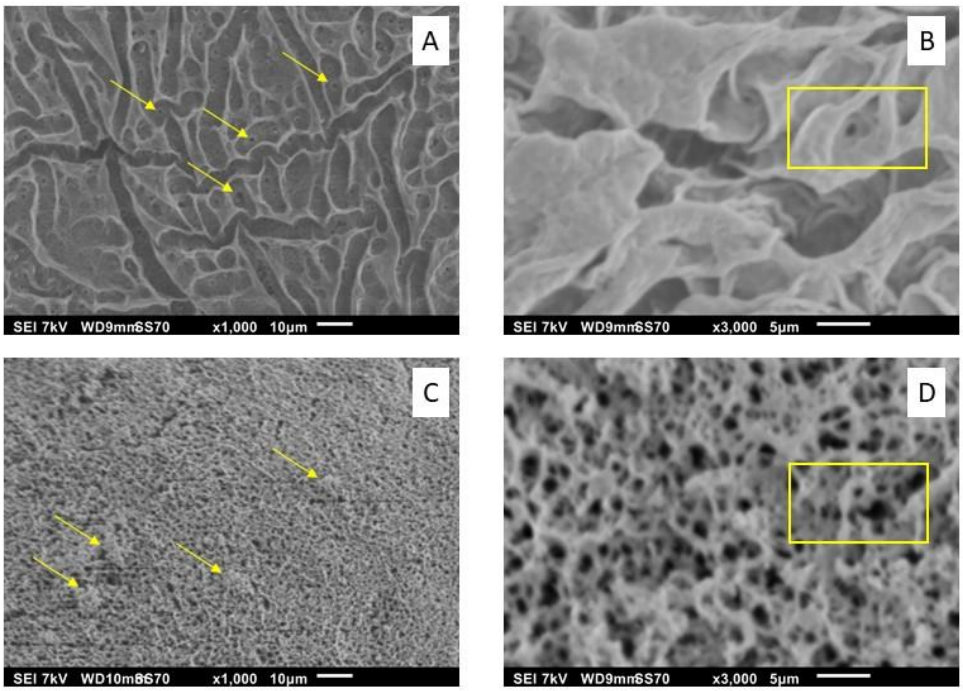

Source: The author.

Legend: Chitosan microspheres cross-linked with sodium tripolyphosphate rough surface with uniform pores (highlighted by yellow arrows) at x 1000 magnification (A), Zoom-in of a pore from chitosan microspheres cross-linked with sodium tripolyphosphate surface (highlighted by a yellow square) at x 3000 magnification (B), “Sponge” aspect and some accumulation of material (highlighted by yellow arrows) on its surface at x 1000 magnification (C), Zoom-in of intercommunicating pores at x 3000 magnification (D).

Figure 14 ((A) – (C)) shows SEM micrographs obtained for CTS–TPP after NOM and Cd(II) contact. As it is possible to notice, the micrographs show an apparent porosity, especially where there is an area of exfoliation indicated by a yellow arrow, and a wrinkled and cracked surface. Similar characteristics were also observed in the work by Araújo et al. (2017) who worked with CTS beads and humic acid (HA). Therefore, these new features may be related to the interaction between CTS–TPP and NOM.

Figure 14 – SEM micrograph images of chitosan microspheres cross-linked with sodium tripolyphosphate after natural organic matter and Cd(II) contact

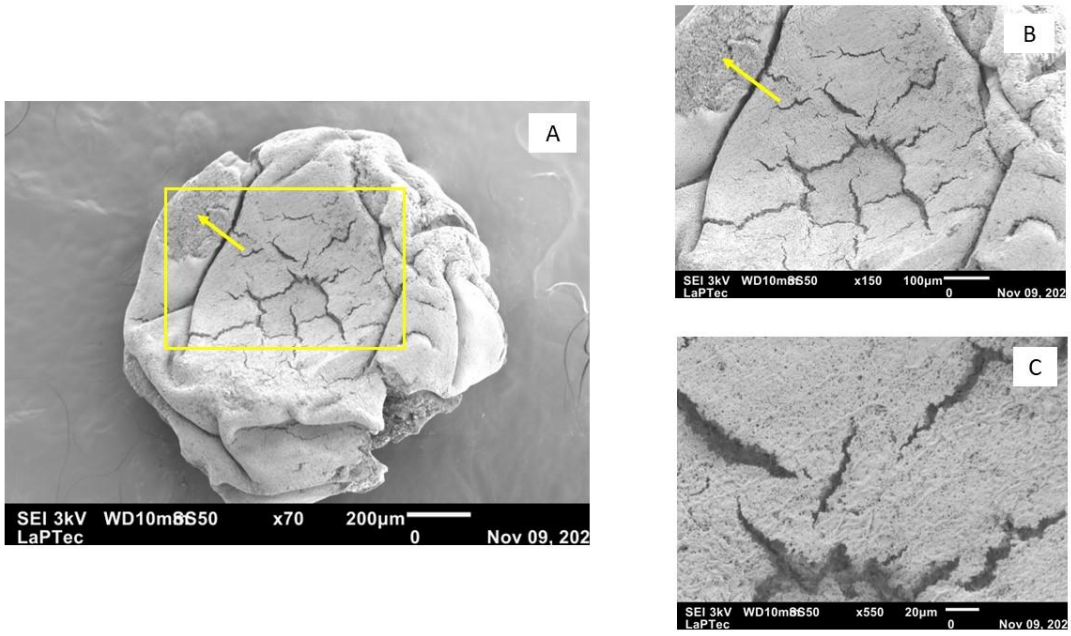

Source: The author.

Legend: chitosan microspheres cross-linked with sodium tripolyphosphate after natural organic matter and Cd(II) contact at x 100 magnification (A), at x 150 magnification (B) and at x 550 magnification (C).

4.2.1.1. SEM – EDS analysis

CTS–TPP surfaces were analyzed with this technique to qualitatively verify if cross-linking with TPP was successful and if there were possible changes before and after the contact with NOM and Cd(II). The EDS analysis of elemental mapping of carbon (C), nitrogen (N), sodium (Na), oxygen (O) and phosphorus (P) (Figure 15 (A) – (J)) showed a homogeneous distribution of the elements across the entire CTS–TPP surface. In Figure 15 (E) and (J) it is possible to observe the presence of remnants of Na on the surface of the CTS–TPP even after the spheres have been washed abundantly in water. In fact, after dissociation of TPP in water (reaction below), the Na element remains in the solution and will not participate in the cross-link reaction.

$$Na_5P_3O_{10} + 5H_2O \rightarrow 5Na^+ + H_5P_3O_{10} + 5OH^-$$

Figure 15 (L) reveals the presence of Cd(II) on the CTS-TPP surface which confirms the successful incorporation of this metal by the adsorbent.

Figure 15 – SEM–EDS micrograph images of chitosan microspheres cross-linked with sodium tripolyphosphate before and after Cd(II) uptake

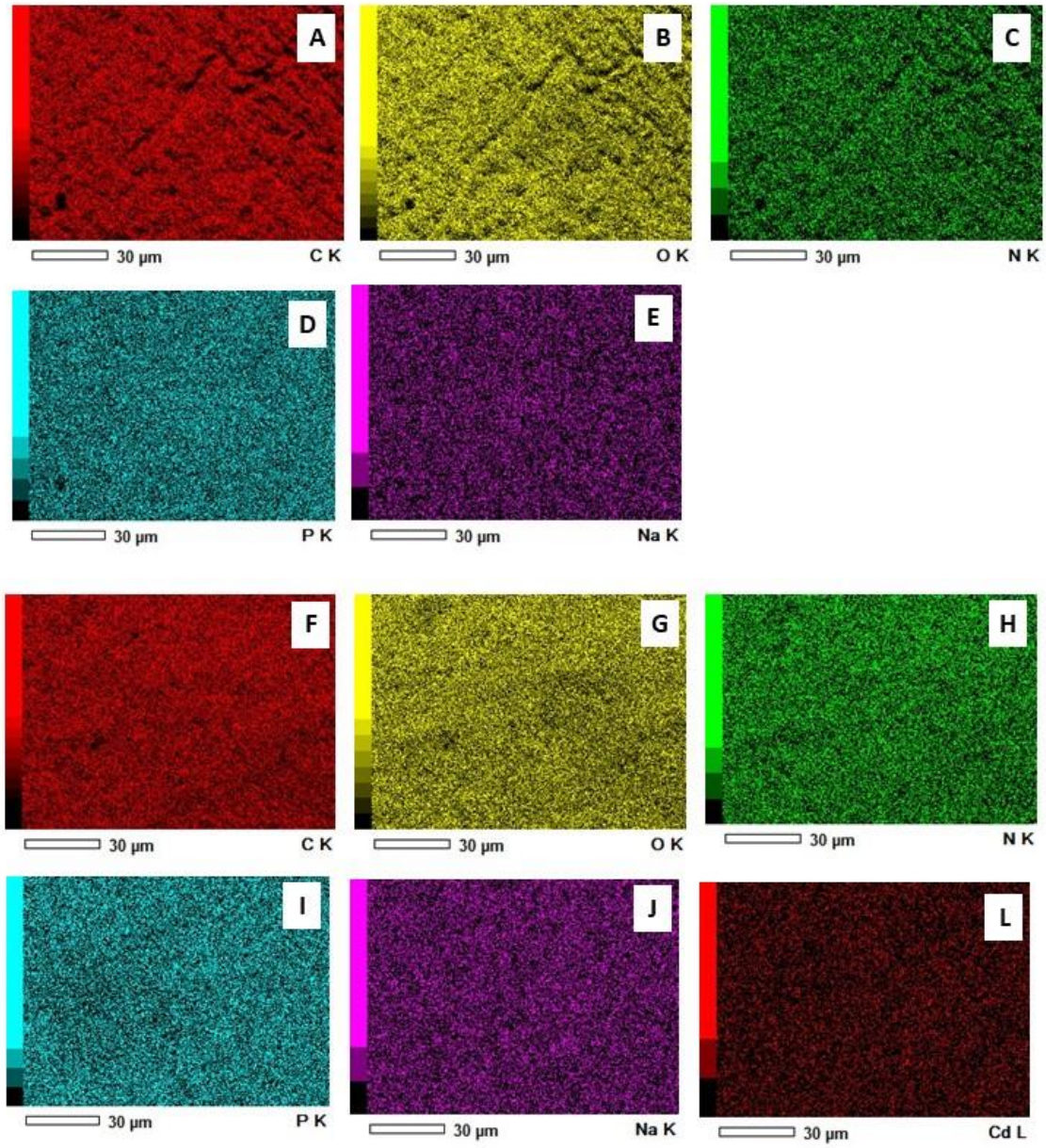

Source: The author.

Legend: Chitosan microspheres cross-linked with sodium tripolyphosphate SEM images before Cd(II) uptake (A–E), Chitosan microspheres cross-linked with sodium tripolyphosphate SEM images after Cd(II) uptake (F–L).

For SEM–EDS micrograph images for CTS–TPP with NOM and Cd(II) (Figure 16), it is possible to notice a homogeneous distribution of the same elements as already discussed in Figure 15.

Figure 16 – SEM–EDS micrograph images of chitosan microspheres cross-linked with sodium tripolyphosphate after natural organic matter and Cd(II) contact

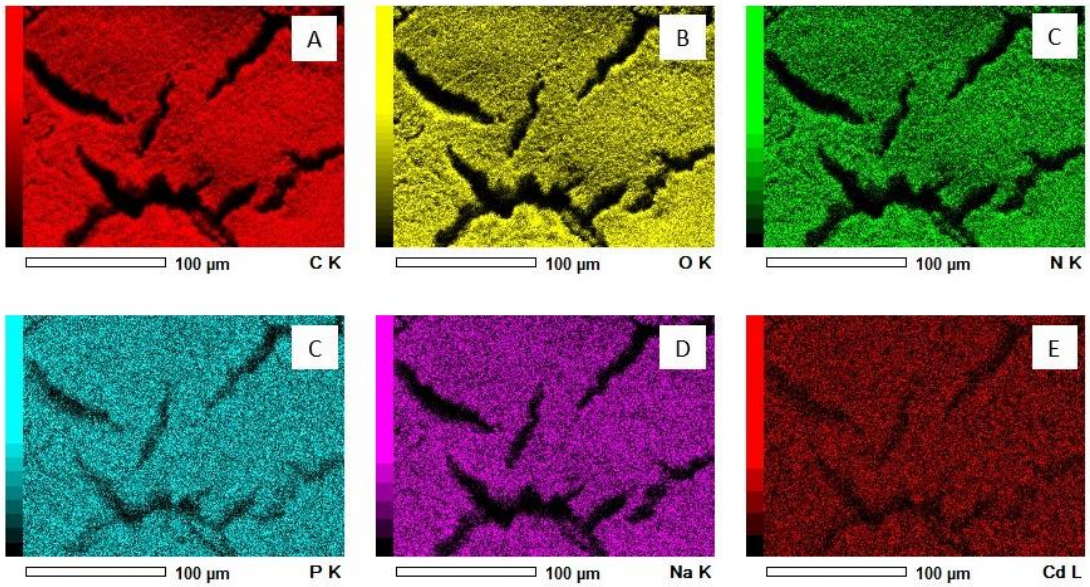

Source: The author.

EDS was applied to confirm the cross-link process between CTS and TPP and the sorption of Cd(II) onto the CTS–TPP. Figure 17 (A) shows the presence of characteristic elements of CTS (C, O and N) and of TPP that correspond to the elements Na, P and O. Figure 17 (B) which gives the characteristic peak for Cd(II) at 3.20 keV (MADALA et al., 2017). This confirms the presence of the Cd(II) on CTS–TPP surface.

Figure 17 – Graph of relative element count as a function of energy in KeV of chitosan microspheres cross-linked with sodium tripolyphosphate

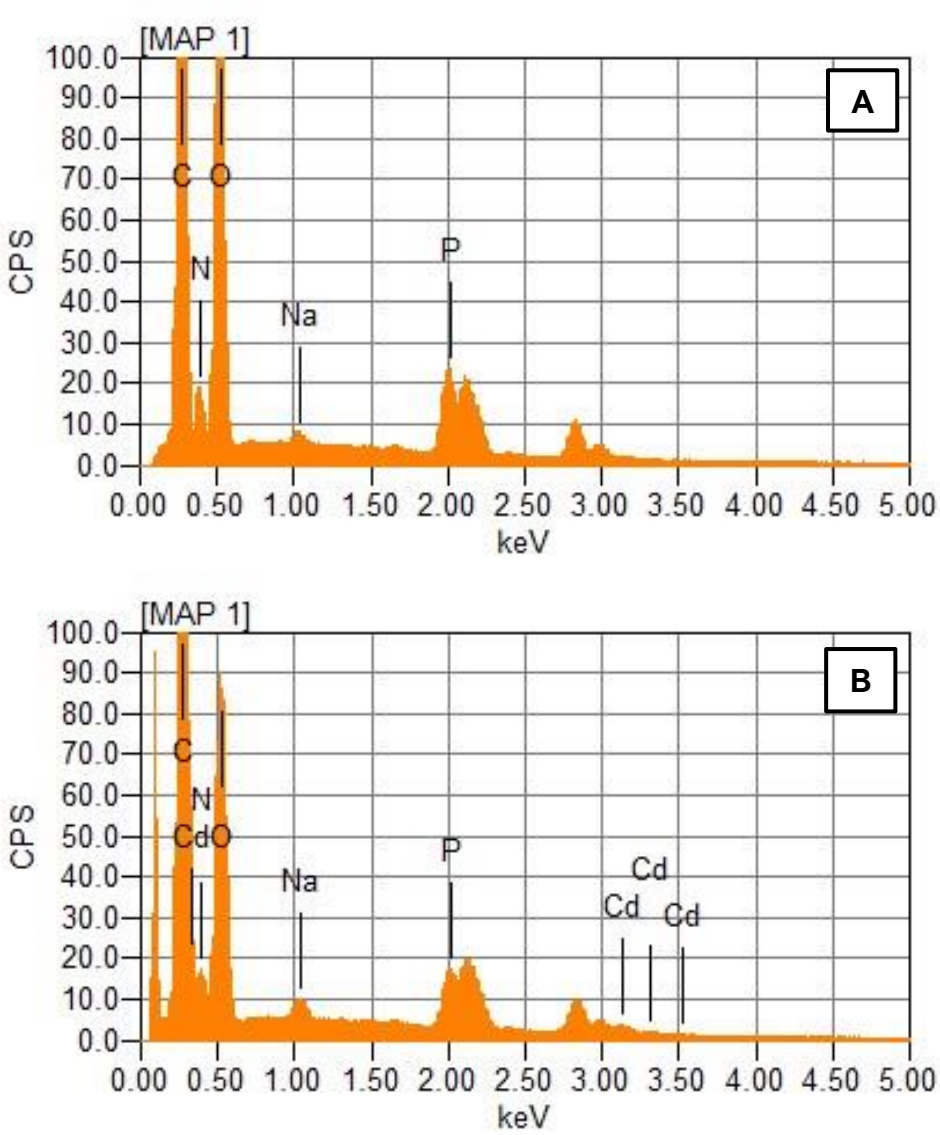

Source: The author.

Legend: CPS: Counts per second; chitosan microspheres cross-linked with sodium tripolyphosphate Cd(II) pre-adsorption (A), chitosan microspheres cross-linked with sodium tripolyphosphate Cd(II) post-adsorption (B).

4.2.3. FTIR

FTIR spectroscopy can provide helpful qualitative information since it is particularly sensitive to the conformational changes and reorganization of intra and intermolecular hydrogen bonds involving the active groups of the compounds (BRANCA et al., 2016). The CTS powder, CTS–TPP (without and with adsorbed Cd(II)) and CTS–TPP with NOM and Cd(II) were characterized using FTIR

spectroscopy. The signature of the CTS molecule can be significantly recognized from the intensity of the amine peak at wavelengths of 3300–3500 cm^{-1} and the strong N–H stretch at 1590–1650 cm^{-1}, as seen from the infrared (IR) spectrum shown in Figure 18.

Figure 18 – IR spectra of chitosan powder

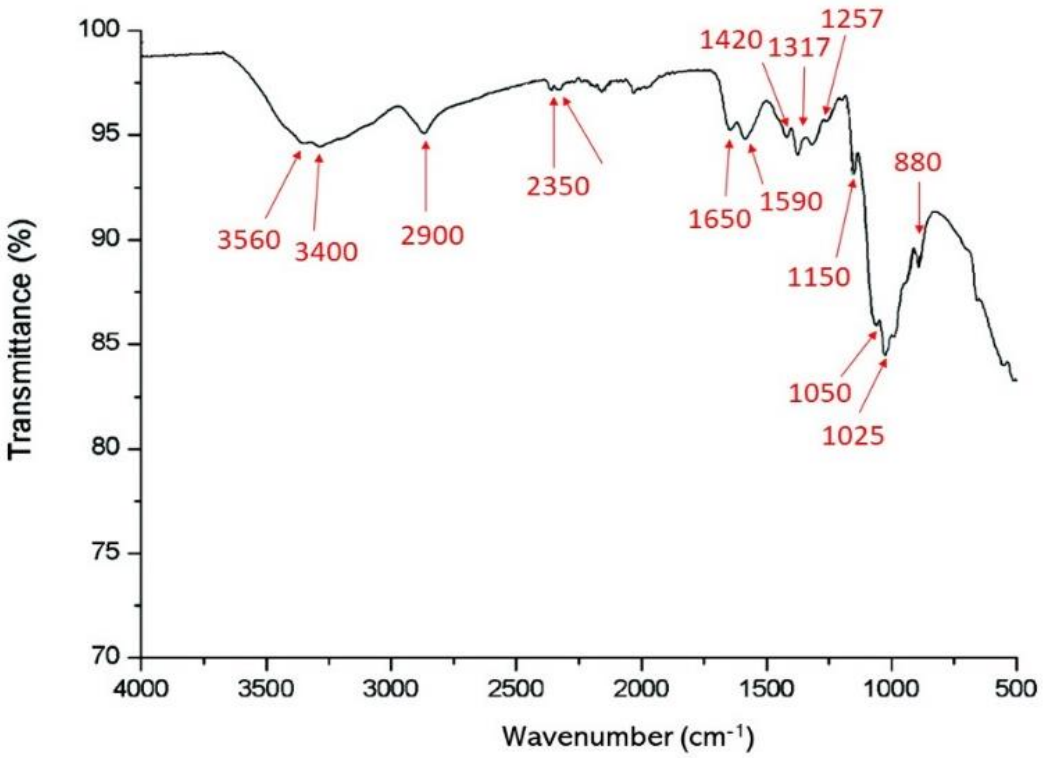

Source: The author.

CTS powder presented some characteristic peaks as shown in Table 7.

Table 7 – FTIR bands of chitosan powder

(continued)

Chitosan wavenumber (cm^{-1})	Assignments
3500–3400	O–H and N–H stretching vibration
2900	C–H stretching
2350	symmetric and asymmetric vibrations of C-H groups
1650	Amide I band
1590	N–H bending of NH_2
1420	CH_2 bending and CH_3 symmetrical deformation
1320	Amide III band

1257	O–H bending
1150	Asymmetric bridge oxygen (C–O–C)
1050	–C–O–C in glycoside linkage
1025	C–O stretching
880	CH_3COH group

Source: Adapted from Fang Feng et al. (2012).

The FTIR spectra of CTS–TPP without and with adsorbed Cd(II) are illustrated in Figure 19.

Figure 19 – FTIR spectra of chitosan microspheres cross-linked with sodium tripolyphosphate without and with sorbed Cd(II)

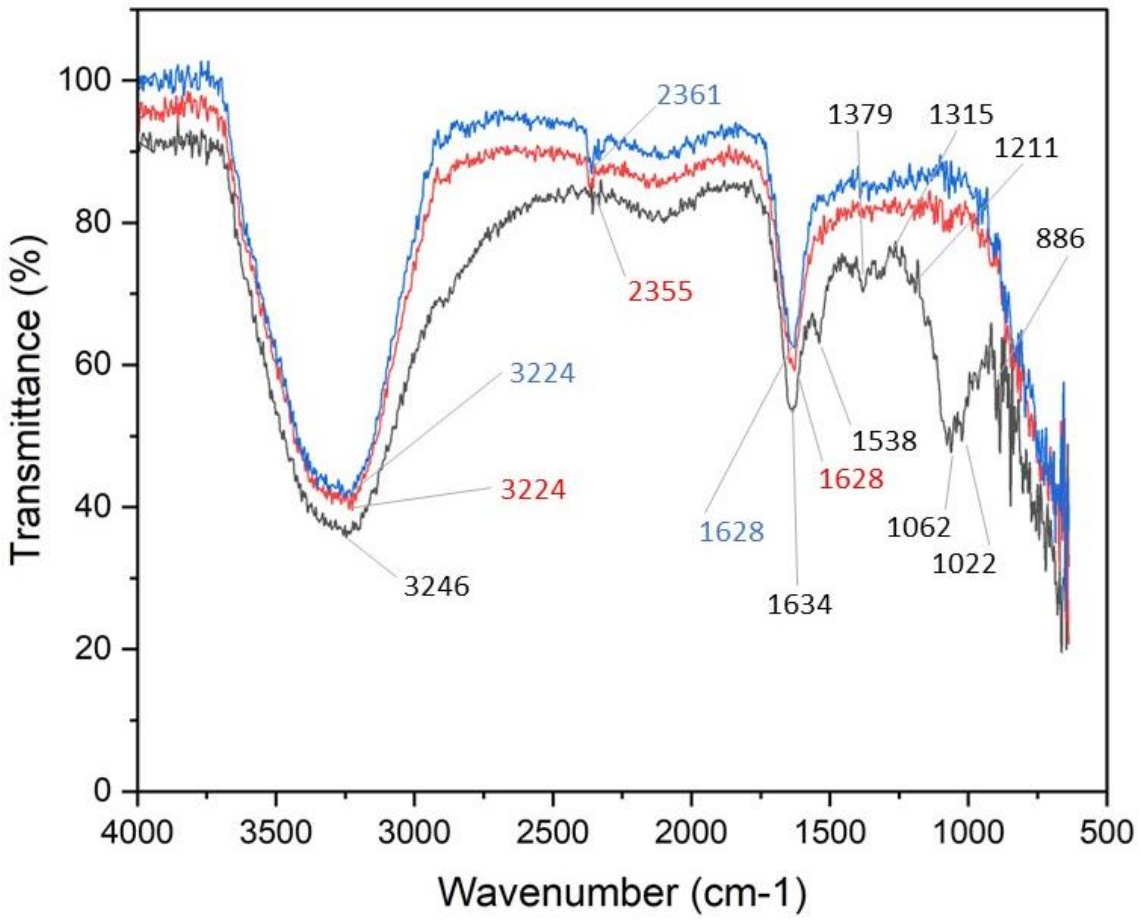

Source: The author.

Legend: IR spectrum of chitosan microspheres cross-linked with sodium tripolyphosphate before Cd(II) uptake is represented by (■) color; IR spectrum after Cd(II) ($[Cd(II)]_o$ = 0.2 mg . L^{-1} solution) uptake is represented by (■) color and after Cd(II) ($[Cd(II)]_o$ = 8.0 mg . L^{-1} solution) uptake by (■) color.

From Figure 19, it is possible to clearly observe the spectral changes in the CTS structure compared to its original state, after the incorporation of TPP and due to the incorporation of Cd(II) after the adsorption process. There is a shift in the absorption peaks assigned to C–O and NH_2 groups stretching vibration (3000 – 3500 cm^{-1}) in the CTS–TPP spectrum compared to CTS powder. Besides that, the absorption peaks of this range eventually became broader and this showed that the $–NH_2$ groups in CTS were protonated to form $–NH_3^+$, as this broader band represented the stretching vibration of $–NH_3$ (CUI et al., 2008). The peak at 2900 corresponding to the C–H stretching has disappeared and there are shifts in the amine peaks from 1650 cm^{-1} (Amide I), 1590 cm^{-1} (N–H bending of NH_2) and 1315 cm^{-1} (Amide III) (PEARSON; MARCHESSAULT; LIANG, 1960; ROEGES; BAAS, 1994) on CTS–TPP which indicate the ionic interaction between the positively charged NH groups of CTS and the negatively charged TPP groups. Therefore, the ionic crosslinking with TPP and CTS took place on the amine groups (DE MOURA et al., 2009; LEE et al., 2001). Apparently, at 1211 cm^{-1} there is a peak that represents P=O stretching characteristic of TPP. This peak disappeared after the uptake test, probably this reflects the interaction between Cd(II) and P=O group. The CH_3 symmetrical deformation observed at 1420 cm^{-1} (SANNAN; KURITA; IWAKURA, 1976; WANG; TURHAN; GUNASEKARAN, 2004) in the CTS powder appears at 1379 cm^{-1} in CTS–TPP, however, this signature and the peaks 1538 cm^{-1} ($–NH_2$ bending in nonacetylated 2-aminoglucose primary amine) and 1315 cm^{-1} (Amide III) disappear in CTS–TPP with adsorbed Cd(II). This feature reflected that these groups participated in binding Cd(II).

The differences between the IR spectra of CTS–TPP before and after the NOM and Cd(II) contact can be observed in Figure 20.

Figure 20 – FTIR spectra of chitosan microspheres cross-linked with sodium tripolyphosphate with natural organic matter and Cd(II) sorbed

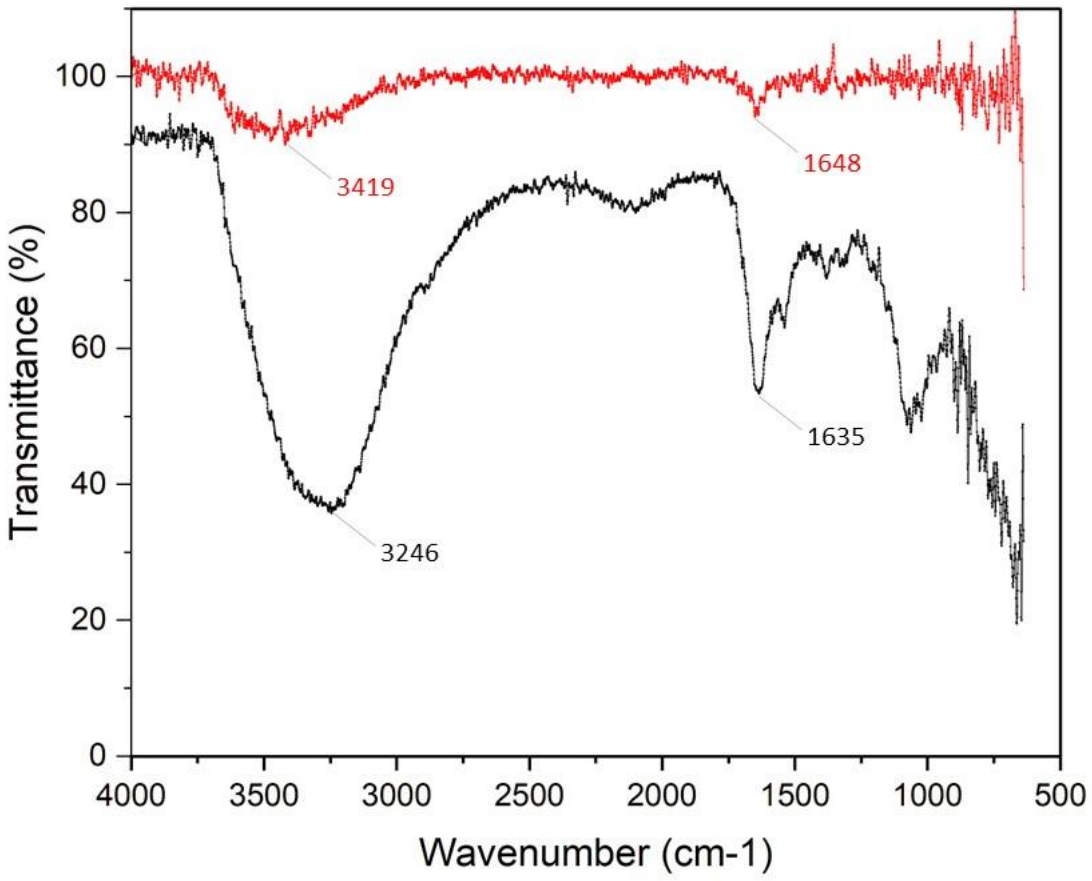

Source: The author.

Legend: IR spectrum of chitosan microspheres cross-linked with sodium tripolyphosphate before natural organic matter and Cd(II) uptake is represented by (■) color; IR spectrum after natural organic matter ($[NOM]_o$ = 10.0 mg . L^{-1} solution) and Cd(II) ($[Cd(II)]_o$ = 0.2 mg . L^{-1} solution) uptake is represented by (■) color.

It is observed that the wide band at 3246 cm^{-1} assigned to amines had a deep change in intensity and displaced to 3419 cm^{-1} due to overlapping stretching of O–H and N–H groups with hydrogen bonds (ARAÚJO et al., 2017). Moreover the band at 1635 cm^{-1}, corresponding to the vibration of NH_2 in amine, decreased considerably in intensity and was displaced to 1648cm^{-1}, indicating that NH_2 took part in adsorption (YUWEI; JIANLONG, 2011). The main binding sites in CTS–TPP for NOM are the amine groups (NGAH; FATINATHAN; YOSOP, 2011) which, in turn, complex with $–RCOO^-$ and $–RO^-$ groups of NOM (YAN; BAI, 2005) under these experimental conditions. In this perspective, at pH 6.5 it is possible the coexistence of protonated and unprotonated $–NH_2$ groups (GUIBAL, 2004).

These results show that the adsorption of NOM and Cd(II) affect the bonds with the N atom, therefore, the nitrogen atom must be the main sorption site of CTS–TPP (NGAH; MUSA, 1998; YAN; BAI, 2005). IR spectrum also shows that some chemical bonds disappeared, if this spectrum (red color) is compared to the spectrum obtained with CTS–TPP after Cd(II) uptake (Figure 19), it is possible to notice that these differences were probably caused by the coordination of NOM with chemical groups of CTS.

4.2.4. XRD analysis

XRD can yield further information regarding the crystalline structure of a solid, and this analysis was applied to detect the crystallinity of CTS powder and CTS–TPP before and after Cd(II) uptake (Figure 21).

Figure 21 – XRD of chitosan powder and microspheres cross-linked with sodium tripolyphosphate with natural organic matter before and after Cd(II) uptake

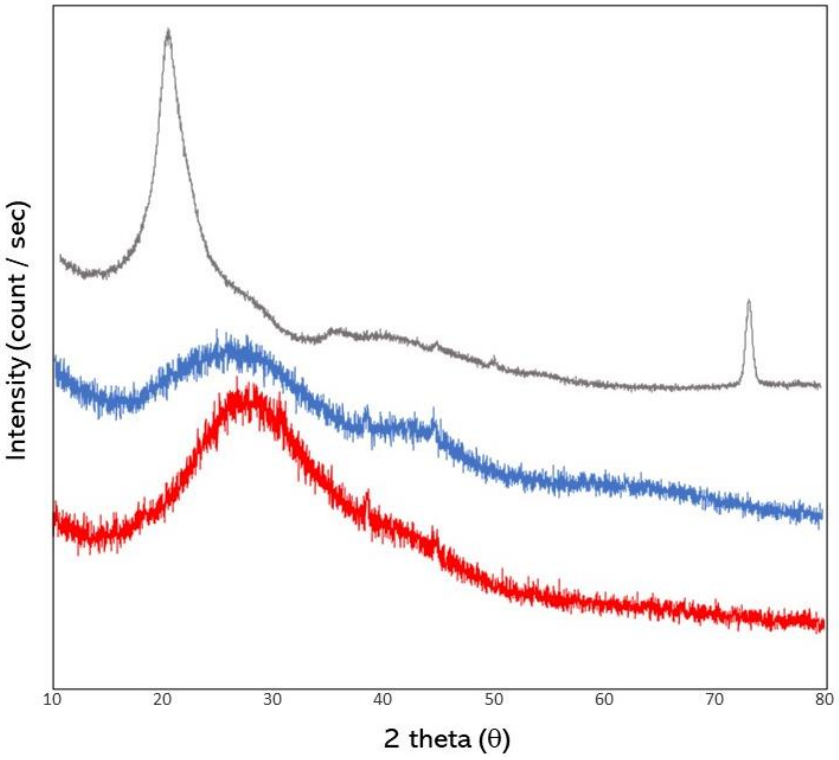

Source: The author.

Legend: XRD of CTS powder (■) color, microspheres cross-linked with sodium tripolyphosphate before Cd(II) uptake (■) color and after Cd(II) uptake (■) color.

As shown in Figure 21, it was observed that the diffractogram of CTS powder showed a consistent peak at 20.0° (crystalline form II) (SAMUELS, 1981) and a

structure located at 10.0° (crystalline form I) (SAMUELS, 1981) can be only partially visualized (as it is possible to notice, the intensity at this degree starts out very high). CTS is a semi-crystalline polymer with regular structure and strong intra and intermolecular interactions, characterized by hydrogen bonds formed between amino, hydroxyl, amide groups and other functional groups that ensure its strong crystallinity and compaction (WANG et al., 2018). Compared with CTS powder, the diffractogram of CTS–TPP exhibited some changes in the intensity and width of the peaks. After ionic gelation using TPP, a broader peak around 24.8° and a smaller and smooth peak around 44.5° were obtained. The XRD peak width reveals crystallite size information. Thus, when the peak appears enlarged, it means that there is an imperfect crystal present (indicating the amorphous nature of CTS–TPP). Therefore, it is likely that the increase in CTS–TPP imperfect crystal is related to the concentration of TPP, leading to a decrease in crystallinity (BABAKHANI; SARTAJ, 2020; JINGOU et al., 2011). The interaction of CTS with TPP promotes the loss of compact inter- and intra-chain bonding of the biopolymer, which is evidenced as a decrease in crystallinity, and it allows better interaction of metal ions with CTS (QI et al., 2004a; QI; XU, 2004b). Our findings on the decrease in crystallinity are in agreement with the earlier studies (DESHPANDE et al., 2017; HAMIDI et al., 2021). The diffractogram of CTS–TPP after Cd(II) uptake exhibited one major broad amorphous peak around 27.7º. The typical diffraction peaks that were presented in the CTS powder were dramatically changed or disappeared, indicating that the degree of crystallinity of this polymer was reduced, possibly due to the loss of free amine/hydroxyl groups after ionic cross-link and the Cd(II) adsorption process.

4.3. BATCH ADSORPTION STUDIES

4.3.1. Effect of contact time and initial concentration on the kinetics

The time taken for the metal ions and the adsorbent to reach equilibrium is of great importance in the adsorption experiment, as it depends on the nature of the system used. The results of the contact time tests allowed to obtain the percentage of adsorption (%) as a function of time in minutes (min) (Figure 22 and Tables 8–10).

Figure 22 – Contact time effect in the removal % of Cd(II) by microspheres cross-linked with sodium tripolyphosphate

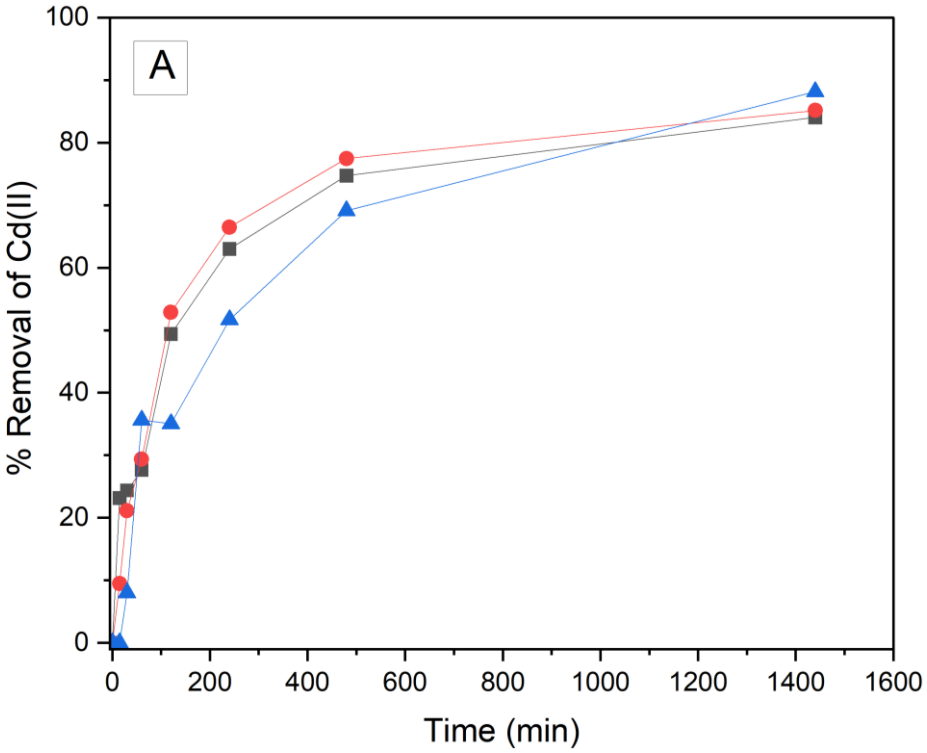

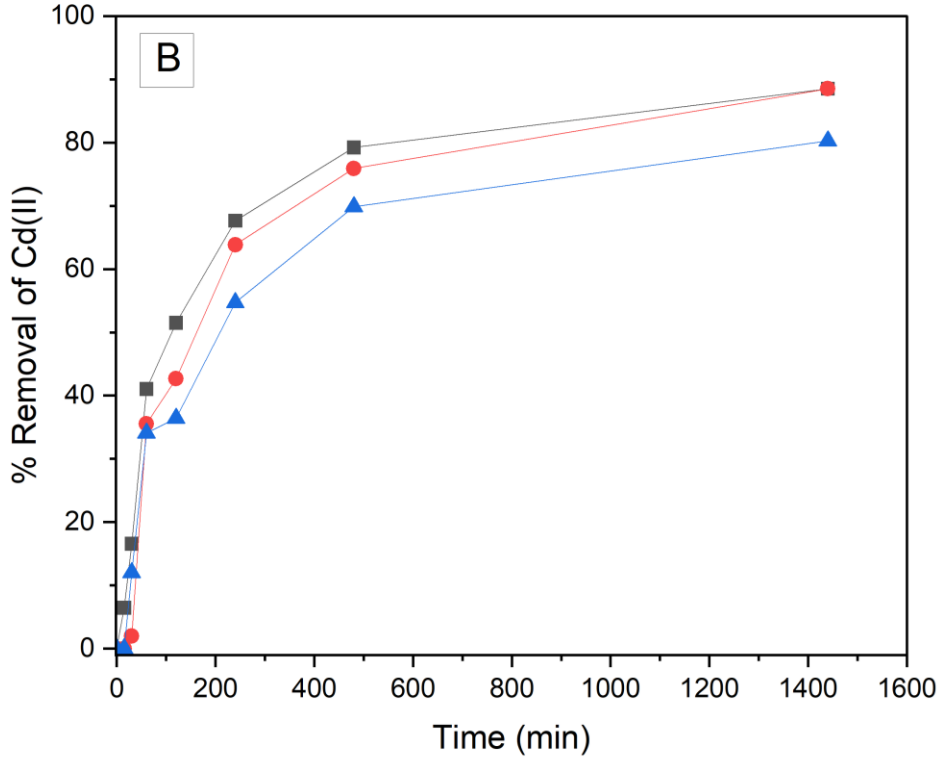

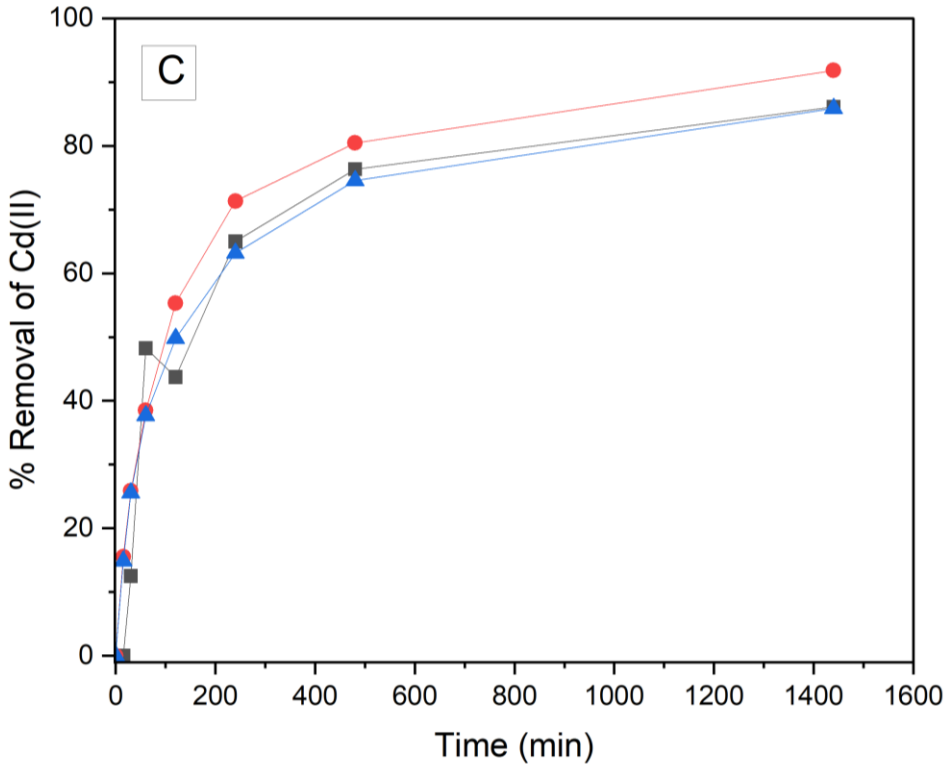

Source: The author.

Legend: Contact time effect of Cd(II) solutions (V = 100 mL, C_0 = 0.1 (■), 0.2 (●) and 5.0 (▲) mg . L^{-1} and 0.5 g of microspheres cross-linked with sodium tripolyphosphate) at 25 ºC and pH 5.5 (A), pH 6.5 (B) and pH 7.0 (C).

Table 8 – Cd(II) removal rate (%) at different times, range of pH and initial concentrations

C_0 (mg L^{-1})	Time (min)	pH	Adsorb. conc. (mg L^{-1})	Cd^{2+} remov. (%)	pH	Adsorb. conc. (mg L^{-1})	Cd^{2+} remov. (%)	pH	Adsorb. conc. (mg L^{-1})	Cd^{2+} remov. (%)
0.1		5.5			6.5			7.0		
	0		0.000	0.000		0.000	0.000		0.000	0.000
	15		0.031	23.147		0.009	6.469		0.000	0.000
	30		0.033	24.375		0.022	16.574		0.016	12.513
	60		0.037	27.633		0.056	41.051		0.063	48.237
	120		0.067	49.383		0.070	51.487		0.057	43.732
	240		0.085	63.000		0.092	67.642		0.085	64.985
	480		0.101	74.713		0.107	79.210		0.100	76.338
	1440		0.114	84.009		0.120	88.524		0.113	86.076
0.2										
	0		0.000	0.000		0.000	0.000		0.000	0.000
	15		0.030	9.469		0.000	0.000		0.030	15.541
	30		0.066	21.115		0.005	2.000		0.050	25.865
	60		0,092	29.374		0.095	35.557		0.075	38.511
	120		0.165	52.871		0.114	42.676		0.107	55.335
	240		0.208	66.480		0.170	63.855		0.138	71.340
	480		0.242	77.461		0.202	75.910		0.156	80.441
	1440		0.267	85.127		0.236	88.523		0.177	91.844
5.0										
	0		0.000	0.000		0.000	0.000		0.0000	0.000
	15		0.000	0.000		0.000	0.000		0.6724	14.875
	30		0.571	7.995		0.824	12.039		1.1568	25.589
	60		2.467	35.600		2.333	34.100		1.7045	37.706
	120		2.426	35.026		2.490	36.398		2.2519	49.814
	240		3.615	51.676		3.744	54.716		2.8559	63.175
	480		4.862	69.138		4.779	69.852		3.3692	74.530
	1440		6.222	88.182		5.492	80.269		3.8810	85.851

Source: The author.

According to the data presented in the plots and table, it is possible to notice that there were two kinetic adsorption behaviors including a fast initial step and a slower second step. The initial stage in which Cd(II) adsorption kinetics is faster took place up to 240 min and the second longer kinetic stage that tends to the steady state over time occurred from 480 min to 1440 min. Similar results regarding the kinetic behavior of Cd(II) when adsorbed by CTS were also observed by EVANS et al. (2002) and BOZORGI et al.(2018). The initial phase probably has an adsorption process dependent on the number of available active sites on the surface of the adsorbent (WEN et al., 2015). Furthermore, the fast rate of adsorption can be attributed to the size and open shape of the pores and also to the stiff structure of

the sphere which increased the internal mass transfer in the adsorption process (PAPELIS; ROBERTS; LECKIE, 1995). The functional groups that are located into the pore walls are also of great importance for the adsorption of Cd(II), as they can provide abundant binding sites for this metal ion (CHEN et al., 2017). Therefore, this fast initial step may have been the result of the combination of these two points discussed here that possibly occurred concomitantly during the first stage of Cd(II) kinetics into CTS–TPP. According to Ramesh et al. (2008), as the adsorption of the metal ion on the external surface of the CTS reaches almost saturation, that is, the active sites become unavailable, the ions begin to diffuse into the CTS–TPP. When this process starts, the diffusion resistance into the pore increases and thus the adsorption rate decreases. As the equilibrium concentration of Cd(II) decreases, the rate of diffusion slowly decreases and the adsorption process tends to reach the final equilibrium stage. According EVANS et al (2002) after the high initial rate, the mass transfer decreases with time and it may take several hundred hours to reach equilibrium uptake, suggesting intraparticle diffusion as the rate-limiting step.

It is also possible to note that after 120 minutes of experiment for solutions with initial concentrations of 0.1 and 0.2 mg L^{-1}, an average of 49.383 ± 4.633% of Cd(II) removal was obtained. However, for the solution with an initial concentration of 5.0 mg L^{-1} a removal rate of 56.522 ± 4.865% was obtained only at 240 min, which indicates a trend towards slower adsorption kinetics. Probably the fixed number of active sites in the CTS–TPP *versus* the number of metal ion molecules present in the solution promoted their rapid saturation (TEYMOURI et al., 2013) and this could explain the difference in removal rate between the different solutions during the experiment. On the other hand, the average removal rates obtained at the end of the experiment (1440 min) for all pH range for the initial concentrations of 0.1, 0.2 and 5.0 mg L^{-1} of Cd(II) (86.203%, 88.498% and 84.767%, respectively) are relatively close, which reveals that the difference in the initial concentration was expressed more clearly in the dynamics of the kinetics in the course of the experiment.

However, it should be considered that the adsorbent dosage applied (m = 0.5 g) may also have masked the effect of increasing the initial concentration, since many active sites were available. Finally, it can be concluded from the high adsorption rates that, although the cross-linking process with TPP consumes $–NH_2$ groups from the CTS, both the porosity of the bead and the cross-linking reaction

(positively affected the access to amine sites by Cd(II). In other words, the $–NH_2$ groups consumed by crosslinking process were presumably compensated by an increase in the number of amine sites exposed by the increased internal surface area (HSIEN; RORRER, 1995).

4.3.2. The effect of pH on adsorption capacity

In order to evaluate the influence of pH on the adsorption of Cd(II), the experiments were made in the pH range of 5.5, 6.5 and 7.0. The experiments could not be conducted at lower pH range to avoid dissolution of CTS–TPP and it could not be conducted above pH 7.0 to avoid the precipitation of the analyte. The Cd(II) removal rates (%) at different pH ranges and initial concentrations are summarized in Table 9. The batch adsorption carried out in this study showed a maximum removal efficiency for Cd(II) at pH 7.0 (91.84%) with initial concentration of 0.2 mg L^{-1}, however, the overall average performance at pH 5.5, 6.5 and 7.0 was, respectively, 82.0%, 82.4% and 81.6%.

Table 9 – Cd(II) removal rates (%) at different pH ranges and initial concentrations

C_0	pH		
	5.5	6.5	7.0
0.1	84.01	88.52	86.08
0.2	85.13	88.52	91.84
0.5	84.18	83.27	77.72
1.5	82.10	75.62	71.19
2.5	78.51	78.50	81.57
5.0	88.18	80.27	85.85
8.0	71.85	82.09	77.03
$\overline{X}$:	81.99	82.40	81.61
σ	5.35	4.86	6.92

Source: The author.

Generally, at acidic media (pH < 5.5), that is, solution with low pH values, protons (H^+) occupy most of the sorption sites on the CTS surface and the adsorption of metal ions is reduced due to electrostatic repulsion (AHMADI et al., 2017). However, according to Guibal (2004), at weak acidity, occurs the coexistence of protonated and unprotonated $–NH_2$ groups (about 50% of $–NH_2$ groups are protonated) (Figure 23). In this pH condition, free electron doublet on nitrogen may bind metal cations and this could be observed with the high removal rates of Cd(II)

obtained in this work when the batch adsorption test was done at pH 5.5. As the pH increases, the $–NH_2$ groups deprotonate due to depletion of H^+ concentration, leading to a reduction in the competition of these ions with Cd(II) for the sorption sites and, thus, the adsorption capacity increases (AHMADI et al., 2017). The suggested mechanism for the interaction of Cd(II) and CTS at higher pH is chelation between uncharged $–NH_2$ or –OH groups (SUTIRMAN et al., 2018). However, understanding the interactions of metal ions with CTS is not so simple, due to the simultaneous mechanisms that occur during these interplays, dominated by adsorption, ion exchange and chelation (ONSOSYEN; SKAUGRUD, 2007).

Figure 23 – Schematic of the chelation mechanism between chitosan and Cd(II)

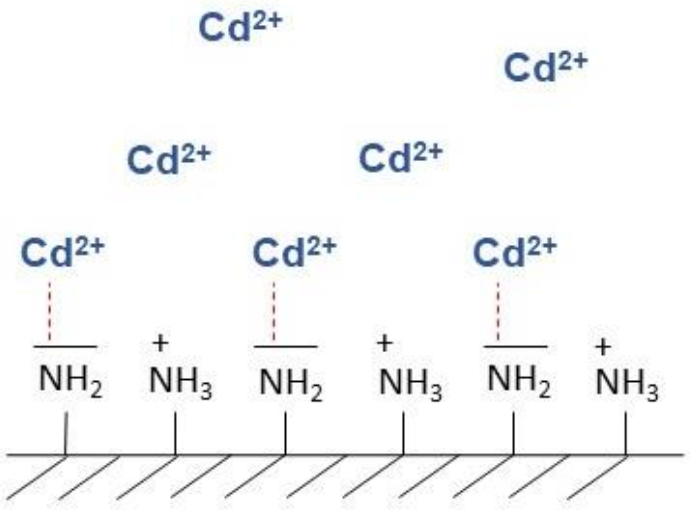

Source: Adapted from Mende et al., 2016.

Legend: Schematically adsorption mechanism of Cd(II) on microspheres cross-linked with sodium tripolyphosphate by formation of chelate complexes.

From the point of view of chemical speciation, Cd in aqueous solution is hydrolyzed and the formation of several species of this element occurs, depending on the pH of the solution. At pH > 8.5, Cd appears as $Cd(OH)_{2(s)}$, therefore, this element is precipitated. In the pH range 5.0–7.0, Cd appears in the hydrolyzed form of $CdOH^+$, $Cd(OH)^0_2$, and $Cd(OH)_3^-$, however, these hydrolyzed forms are at least 5 orders of magnitude lower than the Cd^{2+} concentration in this pH range (HSIEN, 1992). Within pH range 5.0–7.0, Cd ions in aqueous solution are speciated primarily as Cd^{2+}, thus, only this chemical configuration was adsorbed onto CTS–TPP.

INOUE et al. (1988) determined that –NH_2 sites on CTS chelate with transition metal ions according to the overall charge of the metal ions. This way, a metal ion of charge (+2) require two glucosamine units for chelation. Based on this Inoue's findings, two glucosamine units are required to complex one Cd^{2+} ion (Figure 24).

Figure 24 – Cd(II) adsorption mechanisms onto microspheres cross-linked with sodium tripolyphosphate

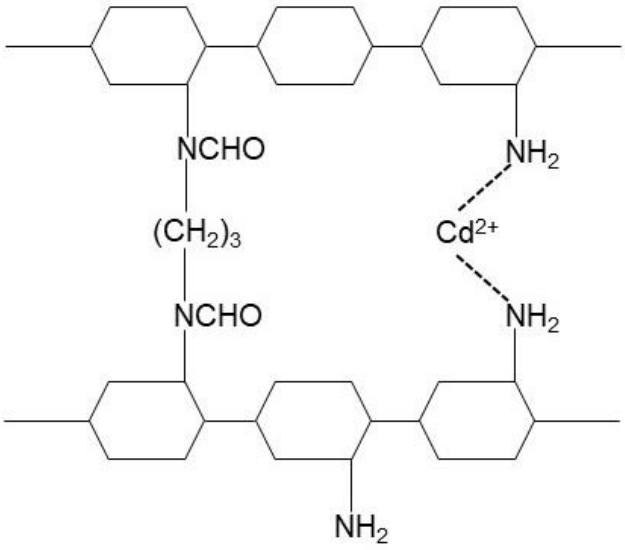

Source: Adapted from Rorrer; Hsien; Way (1993).
Legend: Proposed coordinated chelation of Cd^{2+} in cross-linked chitosan.

According to Gierszewska-Drusynska and Ostrowska-Czubenko (2008), in addition to the –NH_2 sites, depending on the pH (~ pH 6.0), the phosphate groups of TPP can also interact with Cd(II) via ion-exchange/electrostatic attraction and this fact could explain the high rate of adsorption of this metal by CTS–TPP (Figure 25). In general, good removal rates are observed for the entire pH range applied in this work.

Figure 25 – Adsorption mechanisms by sodium tripolyphosphate

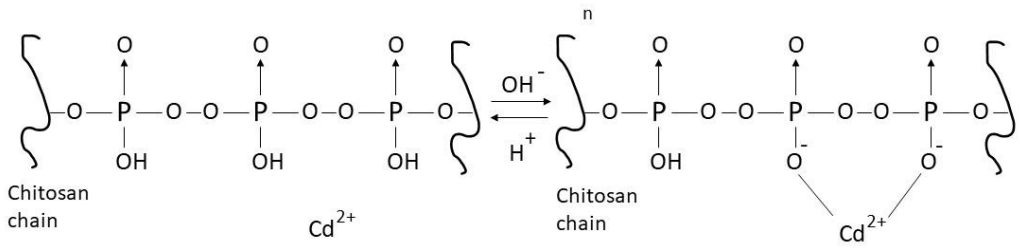

Source: Adapted from Gierszewska-Drusynska and Ostrowska-Czubenko (2008).
Legend: Proposed interaction of Cd^{2+} with sodium tripolyphosphate's P groups.

4.3.3. Kinetic adsorption study

Adsorption kinetic helps elucidate the mechanism of adsorption process. The adsorption data of Cd(II) ions were evaluated according to the pseudo-first order (PSFO) and pseudo-second order (PSSO) kinetic models. The PSFO model assumes that the Cd(II) adsorption rate is directly proportional to the number of vacant sites available for adsorption. The PSFO Equation (5) can be expressed as (LAGERGREN, 1898; TEWARI; VASUDEVAN; GUHA, 2005):

$$\log(q_e - q_t) = log q_e - \frac{K_1}{2.303} t \quad (5)$$

where q_e and q_t represent the amount Cd(II) adsorbed (mg g^{-1}) at equilibrium and at any time t and k_1 is the PSFO rate constant (min^{-1}). From the plots of log (q_e – q_t) against t in Figures 28 – 30, k_1 can be calculated from the slope and theoretical q_e can be obtained from intercepts.

The PSSO is compatible with mechanism of rate-controlling step through chemisorption and assumes that the rate of adsorption is function of the number of sites available for adsorption and the concentration of metal ions in the solution (VIJAYARAGHAVAN et al., 2017). This model predicts that the Cd(II) adsorption rate is proportional to square of difference between amount of Cd(II) absorbed at time t and amount of Cd(II) absorbed at equilibrium. The PSSO rate expression (Equation 6) is as follows (HO; MCKAY, 1999):

$$\frac{t}{q_t} = \frac{1}{k_2 q_e^2} + \left(\frac{1}{q_e}\right) t \quad (6)$$

where k_2 is the rate constant of second-order adsorption. The straight-line plots of t / q_t versus t determine 1 / qe as slope and 1 / $k_2 q_e^2$ as intercepts. The linear plots of PSSO model are shown in Figures 26 – 31.

Figure 26 – Pseudo-first order plots for the adsorption of Cd(II) (C_o = 0.1 mg . L^{-1}) onto chitosan microspheres cross-linked with sodium tripolyphosphate

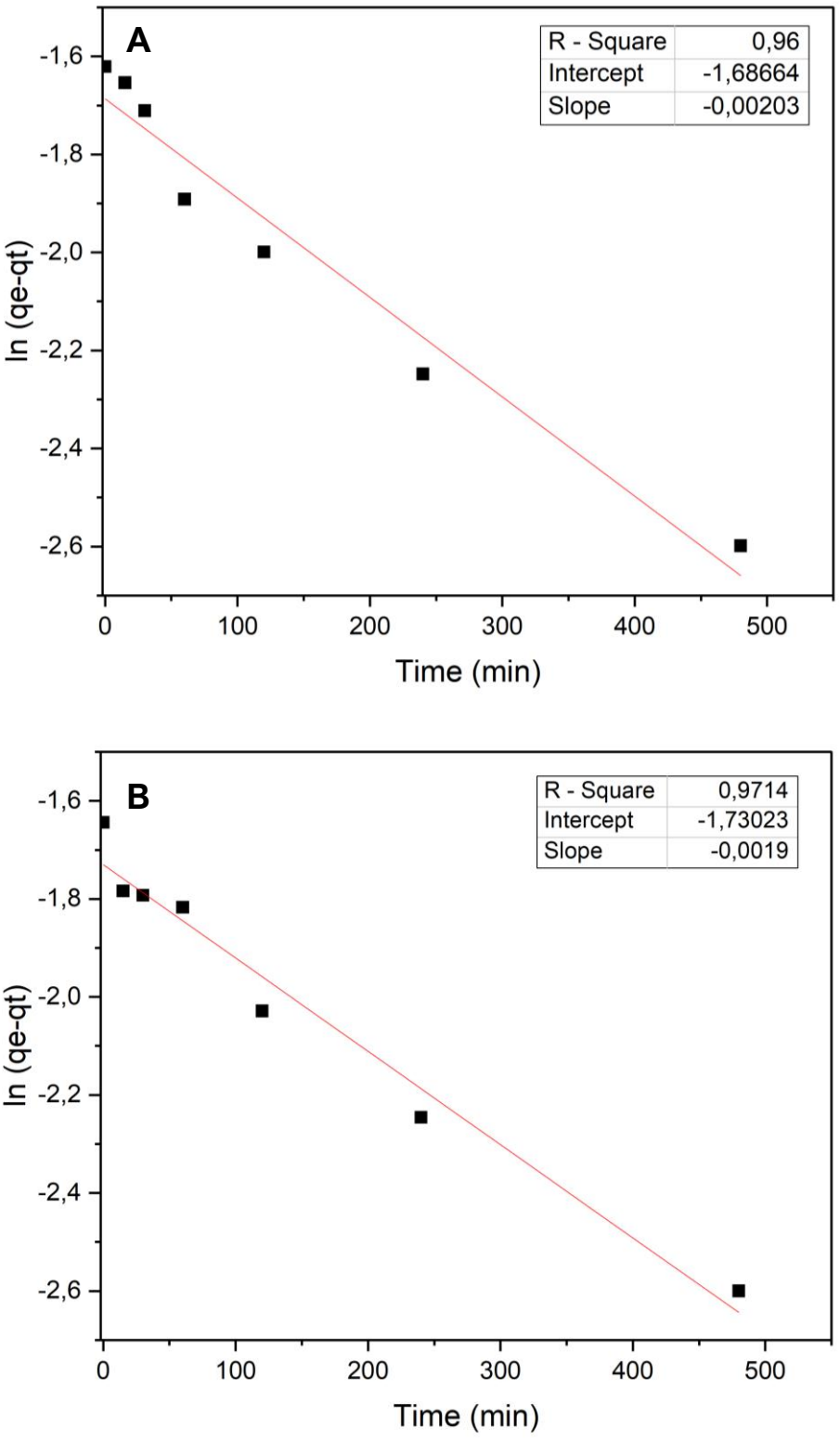

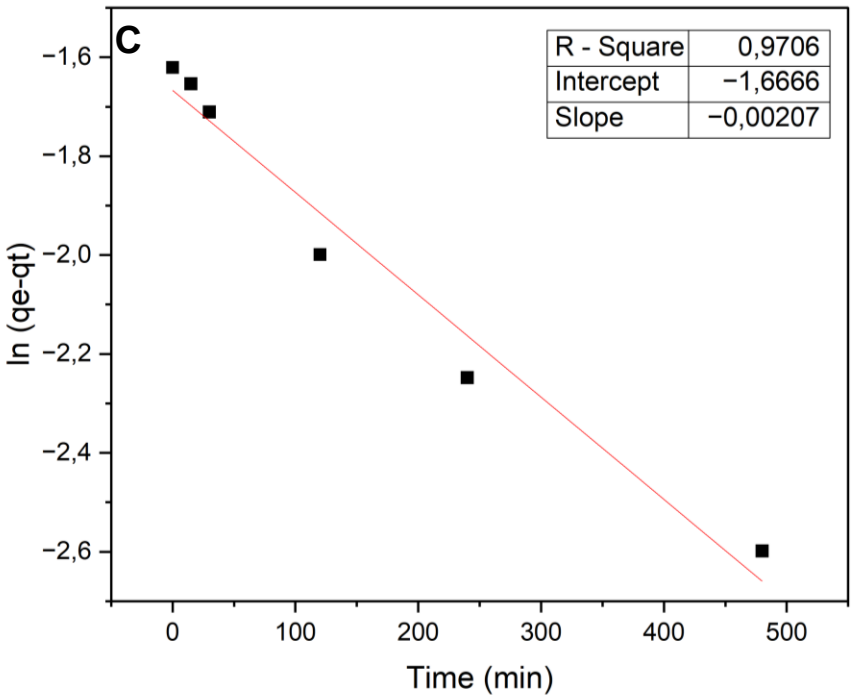

Source: The author.
Legend: Pseudo-first order plots for the adsorption of Cd(II) (V = 100 mL, C_o = 0.1 mg . L^{-1}) at 25 ^oC and pH 5.5 (A), pH 6.5 (B) and pH 7.0 (C) onto chitosan microspheres cross-linked with sodium tripolyphosphate.

Figure 27 – Pseudo-first order plots for the adsorption of Cd(II) (C_o = 0.2 mg . L^{-1}) onto chitosan microspheres cross-linked with sodium tripolyphosphate

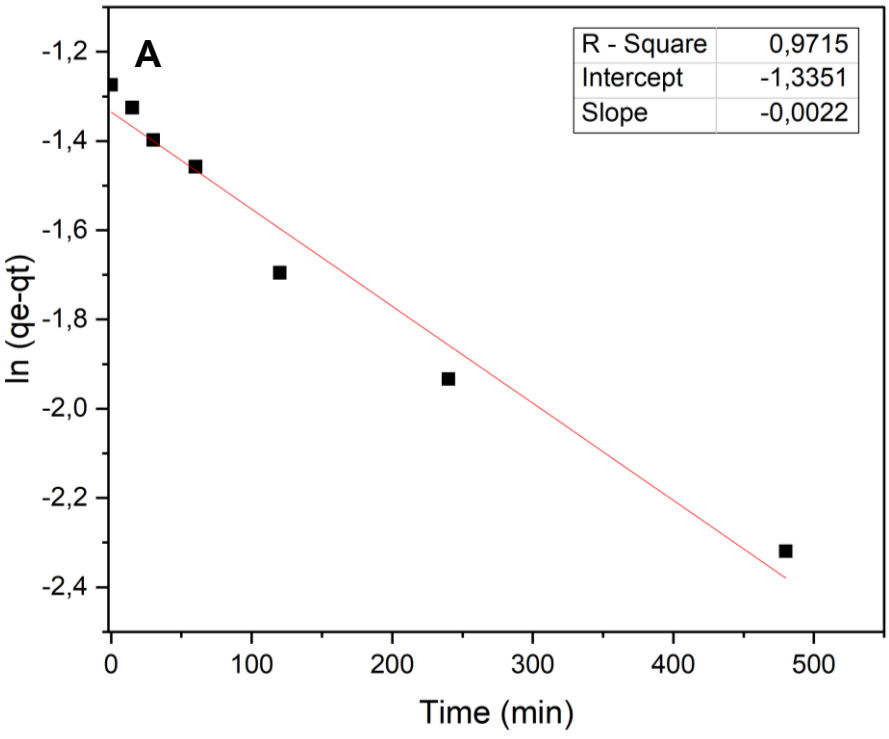

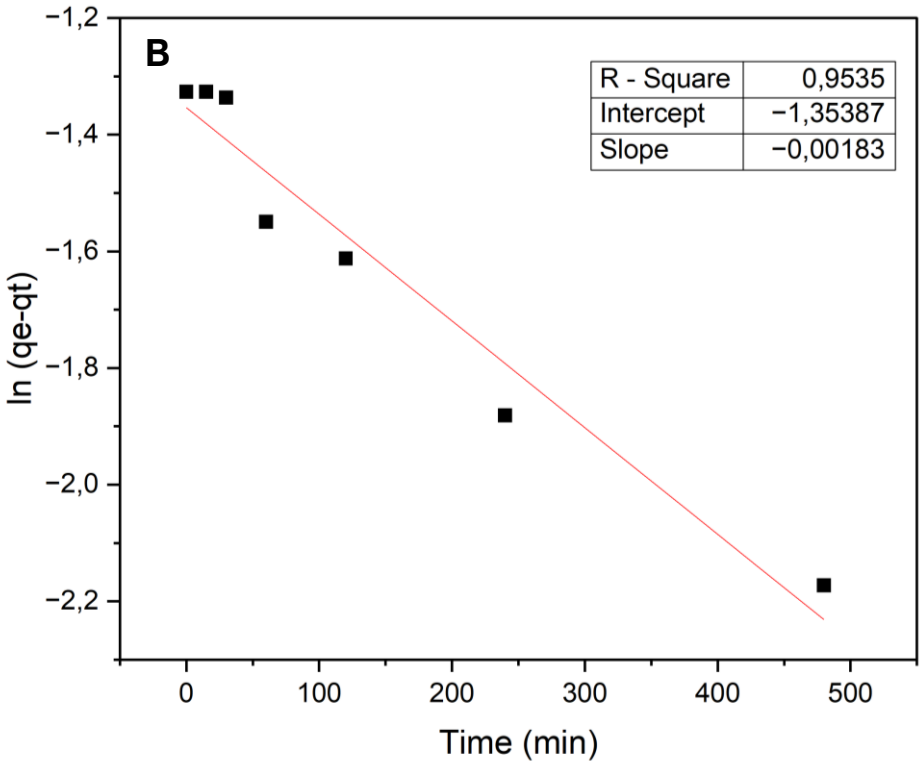

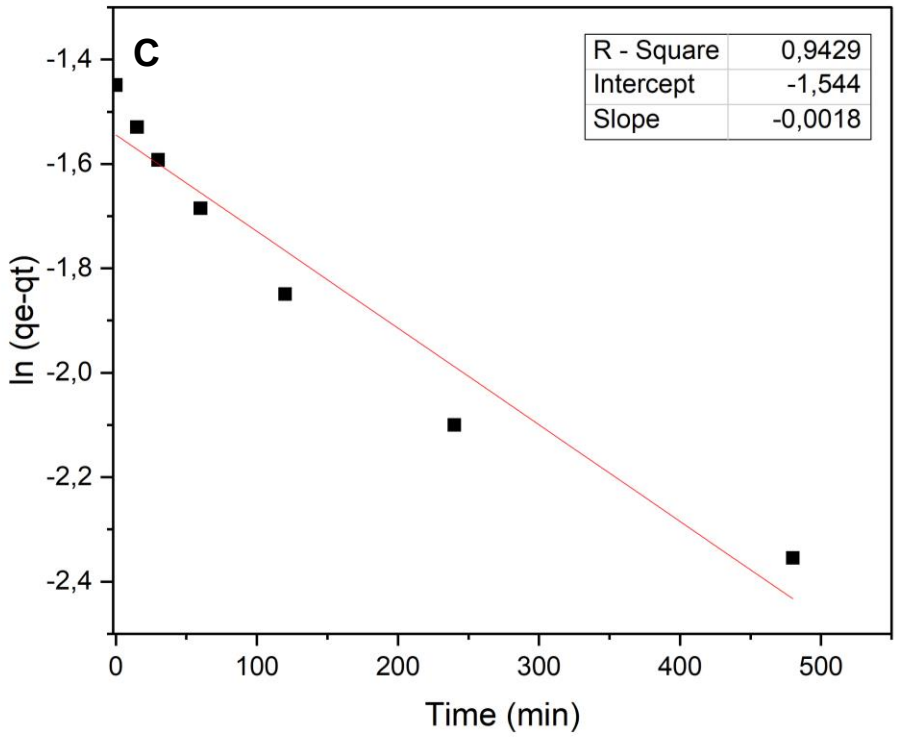

Source: The author.
Legend: Pseudo-first order plots for the adsorption of Cd(II) (V = 100 mL, C_o = 0.2 mg . L^{-1}) at 25 ^oC and pH 5.5 (A), pH 6.5 (B) and pH 7.0 (C) onto chitosan microspheres cross-linked with sodium tripolyphosphate.

Figure 28 – Pseudo-first order plots for the adsorption of Cd(II) (C_o = 5.0 mg . L^{-1}) onto chitosan microspheres cross-linked with sodium tripolyphosphate

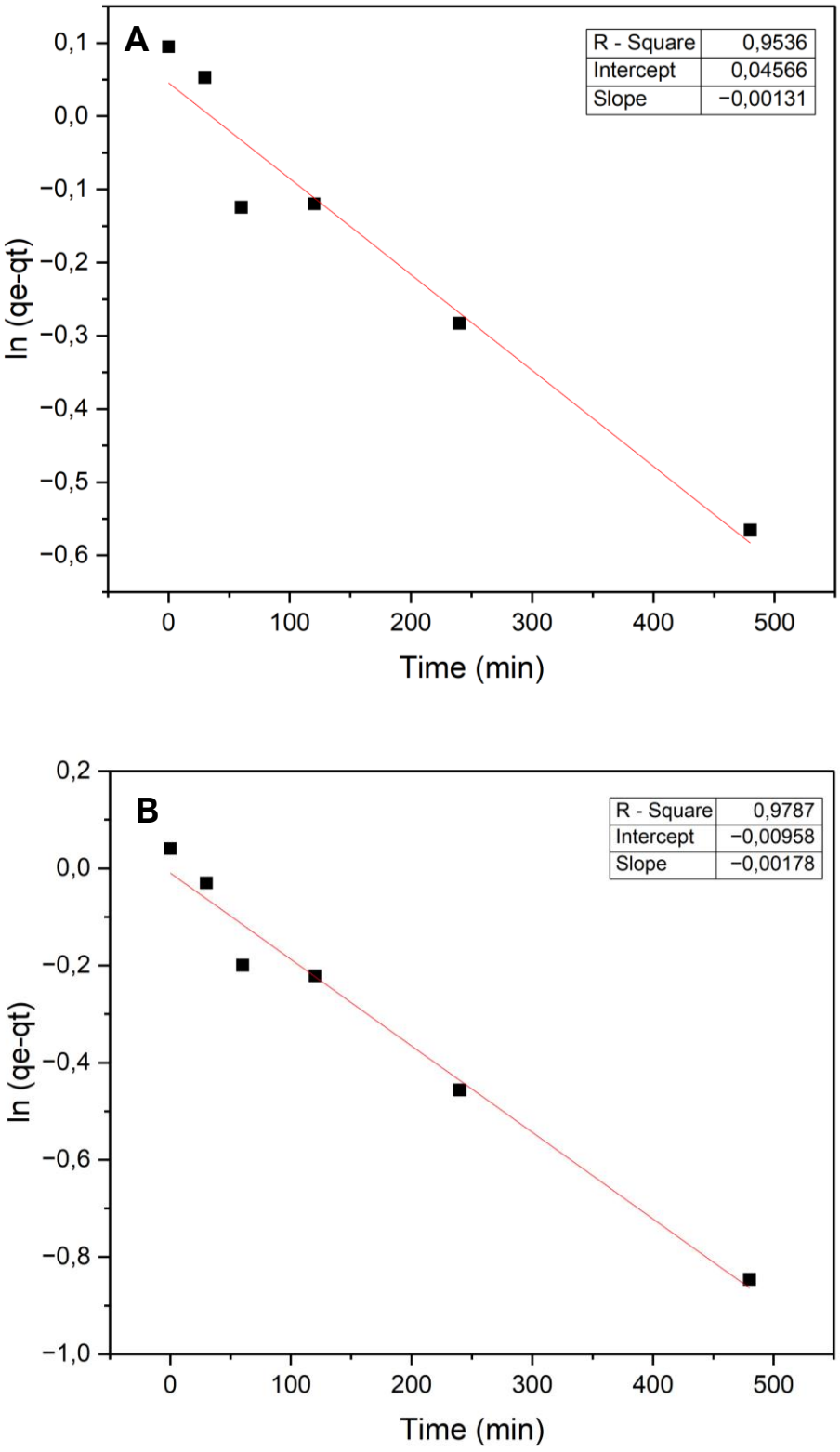

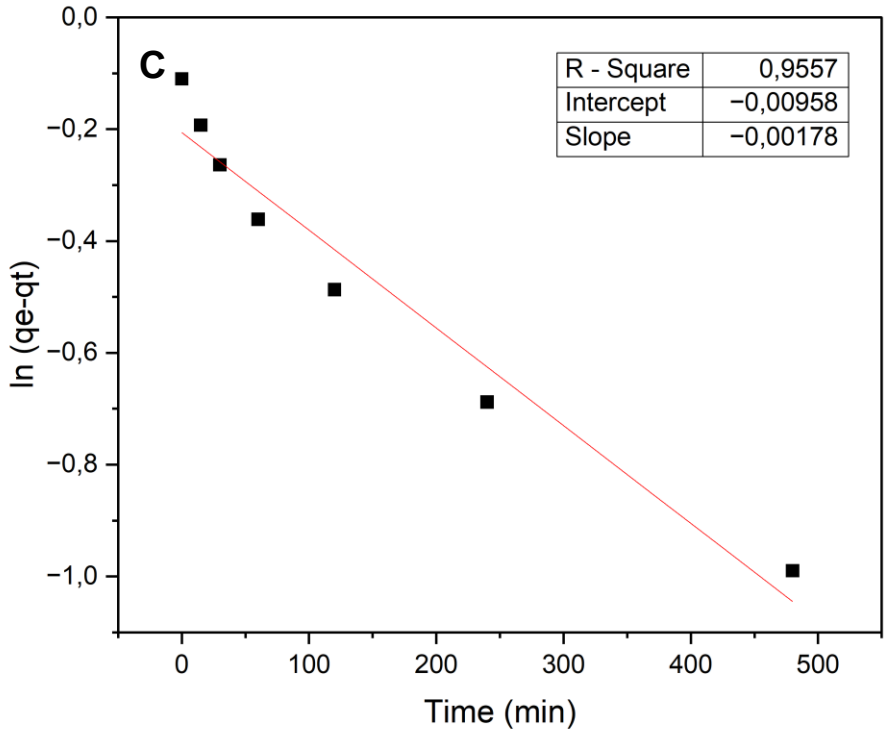

Source: The author.
Legend: Pseudo-first order plots for the adsorption of Cd(II) (V = 100 mL, C_o = 5.0 mg . L^{-1}) at 25 ºC and pH 5.5 (A), pH 6.5 (B) and pH 7.0 (C) onto chitosan microspheres cross-linked with sodium tripolyphosphate.

Figure 29 – Pseudo-second order plots for the adsorption of Cd(II) (C_o = 0.1mg . L^{-1}) onto chitosan microspheres cross-linked with sodium tripolyphosphate

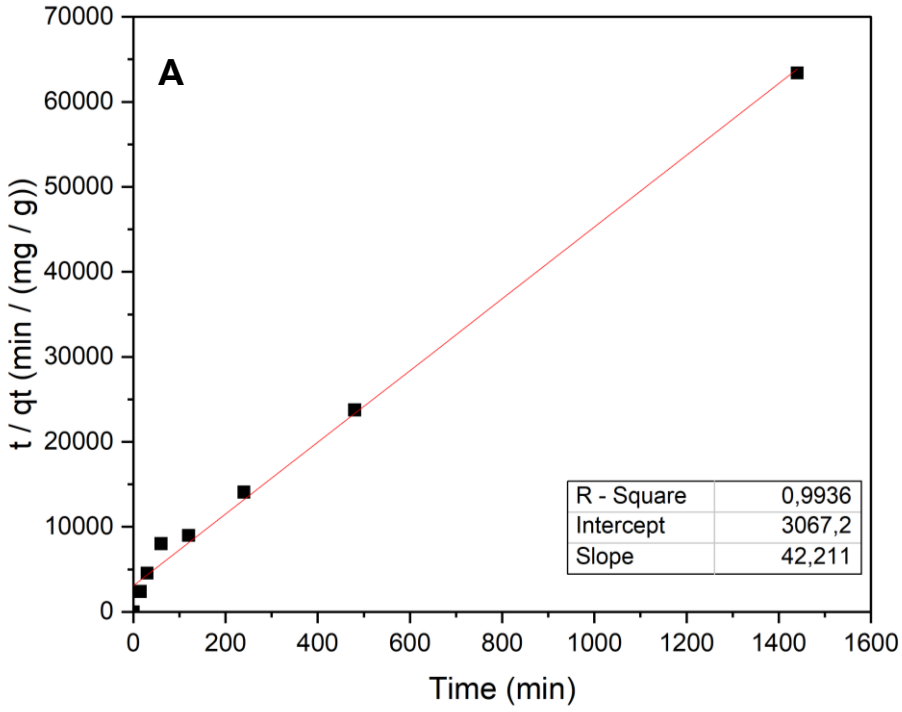

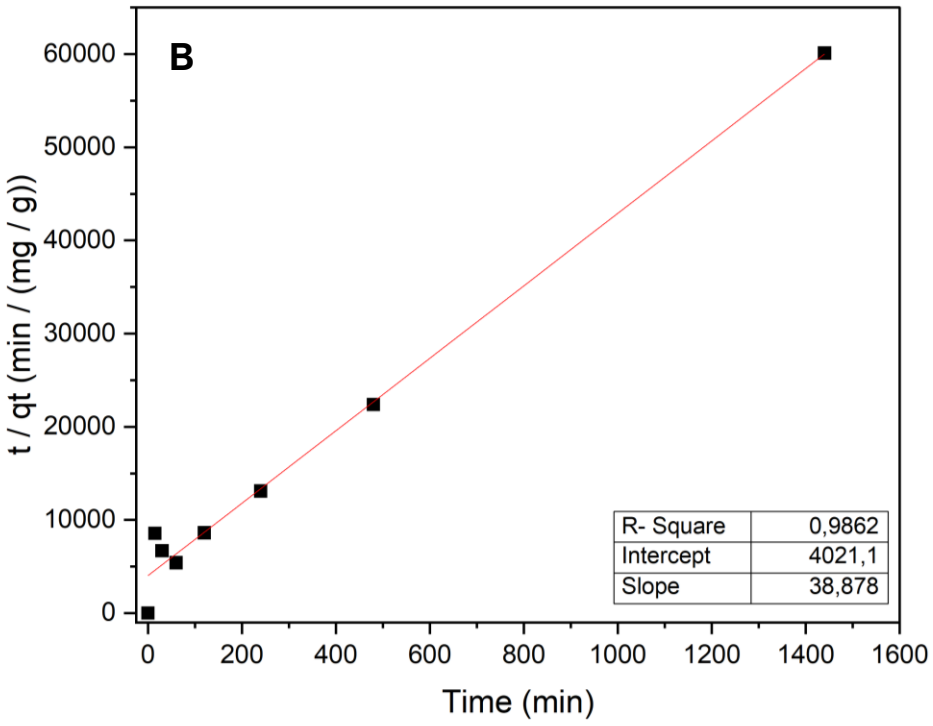

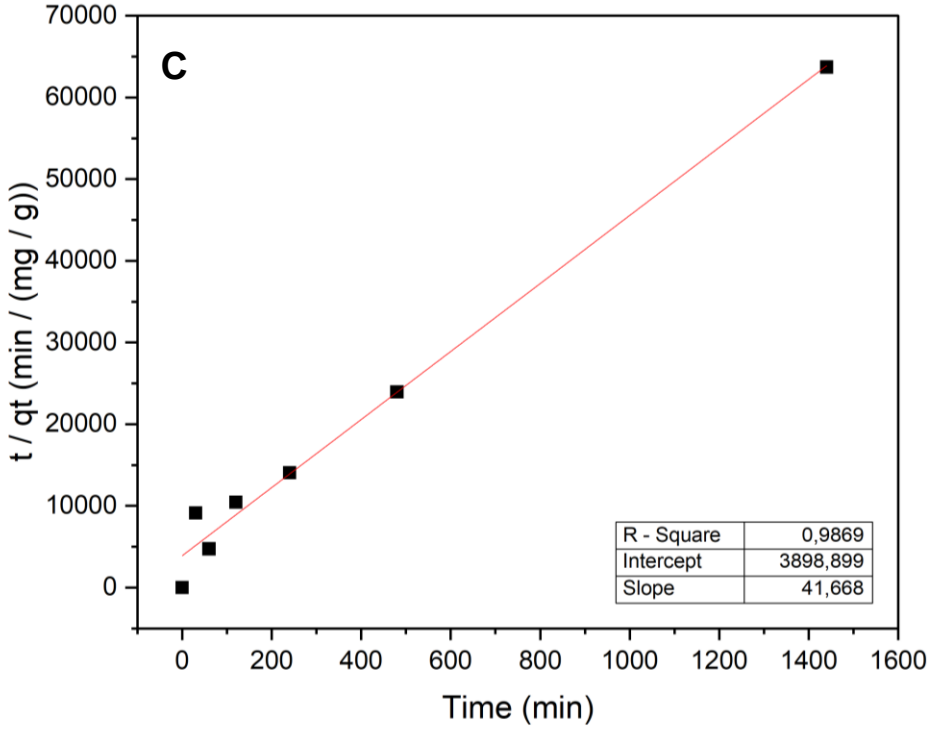

Source: The author.

Legend: Pseudo-second order plots for the adsorption of Cd(II) (V = 100 mL, C_o = 0.1 mg . L^{-1}) at 25 ^{o} C and pH 5.5 (A), pH 6.5 (B) and pH 7.0 (C) onto chitosan microspheres cross-linked with sodium tripolyphosphate.

Figure 30 – Pseudo-second order plots for the adsorption of Cd(II) (C_o = 0.2 mg . L^{-1}) onto chitosan microspheres cross-linked with sodium tripolyphosphate

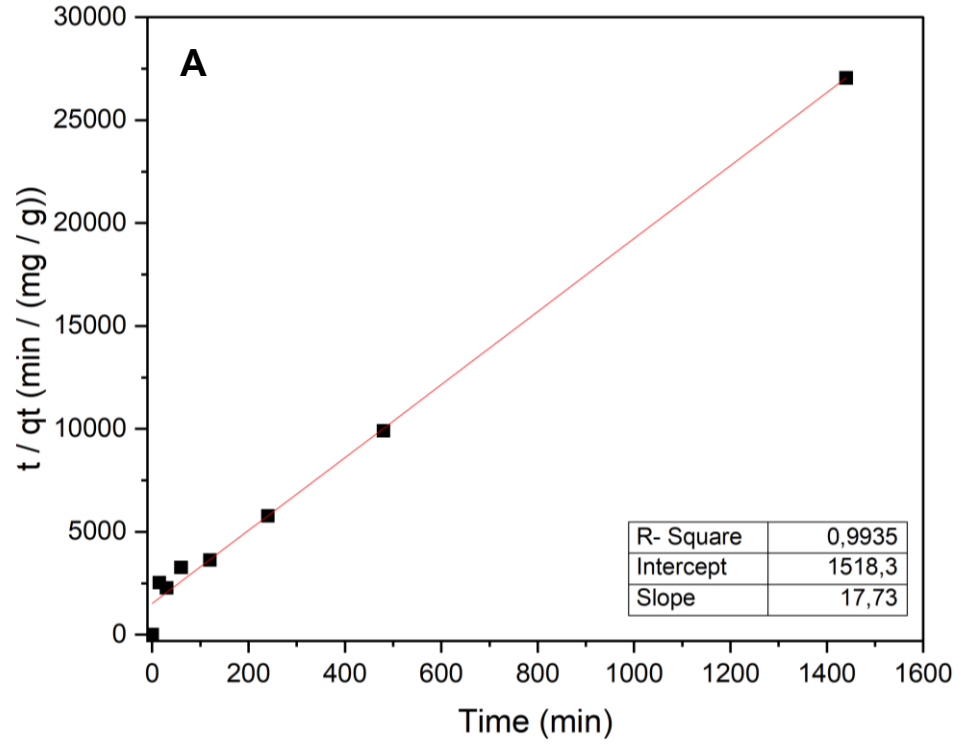

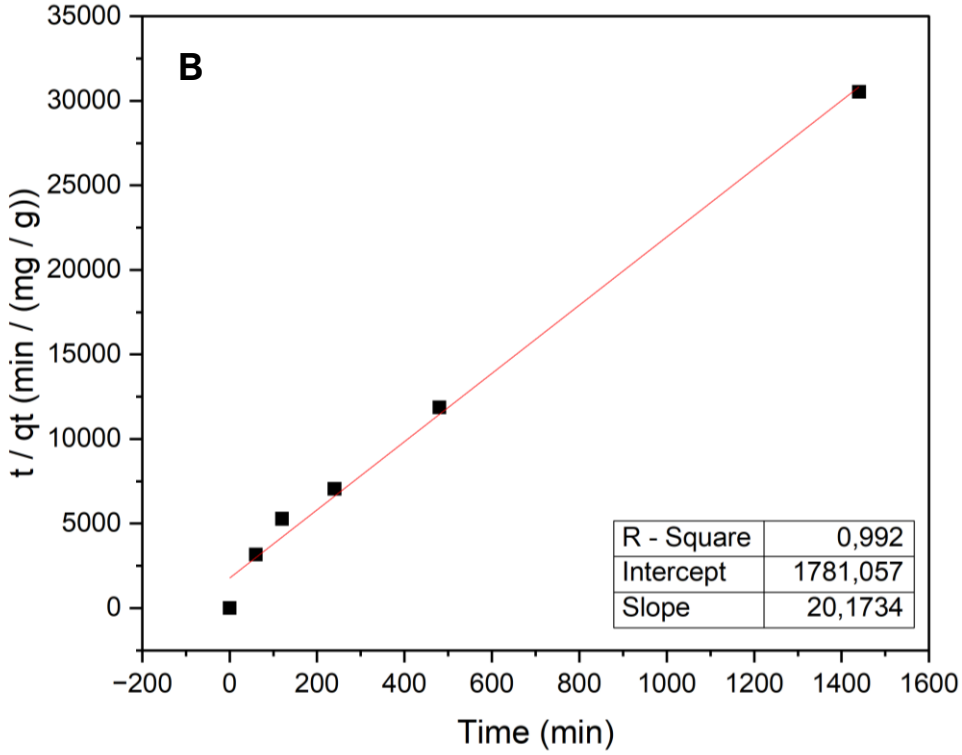

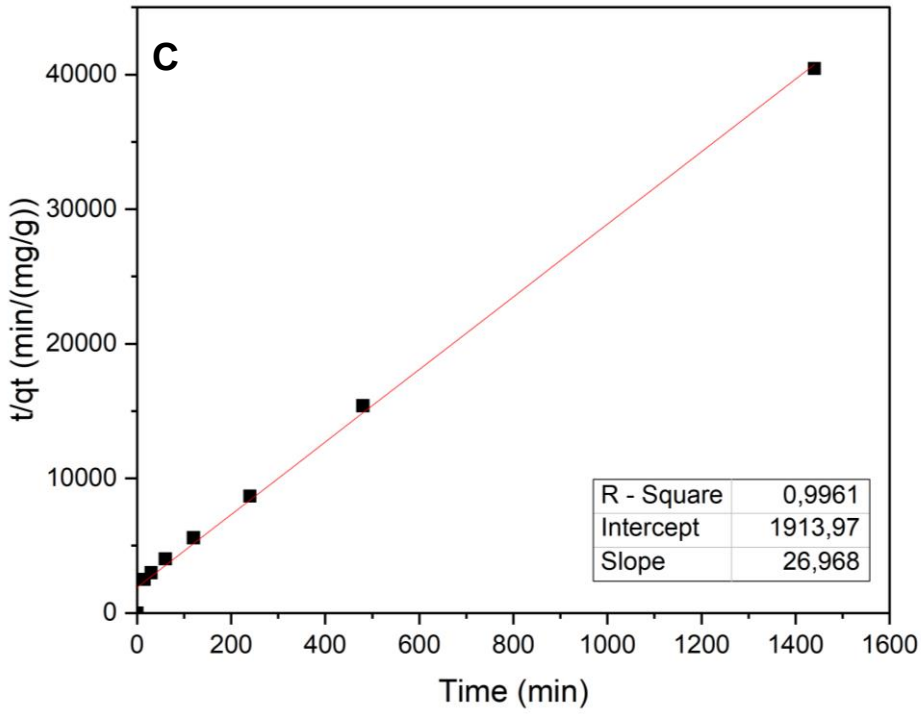

Source: The author.

Legend: Pseudo-second order plots for the adsorption of Cd(II) (V = 100 mL, C_o = 0.2 mg . L^{-1}) at 25 ^oC and pH 5.5 (A), pH 6.5 (B) and pH 7.0 (C) onto chitosan microspheres cross-linked with sodium tripolyphosphate.

Figure 31 – Pseudo-second order plots for the adsorption of Cd(II) (C_o = 5.0 mg . L^{-1}) onto chitosan microspheres cross-linked with sodium tripolyphosphate

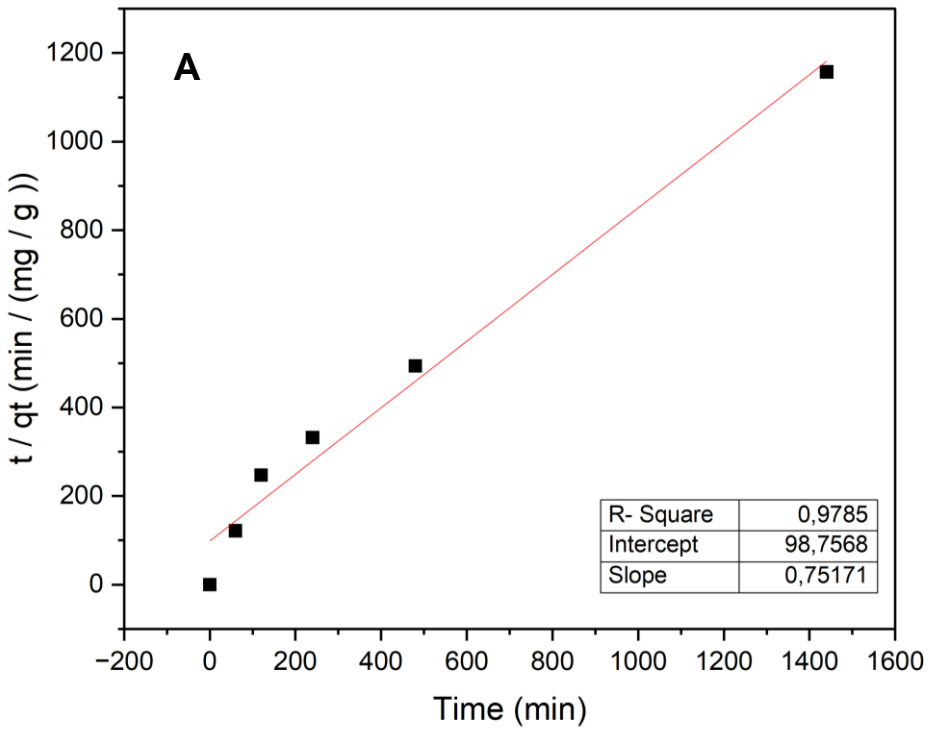

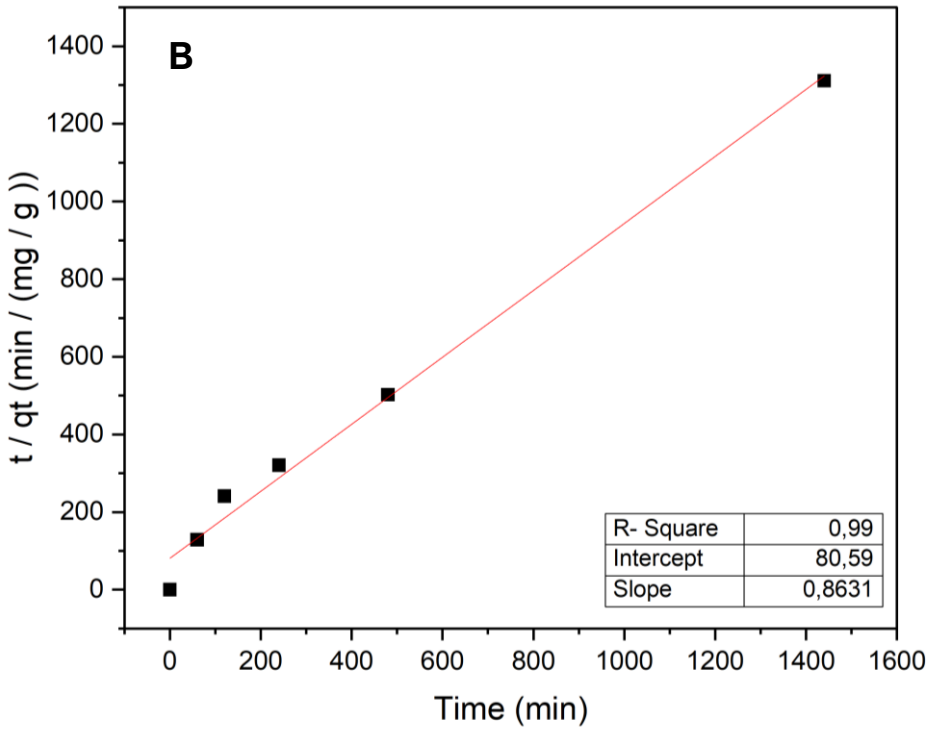

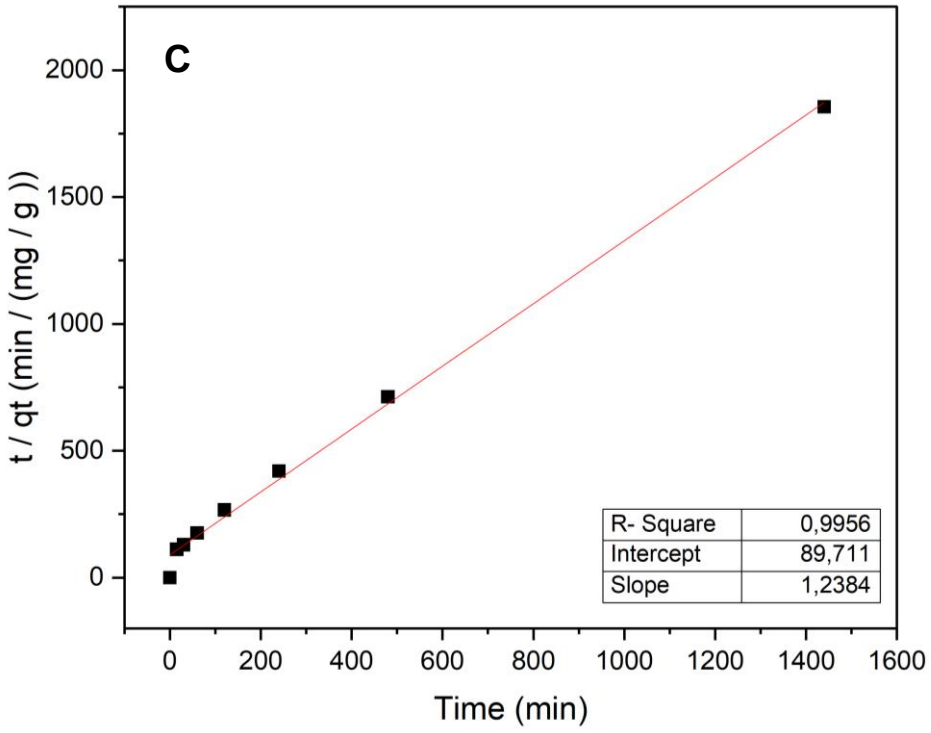

Source: The author.

Legend: Pseudo-second order plots for the adsorption of Cd(II) (V = 100 mL, C_o = 5.0 mg . L^{-1}) at 25 ^oC and pH 5.5 (A), pH 6.5 (B) and pH 7.0 (C) onto chitosan microspheres cross-linked with sodium tripolyphosphate.

Table 10 – Pseudo-first and pseudo-second order equation constants and R^2 for the adsorption of Cd(II) onto chitosan microspheres cross-linked with sodium tripolyphosphate

C_0	pH	Intercept	Slope	R^2	k_1 (min^{-1})	q_e ($mg\ g^{-1}$)	q_{exp} ($mg\ g^{-1}$)
Pseudo-first order model							
0.1	5.5	-1.7302	-0.0019	0.9714	-1.32E-06	0.1772	0.0227
	6.5	-1.6866	-0.0020	0.9599	-1.40E-06	0.1851	0.0239
	7.0	-1.6666	-0.0020	0.9706	-1.43E-06	0.1888	0.0226
0.2	5.5	-1.3350	-0.0021	0.9715	-1.51E-06	0.2631	0.0532
	6.5	-1.3538	-0.0018	0.9535	-1.27E-06	0.2582	0.0472
	7.0	-1.1440	-0.0018	0.9429	-1.28E-06	0.2608	0.0355
5.0	5.5	0.04566	-0.0013	0.9536	-9.09E-07	1.0467	1.2586
	6.5	-0.0095	-0.0018	0.9786	-1,23E-06	0.9904	1.1503
	7.0	-0.2059	-0.0017	0.9557	-1,21E-06	0.8138	0.7871
Pseudo-second order model							
C_0	pH	Intercept	Slope	R^2	k_2 ($g\ mg^{-1}\ min^{-1}$)	q_e ($mg\ g^{-1}$)	q_{exp} ($mg\ g^{-1}$)
0.1	5.5	3067.2	42.211	0.9936	6.06E-01	0.02369	0.0227
	6.5	4021.1	38.878	0.9862	4.03E-01	0.02572	0.0239
	7.0	3898.9	41.668	0.9869	4.72E-01	0.02400	0.0226
0.2	5.5	1518.3	17.730	0.9935	2.19E-01	0.0564	0.0532
	6.5	1781,0	20.173	0.9920	2.40E-01	0.0495	0.0472
	7.0	1913.9	26.969	0.9961	3.95E-01	0.0370	0.0355
5.0	5.5	98.756	0.7517	0.9785	6.05E-03	1.3303	1.2586
	6.5	80.590	0.8631	0.9900	9.75E-03	1.1586	1.1503
	7.0	89.711	1.2384	0.9956	1.75E-02	0.8074	0.7871

Source: The author

According to Table 10, the R^2 values for PSFO kinetics for initial concentration of 0.1, 0.2 and 5.0 mg . L^{-1} at pH 5.5 are 0.9714, 0.9715 and 0.9536, at pH 6.5 are 0.9599, 0.9535 and 0.9786, at pH 7.0 are 0.9706, 09429 and 0.9557. And R^2 values for PSSO kinetics for initial concentration of 0.1, 0.2 and 5.0 mg L^{-1} at pH 5.5 are 0.9936, 0.9935 and 0.9785, at pH 6.5 are 0.9862, 0.9920 and 0.9900, at pH 7.0 are 0.9869, 09961 and 0.9956. Based on these results it is possible to conclude that both kinetic models obtained high values of R^2, however the experimental data had more accurate fit with PSSO model. Furthermore, theoretical values of q_e ($mg\ g^{-1}$) obtained with the PSSO model were compared with the experimental data and result of this evaluation showed that there is no statistically significant difference ($p = 0.05$) between them. The results exposed suggest that the adsorption process of Cd(II) onto CTS–TPP is controlled by the PSSO model,

therefore, the rate-controlling step involves chemisorption or chemical adsorption. This type of sorption, in turn is well supported by the Langmuir isotherm. According to Gautam et al. (2014), normally the chemisorption step (when exchange of electrons takes place between adsorbent-adsorbate by complexation or coordination) is the rate limiting step in the metal ion and CTS adsorption process. In this sense, PSSO takes these valency forces into account which makes this model better than PSFO (UPADHYAY et al., 2021). Table 11 shows some studies that applied chitosan in different chemical configurations to remove metals from water and soil that presented the best fit for the Langmuir isotherm and PSSO kinetic model.

Table 11 – Application of chitosan for metal removal from water and soil

Adsorbent	Adsorbate	Isotherm best fit	Kinetic	Ref.
Cd(II)-imprinted chitosan hydrogel beads TPP crosslinked	Cd(II)	Langmuir	PSSO	Babakhani and Sartaj, 2022
Chitosan-Fe3O4-Modified Fish Bone Char	Cd(II)	Langmuir	PSSO	Yang et al., 2022
Chitosan-Kiwi branch biochar	Cd(II)	Langmuir	PSSO	Yuehui et al., 2022
Electrospun chitosan/polyvinyl alcohol-aminated halloysite nanotubes membranes	Cd(II), Pb(II)	Langmuir	PSSO	Shirazi et al., 2022
Cellulose/chitosan spheres loaded with zero-valent iron	Cd(II)	Langmuir	PSSO	Li et al., 2022
Chitosan/Al_2O_3/Fe_3O_4 nanocomposite	Cd(II), Cu(II), Zn(II)	Langmuir	PSSO	Karimi et al., 2021
N-carboxymethylchitosan hydrogel	Pb(II), Cu(II), Cd(II)	Langmuir	PSSO	Hao and Liang, 2022
Meso-2-3-dimercaptosuccinic acid chitosan beads	Cd(II), Pb(II), Cu(II)	Langmuir	PSSO	Yang et al., 2021b
Functionalized graphene oxide-silica with chitosan	Cd(II)	Langmuir	PSSO	Azizkhani et al., 2021

Source: The author

The values of k_2 and q_e decrease and increase, respectively, with increasing initial concentration. The decrease in k_2 values as the initial concentration increases indicates that there are more Cd(II) ions present in solution and they compete with each other and induce a delay in the attainment of equilibrium and, thus, lower k_2 values are obtained (DEBNATH; GHOSH, 2008; LIU; LEAD; ZHANG, 2013a). Regarding pH, the highest values of k_2 for initial concentration of 0.1, 0.2 and 5.0 mg L^{-1} were, respectively, 4.72E-01, 3.95E-01 and 1.75E-02 g mg^{-1} min^{-1} at pH 7.0. According to Table 8, the removal rate (%) at 60 minutes was higher for all initial concentrations at pH 7.0, therefore, these data corroborate the k_2 values found for this pH.

Regarding the q_e parameter, the initial concentration of 0.2 and 5.0 mg L^{-1} obtained the highest values, respectively, 5.64E-02 and 1.33 mg g^{-1} at pH 5.5. On the other hand, for initial concentration of 0.1 mg L^{-1} the highest q_e value (2.57 E-02 mg g^{-1}) was obtained at pH 6.5. Thus, based on the data presented and discussed so far, it is clear that the entire pH range applied in this work for the removal of Cd(II) ions by CTS–TPP obtained good results.

4.3.4. ADSORPTION EQUILIBRIUM STUDY

Equilibrium isotherm studies can offer important information about the interactive behaviors between the adsorbate and adsorbent while the two phases are reaching the equilibrium state (SUTIRMAN et al., 2018). In addition, these studies provide information on the properties of adsorbents such as the distribution of available adsorption sites on their surface and their capacities (BONILLA-PETRICIOLET; MENDOZA-CASTILLO; REYNEL-ÀVILA, 2017). In this study, the adsorption isotherm experiments were conducted using initial concentration of 0.1 to 8 mg L^{-1} Cd(II), pH range of 5.5–7.0 ± 0.1, 0.5 g adsorbent dosage at 25 ± 1 ^oC and equilibrium was considered reached at 1440 min due to the small variation in value between the penultimate (480 min) and the last contact point. The experimental data were analyzed by applying the linearized form Langmuir and Freundlich isotherm models, as they offered a better fit compared to the non-linearized form.

Freundlich model gives an expression which defines the exponential distribution of active sites and their energies on the adsorbent surface, supports the

heterogeneous interaction between sorbate and sorbent and also predicts non-monolayer coverage (RAO et al., 2009). On the other hand, the Langmuir isotherm model assumes that the maximum adsorption occurs when a saturated monolayer of adsorbate is formed on the adsorbent surface (SUTIRMAN et al., 2018). This monolayer occurs when the adsorbate is chemically adsorbed at a fixed number of specific active sites on the adsorbent surface that are energetically equivalent and identical and there is no migration of adsorbate molecules in the surface plane (LAUS et al., 2010). After fitting the isotherm models to experimental data (Figures 32, 33), the adsorption isotherm parameters and their correlation coefficients (R^2) were calculated and listed in Table 12.

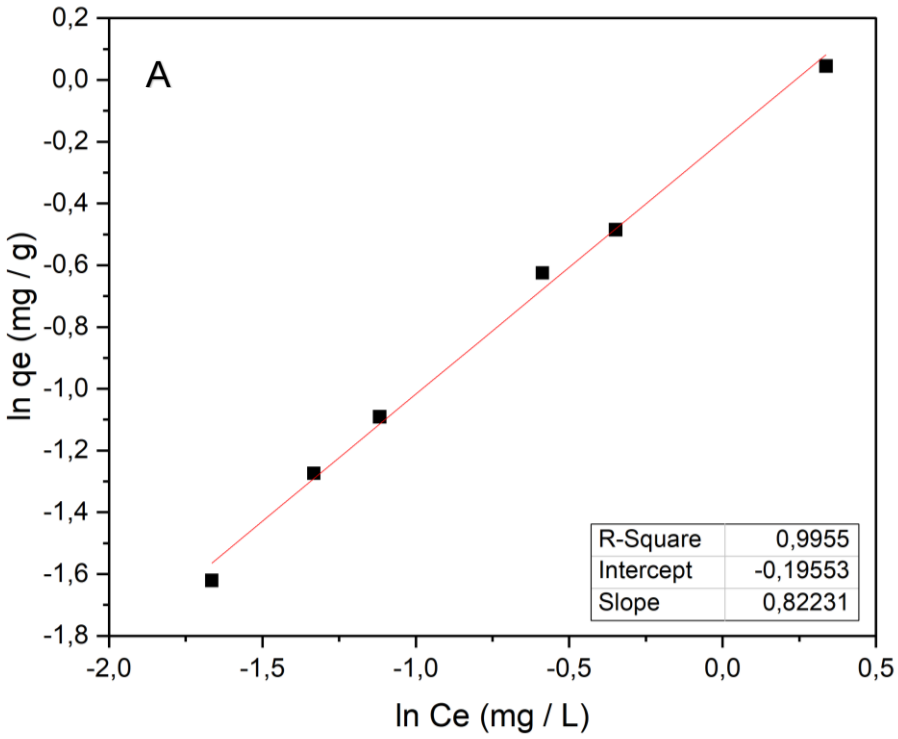

Figure 32 – Freundlich plots of Cd(II) on chitosan microspheres cross-linked with sodium tripolyphosphate at various pHs

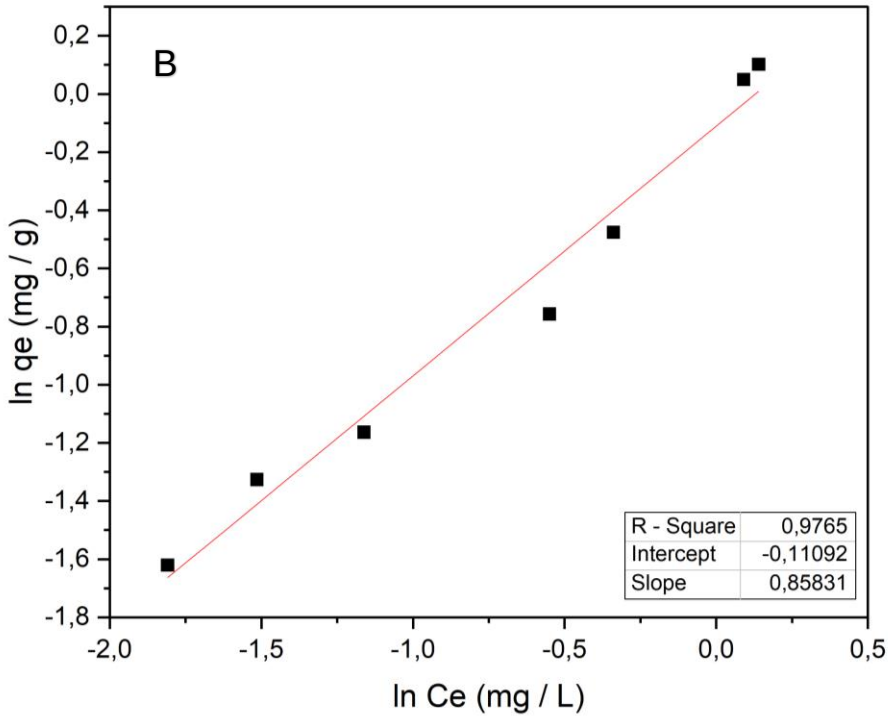

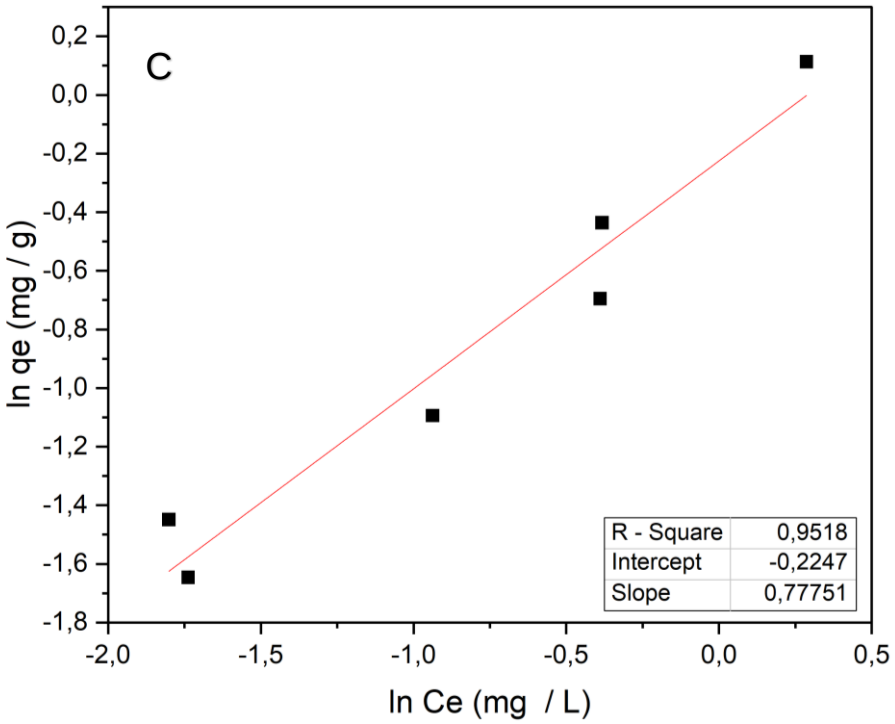

Source: The author

Legend: Freundlich plots (C_o from 0.1 to 8 mg L^{-1} Cd(II), 0.5 g adsorbent dosage, at pH 5.5 (A), 6.5 (B) and 7.0 (C) and 25 ± 1 ^oC).

Figure 33 – Langmuir plots of Cd(II) on chitosan microspheres cross-linked with sodium tripolyphosphate at various pHs

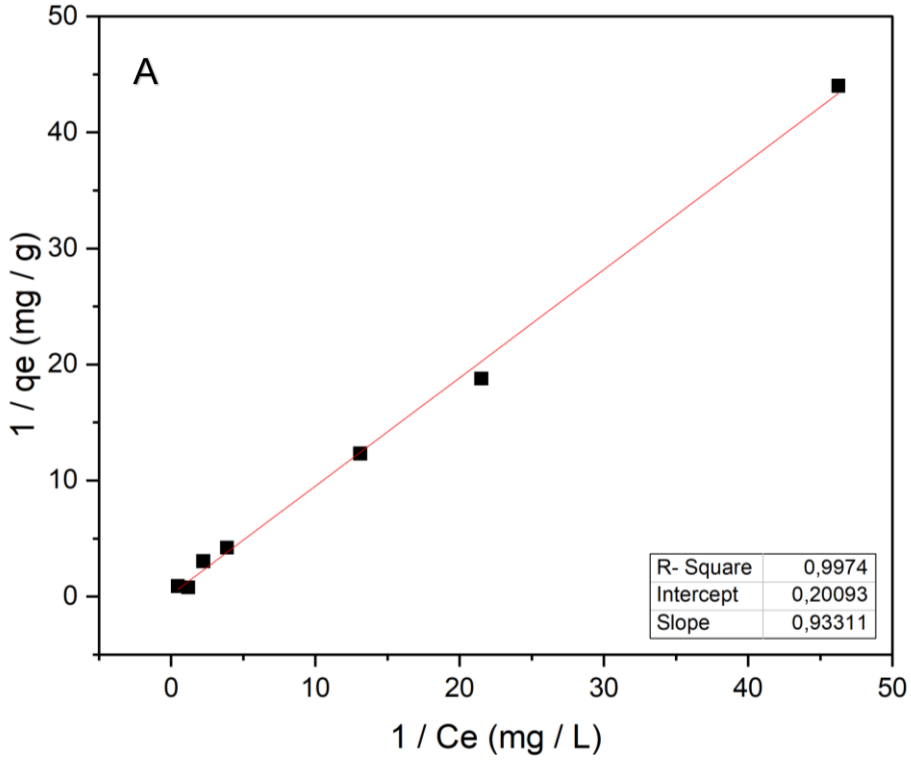

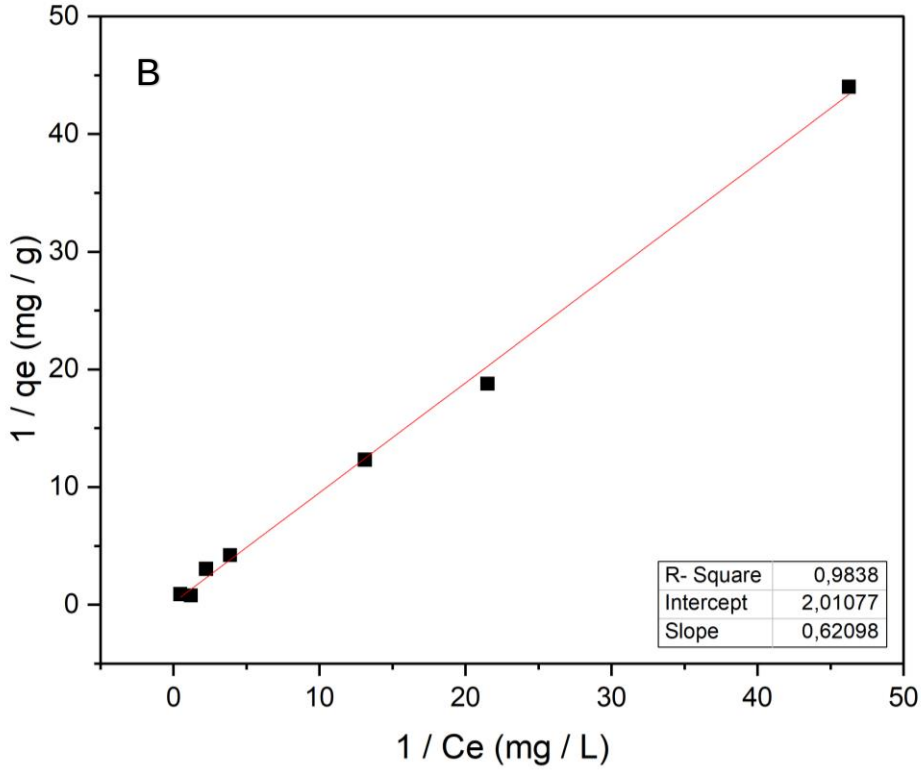

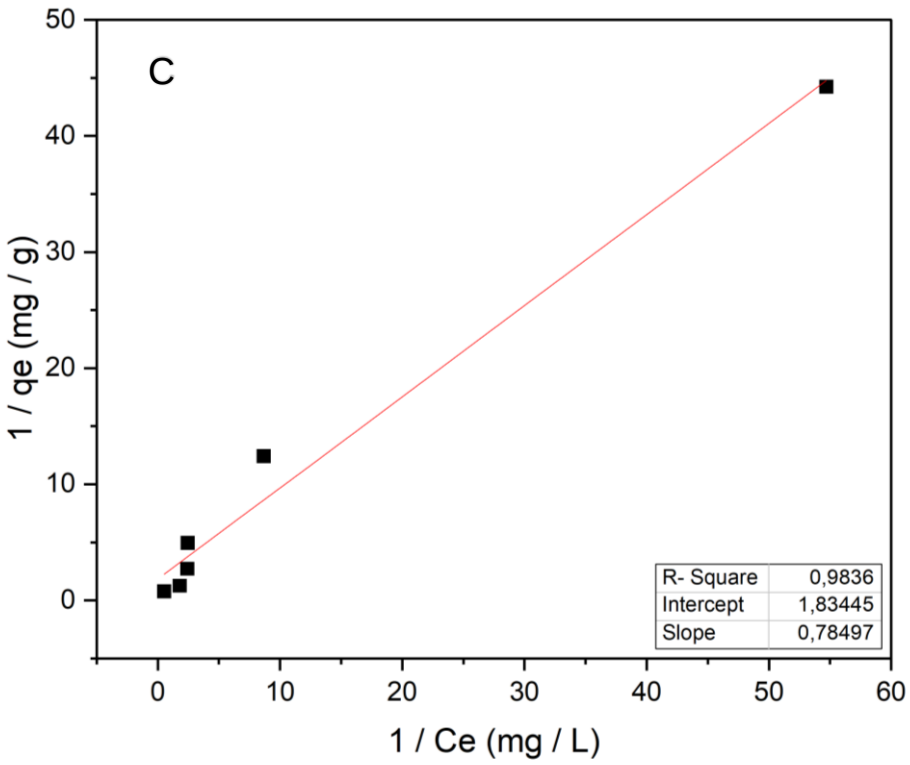

Source: The author

Legend: Langmuir plots (C_o from 0.1 to 8 mg L^{-1} Cd(II), 0.5 g adsorbent dosage, at pH 5.5 (A), 6.5 (B) and 7.0 (C) and 25 ± 1 °C).

Table 12 – Parameters for the Langmuir and Freundlich isotherm models in different pH ranges

(continued)

Adsorption isotherm	pH	Isotherm parameters	Values
Langmuir	5.5	K_L (L . mg^{-1})	4,6440
		q_m (mg . g^{-1})	1.0717
		R_L	0.0271 – 0.6143
		R^2	0.9974
	6.5	K_L (L . mg^{-1})	0.3088
		q_m (mg . g^{-1})	1.6104
		R_L	0.2958 – 0.9599
		R^2	0.9838
	7.0	K_L (L . mg^{-1})	0.3918
		q_m (mg . g^{-1})	1.2739
		R_L	0.2172 – 0.9468
		R^2	0.9836
Freundlich	5.5	K_F (mg . g^{-1}) (L . mg) $^{(1/n)}$	0.6375
		n	1.2161
		R^2	0.9955
	6.5	K_F (mg . g^{-1}) (L . mg) $^{(1/n)}$	0.7746
		n	1.1651
		R^2	0.9765
	7.0	K_F (mg . g^{-1}) (L . mg) $^{(1/n)}$	0.5961

n	1.2862
R^2	0.9518

Source: The author

According to Table 12, based on R^2 values, it is possible to verify that the Langmuir model predicts experimental data of CTS–TPP over all Cd(II) concentrations and pH range studied better than the Freundlich model. Similar results have been reported in the literature (BABAKHANI; SARTAJ, 2020; IGBERASE; OSIFO, 2015; KUCZAJOWSKA-ZADROŻNA; FILIPKOWSKA; JÓŹWIAK, 2020; LAUS et al., 2010) for Langmuir and Freundlich models. Thus, based on these results, it is possible to conclude that the surface of the CTS–TPP was homogeneous and its sites had equivalent energy and were evenly distributed throughout the adsorbent (BABAKHANI; SARTAJ, 2020). Following the Langmuir model, the values of q_m and K_L were obtained from the slope and intercept of (1 / q_e) vs. (1 / C_e) plot, respectively. According to Table 12, the highest value of q_m (1.61 mg g^{-1}), which is the maximum amount of Cd(II) per unit mass of CTS–TPP to form a complete monolayer on the adsorbent surface, was obtained at pH 6.5 and 25 °C. A similar result can be observed in the work by Hasan et al. (2006) . The lowest value of q_m was obtained at pH 5.5 (1.07 mg g^{-1}). The Langmuir constant K_L corresponds to the initial slope of the isotherm curve, and a high value of this constant suggests a high affinity of the adsorbent for the adsorbate (GUIBAL, 2004). Although the highest value of q_m was obtained at pH 6.5, the highest affinity for Cd(II) ions (K_L) was found at pH 5.5 (4.64 L mg^{-1}).

The separation factor (R_L) (dimensionless constant) which is used to predict whether an adsorptive system is favorable or not, and it was obtained following the Equation 7:

$$R_L = \frac{1}{1 + K_L C_0} \tag{7}$$

where the value of R_L indicates the type of Langmuir isotherm to be irreversible ($R_L = 0$), linear ($R_L = 1$), unfavorable ($R_L > 1$), or favorable ($0 < R_L < 1$). The R_L values between 0 and 1 indicate favorable adsorption.

All R_L values obtained in the present investigation were between 0 and 1, indicating, thus, favorable adsorption of the Cd(II) onto CTS–TPP for all pH ranges

at different initial concentrations, as shown in Table 12. This result gives further support to the point that the equilibrium isotherm can be well described by the Langmuir isotherm model.

4.3.5. Competition effect

The average content of total organic carbon used at pH 6.5 to perform this analysis was 10.8 ± 0.5 mg L^{-1}. The rate of Cd(II) adsorbed by CTS–TPP in presence of NOM is shown in Figure 34. At pH 6.5, as it is possible to note that the initial concentration of Cd(II) before the start of the experiment was already extremely low (1.2 E-02 mg L^{-1})

Figure 34 – Rate of Cd(II) adsorbed by chitosan microspheres cross-linked with sodium tripolyphosphate at various pHs in presence of natural organic matter

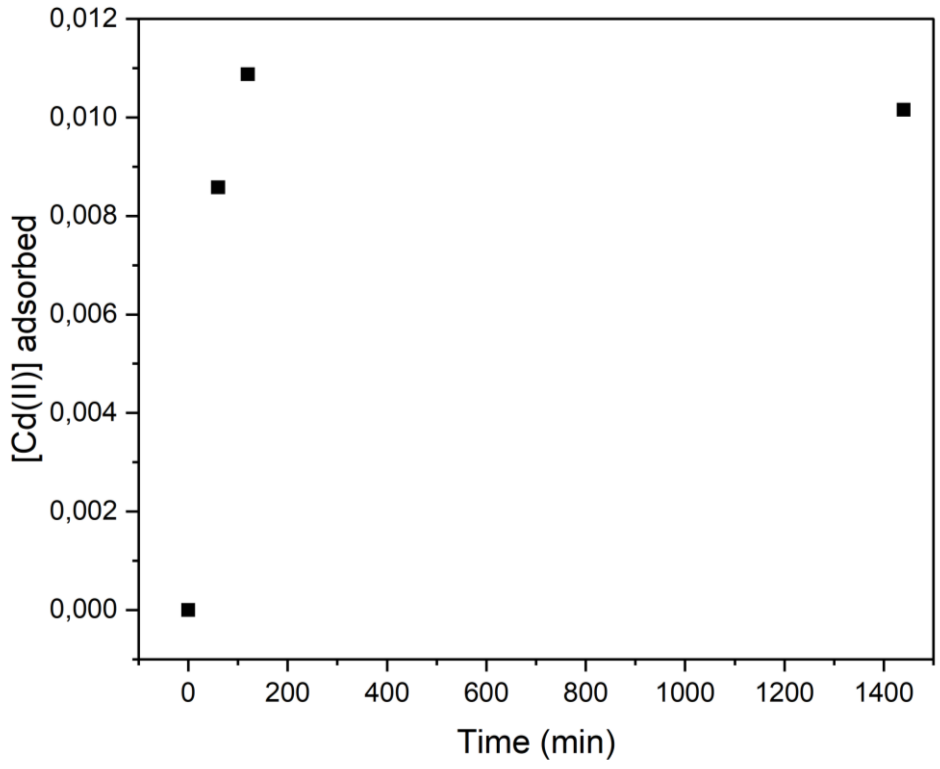

Source: The author

Legend: Plot for the adsorption of Cd(II) in presence of natural organic matter (V = 100 mL, $[Cd(II)]_0$ = 0.2 mg . L^{-1}, $[NOM]_0$ = 10 mg . L^{-1}) at 25 ^oC and pH 6.5 onto 0.5 g of chitosan microspheres cross-linked with sodium tripolyphosphate.

This can be explained by the fact that the Cd(II) and NOM ions remained in contact for about 1 hour until the working solution had its parameters properly

adjusted and finally the CTS spheres were added. Most likely the Cd(II) ions were adsorbed by NOM and the concentration of these ions in solution was reduced to only 6% of the initial concentration used (0.2 mg . L^{-1}). At pH 6.5, NOM have negative ζ potential and this can be attributed to the dissociation of carboxylic (–COOH) and phenolic groups (–OH) (LU; SU, 2007). Thus, an complexation between NOM and Cd(II) ions can be expected due to their opposite ζ potentials at this pH (YAN; BAI, 2005), as shown in Figure 35:

Figure 35 – Cd(II) ion adsorption mechanism on natural organic matter

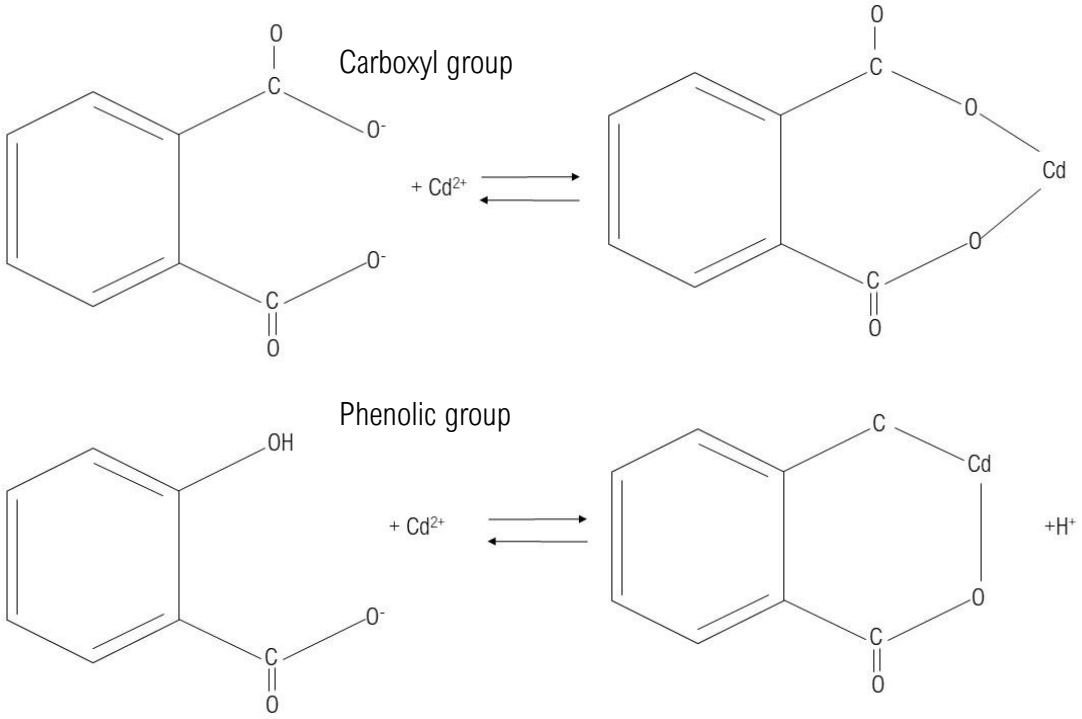

Source: Adapted from Yan and Bai (2005).

However, after the introduction of CTS–TPP in this solution, the beads were able to adsorb about 85% of the Cd(II) concentration that still remained in solution. In comparative terms, the authors Yan and Bai (2005) in their work, prepared a solution containing humic acid (HA) ($[HA]_0$ = 25 mg L^{-1}) and Pb(II) ions ($[Pb^{2+}]_0$ = 15 mg L^{-1}) at pH 6.5 and 25 ºC. This solution was stirred for 1 hour to allow the interaction of HA and Pb(II) before CTS spheres were introduced (m = 2.0 g). Comparing with the control solution, which contained only CTS spheres and Pb(II) ions, they noticed that the concentration of lead ions adsorbed by the CTS spheres

was 90% lower when HA were previously added to the solution. They concluded that the prior presence of HA in the solution significantly affected the interaction of Pb(II) with CTS spheres. If we compare the concentrations of NOM and metal ions applied by Yan and Bai (2005) in their experiment with the concentrations applied in the present work, it can be concluded that, under pH 6.5, there were probably favorable conditions for most of the Cd(II) ions present in the solution to coordinate with the active sites of NOM, even in the presence of CTS–TPP. In other words, there was no major migration of Cd(II) from NOM to CTS–TPP. This fact can be corroborated if we compared the values of Cd(II) ions in solution with CTS–TPP in the absence and presence of NOM. This result suggest that the Cd(II) ions complexed in a stable way with NOM's actives sites and, therefore, less chemical groups were disponible to coordinate with CTS–TPP (YAN; BAI, 2005). Based on the FT–IR characterization discussed above, it is possible to notice that amine groups of CTS–TPP were used to coordinate with the active sites of an adsorbate. Figure 36 shows the interaction between CTS amine groups and NOM.

Figure 36 – Mechanism of adsorption of natural organic matter onto chitosan microspheres cross-linked with sodium tripolyphosphate

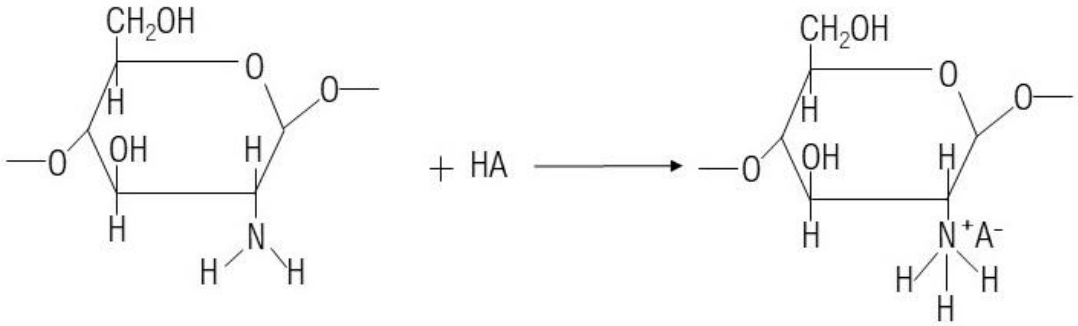

Source: Yan and Bai (2005)

Legend: HA: represents humic acid, and A^- represents R–COO^- or R′–O^-

In this work, the mainly adsorbate sorbed by the spheres was probably represented by NOM that functioned as a "bridge" between Cd(II) and CTS–TPP ions (RANGEL-MENDEZ et al., 2009). However, the CTS–TPP coordination sites were also used directly by Cd(II) ions. The main possible combinations of interaction between CTS–TPP, NOM and Cd(II) in solution are shown in Figure 37:

Figure 37 – Possible interactions between chitosan microspheres cross-linked with sodium tripolyphosphate, natural organic matter and Cd(II) ions in solution

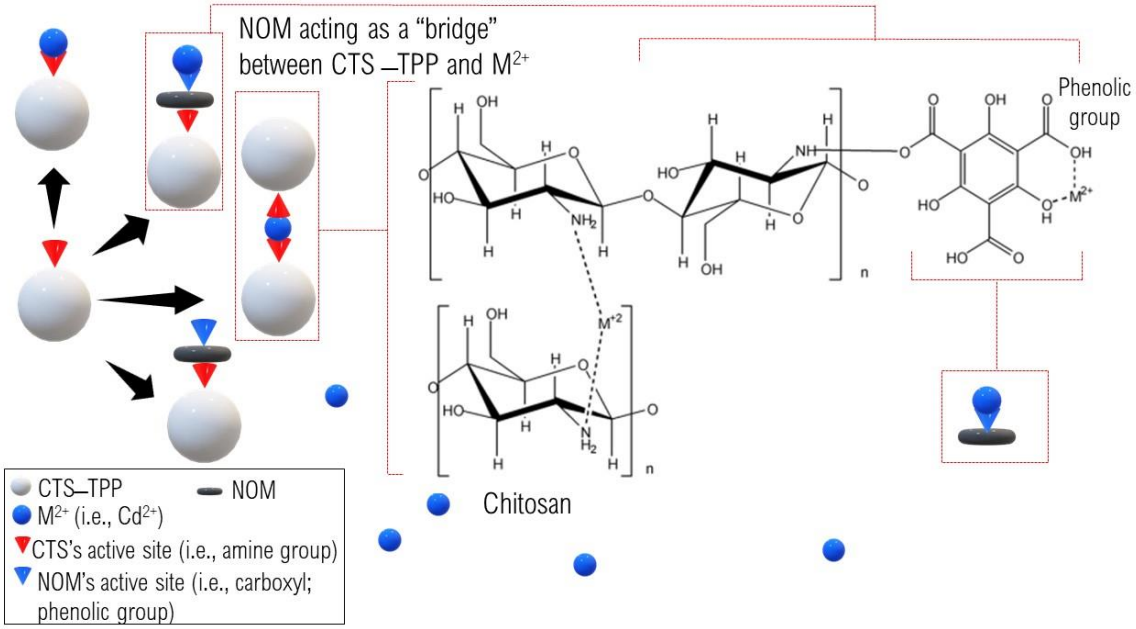

Source: Adapted from Rangel – Mendez et al. (2009).

5. CONCLUSIONS

The CTS–TPP formed by ionic gelation presented a pearly white color, however, after contact with NOM, they obtained a yellow-brown color. This color change proves the adhesion of organic matter to the surface of the spheres. XRD characterization of CTS powder and CTS-TPP before and after contact with Cd(II) revealed that the degree of crystallinity was reduced. The reduction in CTS crystallinity is probably due to the decrease in free amino and hydroxyl groups after the cross-linking process and adsorption of Cd(II) ions. The analysis of the morphology of the spheres with SEM revealed the existence of a large amount of pores regularly distributed over the surface, which probably led to the attainment of high rates of adsorption of Cd(II) ions by CTS–TPP. Through the analysis of the FT-IR spectra, it was possible to observe the incorporation of phosphate groups (from TPP) by the CTS spheres. This modification may also have favored the increase in the adsorption capacity of Cd(II) ions by CTS–TPP, since phosphate groups can interact with metals through different mechanisms (chelation and ion exchange / electrostatic attraction) depending on the pH of the solution. With the analysis of the IR spectra of CTS-TPP before and after contact with Cd(II) and NOM ions, it is very clear the role of the groups $–NH_2$, not only for the success of the cross-linking process, but also for the sorption of Cd(II) ions and / or NOM: The adsorbent used in this study showed good sorption rate (≈ 82%) in all pH ranges and initial concentrations in the absence of NOM. In the competition studies at pH 6.5, since Cd(II) ions and NOM were in previous contact before the CTS beads were added to the solution, about 94% of the Cd(II) ions were adsorbed by NOM, therefore, CTS – TPP suffers great interference from NOM when they are competing for Cd(II) ions. The remaining Cd(II) ions in solution were adsorbed at a rate of 85% by CTS–TPP. At pH 6.5, NOM has a negative ζ potential and this can be attributed to the dissociation of carboxylic (–COOH) and phenolic (–OH) groups. Thus, an complexation between NOM and Cd(II) ions can be expected at this pH and ionic strength. In the contact time studies, it was possible to notice that in the time of 120 min, the initial concentrations of 0.1 and 0.2 mg L^{-1} obtained a Cd(II) removal rate of 50%. However, for the concentration of 5.0 mg L^{-1}, it is possible to observe a slower kinetic process, probably due to the saturation of the surface sites of CTS–TPP. The kinetics of Cd(II) showed two very distinct phases; the first being quite fast

and the second being slower. For the kinetic study, PSFO and PSSO models were applied to the experimental data and the pseudo-second-order kinetics better described the adsorptive process. The study of the adsorption equilibrium was carried out through the non-linear models of Langmuir and Freundlich. The equilibrium data fitted better to the Langmuir model (R2 of 0.98 – 0.99) in the studied pH range. The maximum adsorption capacity achieved by CTS – TPP was 1.61 mg. g^{-1} at pH 6.5. In general, CTS – TPP showed to be very promising in removing Cd(II) ions from aqueous media at different initial concentrations and pH range without the presence of NOM.

REFERENCES

ALFURAYDI, R. T.; ALMINDEREJ, F. M.; MOHAMED, N. A. Evaluation of Antimicrobial and Anti-Biofilm Formation Activities of Novel Poly(vinyl alcohol) Hydrogels Reinforced with Crosslinked Chitosan and Silver Nano-Particles. **Polymers**, v. 14, n. 8, p. 1619, 16 abr. 2022.

ALI, M. M. et al. Environmental Pollution with Heavy Metals: A public health concern. In: **In Heavy Metals-Their Environmental Impacts and Mitigation**. [s.l.] IntechOpen, 2021.

AHMADI, M. et al. Synthesis of chitosan zero-valent iron nanoparticles-supported for cadmium removal: characterization, optimization and modeling approach. **Journal of Water Supply: Research and Technology - Aqua**, v. 66, n. 2, p. 116–130, 15 mar. 2017.

ANISIEI, A. et al. Imination of Microporous Chitosan Fibers—A Route to Biomaterials with “On Demand” Antimicrobial Activity and Biodegradation for Wound Dressings. **Pharmaceutics**, v. 14, n. 1, p. 117, 4 jan. 2022.

ARAÚJO, B. R. et al. Evaluation of the interactions between chitosan and humics in media for the controlled release of nitrogen fertilizer. **Journal of Environmental Management**, v. 190, p. 122–131, abr. 2017.

AZAROVA, YU. A.; PESTOV, A. V.; BRATSKAYA, S. YU. Application of chitosan and its derivatives for solid-phase extraction of metal and metalloid ions: a mini-review. **Cellulose**, v. 23, n. 4, p. 2273–2289, 17 ago. 2016.

AZIZKHANI, S. et al. Synthesis and application of functionalized Graphene oxide-silica with chitosan for removal of Cd (II) from aqueous solution. **Journal of Environmental Health Science and Engineering**, v. 19, n. 1, p. 491–502, 26 jun. 2021.

AZUMA, K. et al. Chitin, Chitosan, and Its Derivatives for Wound Healing: Old and New Materials. **Journal of Functional Biomaterials**, v. 6, n. 1, p. 104–142, 13 mar. 2015.

BABAKHANI, A.; SARTAJ, M. Synthesis, characterization, and performance evaluation of ion-imprinted crosslinked chitosan (with sodium tripolyphosphate) for cadmium biosorption. **Journal of Environmental Chemical Engineering**, v. 10, n. 2, p. 107147, abr. 2022.

BABAKHANI, A.; SARTAJ, M. Removal of Cadmium (II) from aqueous solution using tripolyphosphate cross-linked chitosan. **Journal of Environmental Chemical Engineering**, v. 8, n. 4, p. 103842, ago. 2020.

BAEYENS, W. et al. In situ measurements of micronutrient dynamics in open seawater show that complex dissociation rates may limit diatom growth. **Scientific Reports**, v. 8, n. 1, p. 16125, 31 dez. 2018.

BAKSHI, P. S. et al. Chitosan as an environment friendly biomaterial – a review on recent modifications and applications. **International Journal of Biological Macromolecules**, v. 150, p. 1072–1083, maio 2020.

BANSAL, V. et al. Applications of chitosan and chitosan derivatives in drug delivery. **Advances in Biological Research**, v. 5, n. 1, p. 28–37, 2011.

BASHIR, A. et al. Removal of heavy metal ions from aqueous system by ion-exchange and biosorption methods. **Environmental Chemistry Letters**, v. 17, n. 2, p. 729–754, 5 jun. 2019.

BERGER, J. et al. Structure and interactions in covalently and ionically crosslinked chitosan hydrogels for biomedical applications. **European Journal of Pharmaceutics and Biopharmaceutics**, v. 57, n. 1, p. 19–34, jan. 2004.

BILAL, M.; IQBAL, H. M. N. Naturally-derived biopolymers: Potential platforms for enzyme immobilization. **International Journal of Biological Macromolecules**, v. 130, p. 462–482, jun. 2019.

BILAL, M. et al. Biosorption: An Interplay between Marine Algae and Potentially Toxic Elements—A Review. **Marine Drugs**, v. 16, n. 2, p. 65, 19 fev. 2018.

BODAKOWSKA-BOCZNIEWICZ, J.; GARNCAREK, Z. Immobilization of Naringinase from Penicillium decumbens on Chitosan Microspheres for Debittering Grapefruit Juice. **Molecules**, v. 24, n. 23, p. 4234, 21 nov. 2019.

BONILLA-PETRICIOLET, A.; MENDOZA-CASTILLO, D. I.; REYNEL-ÀVILA, H. E. **Adsorption processes for water treatment and purification**. 2017. ed. Berlin/Heidelberg: Springer, 2017. v. 256

BOZORGI, M. et al. Performance of synthesized cast and electrospun PVA/chitosan/ZnO-NH_2 nano-adsorbents in single and simultaneous adsorption of cadmium and nickel ions from wastewater. **Environmental Science and Pollution Research**, v. 25, n. 18, p. 17457–17472, 14 jun. 2018.

BRANCA, C. et al. Role of the OH and NH vibrational groups in polysaccharide-nanocomposite interactions: A FTIR-ATR study on chitosan and chitosan/clay films. **Polymer**, v. 99, p. 614–622, set. 2016.

BRIFFA, J.; SINAGRA, E.; BLUNDELL, R. Heavy metal pollution in the environment and their toxicological effects on humans. **Heliyon**, v. 6, n. 9, p. e04691, set. 2020.

BRYAN, G. W. The effects of heavy metals (other than mercury) on marine and estuarine organisms. **Proceedings of the Royal Society of London. Series B. Biological Sciences**, v. 177, n. 1048, p. 389–410, 13 abr. 1971.

CALVO, P. et al. Novel hydrophilic chitosan-polyethylene oxide nanoparticles as protein carriers. **Journal of Applied Polymer Science**, v. 63, n. 1, p. 125–132, 3 jan. 1997.

CERAMELLA, J. et al. A Review on the Antimicrobial Activity of Schiff Bases: Data Collection and Recent Studies. **Antibiotics**, v. 11, n. 2, p. 191, 1 fev. 2022.

CHEN, A. et al. Carbon disulfide-modified magnetic ion-imprinted chitosan-Fe(III): A novel adsorbent for simultaneous removal of tetracycline and cadmium. **Carbohydrate Polymers**, v. 155, p. 19–27, jan. 2017.

CHO, A. R. et al. Preparation of alginate–CaCl2 microspheres as resveratrol carriers. **Journal of Materials Science**, v. 49, n. 13, p. 4612–4619, 27 jul. 2014.

CRINI, G. Historical review on chitin and chitosan biopolymers. **Environmental Chemistry Letters**, v. 17, n. 4, p. 1623–1643, 15 dez. 2019.

CUI, Z. et al. Ionic interactions between sulfuric acid and chitosan membranes. **Carbohydrate Polymers**, v. 73, n. 1, p. 111–116, jul. 2008.

DEBNATH, S.; GHOSH, U. C. Kinetics, isotherm and thermodynamics for Cr(III) and Cr(VI) adsorption from aqueous solutions by crystalline hydrous titanium oxide. **The Journal of Chemical Thermodynamics**, v. 40, n. 1, p. 67–77, jan. 2008.

DE FARIA, C. C. et al. Application of chitosan film as a binding phase in the diffusive gradients in thin films technique (DGT) for measurement of metal ions in aqueous solution. **Analytical and Bioanalytical Chemistry**, v. 412, n. 3, p. 703–714, 11 jan. 2020.

DE FREITAS, G. R.; DA SILVA, M. G. C.; VIEIRA, M. G. A. Biosorption technology for removal of toxic metals: a review of commercial biosorbents and patents. **Environmental Science and Pollution Research**, v. 26, n. 19, p. 19097–19118, 19 jul. 2019.

DE MOURA, M. R. et al. Improved barrier and mechanical properties of novel hydroxypropyl methylcellulose edible films with chitosan/tripolyphosphate nanoparticles. **Journal of Food Engineering**, v. 92, n. 4, p. 448–453, jun. 2009.

DESBRIÈRES, J.; GUIBAL, E. Chitosan for wastewater treatment. **Polymer International**, v. 67, n. 1, p. 7–14, jan. 2018.
DEVLIEGHERE, F.; VERMEULEN, A.; DEBEVERE, J. Chitosan: antimicrobial activity, interactions with food components and applicability as a coating on fruit and vegetables. **Food Microbiology**, v. 21, n. 6, p. 703–714, dez. 2004.

DESHPANDE, P. et al. Zinc complexed chitosan/TPP nanoparticles: A promising micronutrient nanocarrier suited for foliar application. **Carbohydrate Polymers**, v. 165, p. 394–401, jun. 2017.

DOSHI, B. et al. Effectiveness of N,O-carboxymethyl chitosan on destabilization of Marine Diesel, Diesel and Marine-2T oil for oil spill treatment. **Carbohydrate Polymers**, v. 167, p. 326–336, jul. 2017.

DOS SANTOS PEREIRA, T. et al. Chitosan-Sugarcane Bagasse Microspheres as Fertilizer Delivery: On/Off Water Availability System. **Journal of Polymers and the Environment**, v. 28, n. 11, p. 2977–2987, 18 nov. 2020.

DUTTA, J. Isolation, Purification, and Nanotechnological Applications of Chitosan. In: **Polysaccharides**. Cham: Springer International Publishing, 2015. p. 1029–1063.

DYBERN, B. **Water pollution: a problem with global dimensions**. [s.l.] Ambio, 1974.

ELANCHEZHIYAN, S. SD. et al. Magnetic kaolinite immobilized chitosan beads for the removal of Pb(II) and Cd(II) ions from an aqueous environment. **Carbohydrate Polymers**, v. 261, p. 117892, jun. 2021.

ELIEH-ALI-KOMI, D.; HAMBLIN, M. R. Chitin and Chitosan: Production and Application of Versatile Biomedical Nanomaterials. **International journal of advanced research**, v. 4, n. 3, p. 411–427, mar. 2016.

ERDOGAN, S.; KAYA, M.; AKATA, I. **Chitin extraction and chitosan production from cell wall of two mushroom species (Lactarius vellereus and Phyllophora ribis)** In: AIP CONFERENCE PROCEEDINGS. v. 1809, n. 1, p. 020012, Fev. 2017.

EVANS, J. R. et al. Kinetics of cadmium uptake by chitosan-based crab shells. **Water Research**, v. 36, n. 13, p. 3219–3226, jul. 2002.

FENG, F. et al. Characterization of half N-acetylated chitosan powders and films. **Procedia Engineering**, v. 27, p. 718–732, 2012.

FRIBERG, L. T. et al. **Cadmium and health: A toxicological and epidemiological appraisal**. [s.l.] CRC press, 2019. v. 2

GALCERAN, J. et al. Speciation of Inorganic Compounds in Aquatic Systems Using Diffusive Gradients in Thin-Films: A Review. **Frontiers in Chemistry**, v. 9, 6 abr. 2021.

GAUTAM, R. K. et al. Biomass-derived biosorbents for metal ions sequestration: Adsorbent modification and activation methods and adsorbent regeneration. **Journal of Environmental Chemical Engineering**, v. 2, n. 1, p. 239–259, mar. 2014.

GHIMICI, L.; NICHIFOR, M. Flocculation characteristics of a biodegradable polymer based on dextran. **Separation and Purification Technology**, v. 194, p. 48–55, abr. 2018.

GIERSZEWSKA-DRUSYNSKA, M.; OSTROWSKA-CZUBENKO, J. **Sorption of heavy metal ions by polyelectrolyte complex hydrogel membranes**. ARS Separatoria, XIII. **Anais**...Toruń, Poland: 2008.

GODAGE, N. H.; GIONFRIDDO, E. Use of natural sorbents as alternative and green extractive materials: A critical review. **Analytica Chimica Acta**, v. 1125, p. 187–200, ago. 2020.

GEROMEL-COSTA, C. G. A. et al. Adsorption of metals by crosslinked chitosan beads in sugarcane contaminated streams. **Biomass and Bioenergy**, v. 119, p. 128–134, dez. 2018.

GUIBAL, E. Interactions of metal ions with chitosan-based sorbents: a review. **Separation and Purification Technology**, v. 38, n. 1, p. 43–74, jul. 2004.

GUIBAL, E. et al. Influence of polymer structural parameters and experimental conditions on metal anion sorption by chitosan. **Polymer International**, v. 48, n. 8, p. 671–680, 1999.

HAMZA, M. F. et al. Efficient removal of uranium, cadmium and mercury from aqueous solutions using grafted hydrazide-micro-magnetite chitosan derivative. **Journal of Materials Science**, v. 55, n. 10, p. 4193–4212, 1 abr. 2020.

HAMED, I.; ÖZOGUL, F.; REGENSTEIN, J. M. Industrial applications of crustacean by-products (chitin, chitosan, and chitooligosaccharides): A review. **Trends in Food Science & Technology**, v. 48, p. 40–50, fev. 2016.
HAO, D.; LIANG, Y. Adsorption of Cu^{2+} , Cd^{2+} and Pb^{2+} in wastewater by modified chitosan hydrogel. **Environmental Technology**, v. 43, n. 6, p. 876–884, 8 mar. 2022.

HARRIS, R. et al. Chitosan nanoparticles and microspheres for the encapsulation of natural antioxidants extracted from Ilex paraguariensis. **Carbohydrate Polymers**, v. 84, n. 2, p. 803–806, 1 mar. 2011.

HASAN, S. et al. Adsorption of Divalent Cadmium (Cd(II)) from Aqueous Solutions onto Chitosan-Coated Perlite Beads. **Industrial & Engineering Chemistry Research**, v. 45, n. 14, p. 5066–5077, 1 jul. 2006.

HAYAT, M. T. et al. Environmental Hazards of Cadmium: Past, Present, and Future. In: **Cadmium Toxicity and Tolerance in Plants**. [s.l.] Elsevier, 2019. p. 163–183.

HILLER, E.; JURKOVIČ, Ľ.; ŠUTRIEPKA, M. Metals in the Surface Sediments of Selected Water Reservoirs, Slovakia. **Bulletin of Environmental Contamination and Toxicology**, v. 84, n. 5, p. 635–640, 22 maio 2010.

HO, Y. S.; MCKAY, G. A kinetic study of dye sorption by biosorbent waste product pith. **Resources, Conservation and Recycling**, v. 25, n. 3–4, p. 171–193, mar. 1999.

HOPPE-SEYLER, F. Ueber Chitin und Cellulose. **Berichte der deutschen chemischen Gesellschaft**, v. 27, n. 3, p. 3329–3331, 28 out. 1894.

HSIEN, T. Y. **Synthesis of Porous Magnetic Chitoean Beads and Application to Cadmium Ion Adsorption**. Oregon: Department of Chemical Engineering, Oregon State University, 1992.

HSIEN, T.-Y.; RORRER, G. L. Effects of Acylation and Crosslinking on the Material Properties and Cadmium Ion Adsorption Capacity of Porous Chitosan Beads. **Separation Science and Technology**, v. 30, n. 12, p. 2455–2475, jul. 1995.

IARC. **Working Group on the Evaluation of Carcinogenic Risks to Humans. Cadmium and cadmium compounds**. International Agency for Research on Cancer. **Anais**...1993.

IGBERASE, E.; OSIFO, P. Equilibrium, kinetic, thermodynamic and desorption studies of cadmium and lead by polyaniline grafted cross-linked chitosan beads from aqueous solution. **Journal of Industrial and Engineering Chemistry**, v. 26, p. 340–347, jun. 2015.

INOUE, K. et al. Selectivity Series in the Adsorption of Metal Ions on a Resin Prepared by Crosslinking Copper(II)-Complexed Chitosan. **Chemistry Letters**, v. 17, n. 8, p. 1281–1284, 5 ago. 1988.

JÄRUP, L.; ÅKESSON, A. Current status of cadmium as an environmental health problem. **Toxicology and applied pharmacology**, v. 238, n. 3, p. 201–208, 2009.

JAYAN, S. C. et al. Design and in-vitro evaluation of gelatin microspheres of salbutamol sulphate. **Hygeia**, v. 1, n. 1, p. 17–20, 2009.

JEYASEELAN, A.; MEZNI, A.; VISWANATHAN, N. Facile hydrothermal fabrication of functionalized multi-layer graphene oxide encapsulated chitosan beads for enriched fluoride adsorption. **Journal of Applied Polymer Science**, v. 139, n. 9, p. 51703, 5 mar. 2022.

JI, M. et al. A biodegradable chitosan-based composite film reinforced by ramie fibre and lignin for food packaging. **Carbohydrate Polymers**, v. 281, p. 119078, abr. 2022.

JIANG, P. et al. Chitosan–Polycaprolactone Core–Shell Microparticles for Sustained Delivery of Bevacizumab. **Molecular Pharmaceutics**, v. 17, n. 7, p. 2570–2584, 6 jul. 2020.

JINGOU, J. et al. Preparation, characterization of hydrophilic and hydrophobic drug in combine loaded chitosan/cyclodextrin nanoparticles and in vitro release study. **Colloids and Surfaces B: Biointerfaces**, v. 83, n. 1, p. 103–107, mar. 2011.

JONGPAIBOONKIT, L.; FRANKLIN-FORD, T.; MURPHY, W. L. Growth of Hydroxyapatite Coatings on Biodegradable Polymer Microspheres. **ACS Applied Materials & Interfaces**, v. 1, n. 7, p. 1504–1511, 29 jul. 2009.

JOTHI, N.; NACHIYAR, R. K. Identification and isolation of chitin and chitosan from cuttlebone of Sepla prashadi Winckworth, 1936. **Current Biotica**, v. 6, n. 3, p. 304–313, 2012.

KAN, Y. et al. Diminishing Cohesion of Chitosan Films in Acidic Solution by Multivalent Metal Cations. **Langmuir**, v. 36, n. 18, p. 4964–4974, 12 maio 2020.

KANMANI, P. et al. Environmental applications of chitosan and cellulosic biopolymers: A comprehensive outlook. **Bioresource Technology**, v. 242, p. 295–303, out. 2017.

KARIMI, F. et al. Removal of metal ions using a new magnetic chitosan nano-bio-adsorbent; A powerful approach in water treatment. **Environmental Research**, v. 203, p. 111753, jan. 2022.

KAŠPAR, O.; JAKUBEC, M.; ŠTĚPÁNEK, F. Characterization of spray dried chitosan–TPP microparticles formed by two- and three-fluid nozzles. **Powder Technology**, v. 240, p. 31–40, maio 2013.

KAYA, M.; ASAN-OZUSAGLAM, M.; ERDOGAN, S. Comparison of antimicrobial activities of newly obtained low molecular weight scorpion chitosan and medium molecular weight commercial chitosan. **Journal of Bioscience and Bioengineering**, v. 121, n. 6, p. 678–684, jun. 2016.

KLEBER, M.; LEHMANN, J. Humic Substances Extracted by Alkali Are Invalid Proxies for the Dynamics and Functions of Organic Matter in Terrestrial and Aquatic Ecosystems. **Journal of Environmental Quality**, v. 48, n. 2, p. 207–216, mar. 2019.

KRSTIĆ, V.; UROŠEVIĆ, T.; PEŠOVSKI, B. A review on adsorbents for treatment of water and wastewaters containing copper ions. **Chemical Engineering Science**, v. 192, p. 273–287, dez. 2018.
KOU, S. G.; PETERS, L.; MUCALO, M. Chitosan: A review of molecular structure, bioactivities and interactions with the human body and micro-organisms. **Carbohydrate Polymers**, v. 282, p. 119132, abr. 2022.

KUCZAJOWSKA-ZADROŻNA, M.; FILIPKOWSKA, U.; JÓŹWIAK, T. Adsorption of Cu (II) and Cd (II) from aqueous solutions by chitosan immobilized in alginate beads. **Journal of Environmental Chemical Engineering**, v. 8, n. 4, p. 103878, ago. 2020.

KUMAR, A. et al. Entry, colonization, and distribution of endophytic microorganisms in plants. In: **Microbial Endophytes**. [s.l.] Elsevier, 2020. p. 1–33.

KURNIAWAN, T. A.; BABEL, S. A. **A research study on Cr (VI) removal from contaminated wastewater using low-cost adsorbents and commercial**

activated carbon. SECOND INT. CONF. ON ENERGY TECHNOLOGY TOWARDS A CLEAN ENVIRONMENT (RCETE). v. 2, p. 1110-1117, Fev. 2003.

LAGERGREN, S. Zur theorie der sogenannten adsorption gelõster stoffe, Kungliga Svenska Vetenskapsakademiens. v. 24, p. 1–39, 1898.

LAUS, R. et al. Adsorption and desorption of Cu(II), Cd(II) and Pb(II) ions using chitosan crosslinked with epichlorohydrin-triphosphate as the adsorbent. **Journal of Hazardous Materials**, v. 183, n. 1–3, p. 233–241, nov. 2010.

LEE, S.-T. et al. Equilibrium and kinetic studies of copper(II) ion uptake by chitosan-tripolyphosphate chelating resin. **Polymer**, v. 42, n. 5, p. 1879–1892, mar. 2001.

LI, B.; ELANGO, J.; WU, W. Recent Advancement of Molecular Structure and Biomaterial Function of Chitosan from Marine Organisms for Pharmaceutical and Nutraceutical Application. **Applied Sciences**, v. 10, n. 14, p. 4719, 8 jul. 2020.

LI, B. et al. Remediation of Cd (II) ions in aqueous and soil phases using novel porous cellulose/chitosan composite spheres loaded with zero-valent iron nanoparticles. **Reactive and Functional Polymers**, v. 173, p. 105210, abr. 2022.

LI, C. et al. Spatial distribution and risk assessment of heavy metals in sediments of Shuangtaizi estuary, China. **Marine Pollution Bulletin**, v. 98, n. 1–2, p. 358–364, set. 2015.

LI, J.; DENG, L.; YAO, F. Chitosan Derivatives. **Chitosan-Based Hydrogels: Functions and Applications**. v. 39, Jul., 2011.

LIU, H. et al. Binding characteristics of humic substances with Cu and Zn in response to inorganic mineral additives during swine manure composting. **Journal of Environmental Management**, v. 305, p. 114387, mar. 2022.

LIU, R.; LEAD, J. R.; ZHANG, H. Combining cross flow ultrafiltration and diffusion gradients in thin-films approaches to determine trace metal speciation in freshwaters. **Geochimica et Cosmochimica Acta**, v. 109, p. 14–26, 2013.

LIU, Y. et al. Biosorption of copper(II) from aqueous solution by Bacillus subtilis cells immobilized into chitosan beads. **Transactions of Nonferrous Metals Society of China**, v. 23, n. 6, p. 1804–1814, jun. 2013.

LIVENS, F. R. Chemical reactions of metals with humic material. **Environmental Pollution**, v. 70, n. 3, p. 183–208, 1991.

LODEIRO, P. et al. Acid-base properties of dissolved organic matter extracted from the marine environment. **Science of The Total Environment**, v. 729, p. 138437, ago. 2020.

LU, C.; SU, F. Adsorption of natural organic matter by carbon nanotubes. **Separation and Purification Technology**, v. 58, n. 1, p. 113–121, 1 dez. 2007.

MA, X. et al. Assessment of heavy metals contamination in sediments from three adjacent regions of the Yellow River using metal chemical fractions and multivariate analysis techniques. **Chemosphere**, v. 144, p. 264–272, fev. 2016.

MADALA, S. et al. Equilibrium, kinetics and thermodynamics of Cadmium (II) biosorption on to composite chitosan biosorbent. **Arabian Journal of Chemistry**, v. 10, p. S1883–S1893, maio 2017.

MADNI, A. et al. Drug-Polymer Interaction Studies of Cytarabine Loaded Chitosan Nanoparticles. **Journal of the Chemical Society of Pakistan**, v. 39, n. 6, 2017.

MAI, N. X. D.; HOANG, T. L. H.; PHAN, B. T. Evaluation of removal efficiency of Fe (III) and Al (III) ions in acid sulfate water using agarose-based magnesium oxide composite. **Vietnam Journal of Science**, v. 63, n. 3, 2021.

MANISALIDIS, I. et al. Environmental and Health Impacts of Air Pollution: A Review. **Frontiers in Public Health**, v. 8, 20 fev. 2020.

MANZOOR, K.; AHMAD, M.; AHMAD, S.; IKRAM, S. Removal of Pb (ii) and Cd (ii) from wastewater using arginine cross-linked chitosan–carboxymethyl cellulose beads as green adsorbent. **RSC Advances**, v. 9, n. 14, p. 7890–7902, 2019.

MEINELT, T. et al. Reduction in vegetative growth of the water mold Saprolegnia parasitica (Coker) by humic substance of different qualities. **Aquatic Toxicology**, v. 83, n. 2, p. 93–103, jun. 2007.

MENDE, M. et al. Simultaneous adsorption of heavy metal ions and anions from aqueous solutions on chitosan—Investigated by spectrophotometry and SEM-EDX analysis. **Colloids and Surfaces A: Physicochemical and Engineering Aspects**, v. 510, p. 275–282, dez. 2016.

MENG, X. et al. A soft Pickering emulsifier made from chitosan and peptides endows stimuli-responsiveness, bioactivity and biocompatibility to emulsion. **Carbohydrate Polymers**, v. 277, p. 118768, fev. 2022.

MIRDA, E. et al. Synthesis of Chitosan-Silver Nanoparticle Composite Spheres and Their Antimicrobial Activities. **Polymers**, v. 13, n. 22, p. 3990, 18 nov. 2021.

MITRA, A.; DEY, B. Chitosan microspheres in novel drug delivery systems. **Indian journal of pharmaceutical sciences**, v. 73, n. 4, p. 355–66, jul. 2011.

MORALES, J. et al. Degradation of carbofuran and carbofuran-derivatives in presence of humic substances under basic conditions. **Chemosphere**, v. 89, n. 11, p. 1267–1271, nov. 2012.

MOREL F; HERING J. **Principles and Applications of Aquatic Chemistry**. [s.l.] John Wiley, New York, 1993.

MORIN-CRINI, N. et al. Applications of chitosan in food, pharmaceuticals, medicine, cosmetics, agriculture, textiles, pulp and paper, biotechnology, and environmental chemistry. **Environmental Chemistry Letters**, v. 17, n. 4, p. 1667–1692, 13 dez. 2019.

MUXIKA, A. et al. Chitosan as a bioactive polymer: Processing, properties and applications. **International Journal of Biological Macromolecules**, v. 105, p. 1358–1368, dez. 2017.

NGAH, W. S. W.; FATINATHAN, S.; YOSOP, N. A. Isotherm and kinetic studies on the adsorption of humic acid onto chitosan-H2SO4 beads. **Desalination**, v. 272, n. 1–3, p. 293–300, maio 2011.

NGAH, W. W.; MUSA, A. Adsorption of humic acid onto chitin and chitosan. **Journal of Applied Polymer Science**, v. 69, n. 12, p. 2305–2310, 1998.

NGUYEN, T. A.; NGUYEN, T. H. Study on Fabrication of Antibacterial Low Molecular Weight Nanochitosan Using Sodium Tripolyphosphate and Hydrogen Peroxide. **Journal of Nanotechnology**, v. 2022, p. 1–10, 17 jan. 2022.

NINA, M., FATHANA, H., IQHRAMMULLAH, M. Preparation and characterization of new magnetic chitosan-glycine-PEGDE (Fe3O4/Ch-GP) beads for aqueous Cd (II) removal. **Journal of Water Process Engineering**, 45, 102493, 2022.

OMWENE, P. I. et al. Heavy metal pollution and spatial distribution in surface sediments of Mustafakemalpaşa stream located in the world's largest borate basin (Turkey). **Chemosphere**, v. 208, p. 782–792, out. 2018.

ONSØSYEN, E.; SKAUGRUD, O. Metal recovery using chitosan. **Journal of Chemical Technology & Biotechnology**, v. 49, n. 4, p. 395–404, 24 abr. 2007.

PAL, P.; PAL, A. Surfactant-modified chitosan beads for cadmium ion adsorption. **International Journal of Biological Macromolecules**, v. 104, p. 1548–1555, nov. 2017.

PAL, P. et al. Applications of chitosan in environmental remediation: A review. **Chemosphere**, v. 266, p. 128934, mar. 2021.

PALANISAMY, K. et al. Biopolymer Technologies for Environmental Applications. In: [s.l: s.n.]. p. 55–83.

PAPELIS, CHARALAMBOS.; ROBERTS, P. V.; LECKIE, J. O. Modeling the Rate of Cadmium and Selenite Adsorption on Micro- and Mesoporous Transition Aluminas. **Environmental Science & Technology**, v. 29, n. 4, p. 1099–1108, 1 abr. 1995.

PEARSON, F. G.; MARCHESSAULT, R. H.; LIANG, C. Y. Infrared spectra of crystalline polysaccharides. V. Chitin. **Journal of Polymer Science**, v. 43, n. 141, p. 101–116, mar. 1960.

PEI, X. et al. Robust cellulose-based composite adsorption membrane for heavy metal removal. **Journal of Hazardous Materials**, v. 406, p. 124746, mar. 2021.
PHILIBERT, T.; LEE, B. H.; FABIEN, N. Current Status and New Perspectives on Chitin and Chitosan as Functional Biopolymers. **Applied Biochemistry and Biotechnology**, v. 181, n. 4, p. 1314–1337, 27 abr. 2017.

POPOVICH, D. et al. **Composite Films Based on Chitosan Succinate and Food Chitosan as Anticoagulant Coatings**. 2022 Conference of Russian Young Researchers in Electrical and Electronic Engineering (ElConRus). **Anais**...IEEE, 25 jan. 2022.

QI, L.; XU, Z. Lead sorption from aqueous solutions on chitosan nanoparticles. **Colloids and Surfaces A: Physicochemical and Engineering Aspects**, v. 251, n. 1–3, p. 183–190, dez. 2004.

QI, L. et al. Preparation and antibacterial activity of chitosan nanoparticles. **Carbohydrate Research**, v. 339, n. 16, p. 2693–2700, nov. 2004.

QIU, Z. et al. A study of cadmium remediation and mechanisms: Improvements in the stability of walnut shell-derived biochar. **Science of The Total Environment**, v. 636, p. 80–84, set. 2018.

RAHANGDALE, D.; KUMAR, A. Derivatized Chitosan: Fundamentals. In: **Biopolymer Grafting: Applications**. [s.l: s.n.]. v. 251.

RAHMI et al. Preparation of magnetic chitosan using local iron sand for mercury removal. **Heliyon**, v. 5, n. 5, p. e01731, maio 2019.

RAHIM, M.; MAS HARIS, M. R. H. Application of biopolymer composites in arsenic removal from aqueous medium: A review. **Journal of Radiation Research and Applied Sciences**, v. 8, n. 2, p. 255–263, abr. 2015.

RAHMAN, M. S.; SAHA, N.; MOLLA, A. H. Potential ecological risk assessment of heavy metal contamination in sediment and water body around Dhaka export processing zone, Bangladesh. **Environmental Earth Sciences**, v. 71, n. 5, p. 2293–2308, 20 mar. 2014.

RAMESH, A. et al. Adsorption of gold(III), platinum(IV) and palladium(II) onto glycine modified crosslinked chitosan resin. **Bioresource Technology**, v. 99, n. 9, p. 3801–3809, jun. 2008.

RANGEL-MENDEZ, J. R. et al. Chitosan selectivity for removing cadmium (II), copper (II), and lead (II) from aqueous phase: pH and organic matter effect. **Journal of Hazardous Materials**, v. 162, n. 1, p. 503–511, fev. 2009.

RANI, A. et al. Cellular mechanisms of cadmium-induced toxicity: a review. **International Journal of Environmental Health Research**, v. 24, n. 4, p. 378–399, 4 jul. 2014.

RANJBARI, S. et al. The surfactant-ionic liquid bi-functionalization of chitosan beads for their adsorption performance improvement toward Tartrazine. **Environmental Research**, v. 204, p. 111961, mar. 2022.

RAO, M. M. et al. Removal of some metal ions by activated carbon prepared from Phaseolus aureus hulls. **Journal of Hazardous Materials**, v. 166, n. 2–3, p. 1006–1013, jul. 2009.

RATTE, H. T. Bioaccumulation and toxicity of silver compounds: A review. **Environmental Toxicology and Chemistry**, v. 18, n. 1, p. 89–108, jan. 1999.

RAZA, S. et al. Biomass furfural-derived green polymer microspheres: Synthesis and applications for the removal of environmental pollutants from wastewater. **Microporous and Mesoporous Materials**, v. 318, p. 110966, abr. 2021.

RAZA, Z. A. et al. Recent developments in chitosan encapsulation of various active ingredients for multifunctional applications. **Carbohydrate Research**, v. 492, p. 108004, jun. 2020.

REHMAN, A. et al. Biochar potential to relegate metal toxicity effects is more soil driven than plant system: A global meta-analysis. **Journal of Cleaner Production**, v. 316, p. 128276, set. 2021.

REY-CASTRO, C. et al. Effective Affinity Distribution for the Binding of Metal Ions to a Generic Fulvic Acid in Natural Waters. **Environmental Science & Technology**, v. 43, n. 19, p. 7184–7191, 1 out. 2009.

RINAUDO, M. Chitin and chitosan: Properties and applications. **Progress in Polymer Science**, v. 31, n. 7, p. 603–632, jul. 2006.

ROBERTS, G. A. F. Thirty years of progress in chitin and chitosan. **Progress on chemistry and application of chitin**, v. 13, p. 7–15, 2008.

ROEGES, N. P. G.; BAAS, J. M. A. **A guide to the complete interpretation of infrared spectra of organic structures**. New York: Wiley, 1994.

RORRER, G. L.; HSIEN, T. Y.; WAY, J. D. Synthesis of porous-magnetic chitosan beads for removal of cadmium ions from wastewater. **Industrial & Engineering Chemistry Research**, v. 32, n. 9, p. 2170–2178, 1 set. 1993.

SACHS, S.; BERNHARD, G. Influence of humic acids on the actinide migration in the environment: suitable humic acid model substances and their application in studies with uranium—a review. **Journal of Radioanalytical and Nuclear Chemistry**, v. 290, n. 1, p. 17–29, 20 out. 2011.

SAKAI, Y.; NAKAMURA, C.; KISHI, T. Evaluation of mass transfer resistance of concrete based on representative pore size of permeation resistance. **Construction and Building Materials**, v. 51, p. 40–46, jan. 2014.

SALEHI, M. Global water shortage and potable water safety; Today's concern and tomorrow's crisis. **Environment International**, v. 158, p. 106936, jan. 2022.

SAMUELS, R. J. Solid state characterization of the structure of chitosan films. **Journal of Polymer Science: Polymer Physics Edition**, v. 19, n. 7, p. 1081–1105, jul. 1981.

SANNAN, T.; KURITA, K.; IWAKURA, Y. Studies on chitin, 2. Effect of deacetylation on solubility. **Die Makromolekulare Chemie**, v. 177, n. 12, p. 3589–3600, dez. 1976.

SCHULTEN, H.-R.; SCHNITZER, M. A state of the art structural concept for humic substances. **Naturwissenschaften**, v. 80, n. 1, p. 29–30, jan. 1993.

SCHWARZENBACH, R. P. et al. Global Water Pollution and Human Health. **Annual Review of Environment and Resources**, v. 35, n. 1, p. 109–136, 21 nov. 2010.

SEYEDI, S. M.; ANVARIPOUR, B.; MOTAVASSEL, M.; JADIDI, N. Comparative cadmium adsorption from water by nanochitosan and chitosan. **International Journal of Engineering and Innovative Technology**, 2(9), 145-148, 2013.

SHAHJAHAN, M. et al. Effects of heavy metals on fish physiology – A review. **Chemosphere**, v. 300, p. 134519, ago. 2022.

SHAO, Z. et al. Novel green chitosan-pectin gel beads for the removal of Cu(II), Cd(II), Hg(II) and Pb(II) from aqueous solution. **International Journal of Biological Macromolecules**, v. 176, p. 217–225, abr. 2021.

SHARP, R. A Review of the Applications of Chitin and Its Derivatives in Agriculture to Modify Plant-Microbial Interactions and Improve Crop Yields. **Agronomy**, v. 3, n. 4, p. 757–793, 21 nov. 2013.

SHETH, Y. et al. An environment friendly approach for heavy metal removal from industrial wastewater using chitosan based biosorbent: A review. **Sustainable Energy Technologies and Assessments**, v. 43, p. 100951, fev. 2021.

SHIRAZI, R.H.M.T; MOHAMMADI, T.; ASADI, A. A. Incorporation of amine-grafted halloysite nanotube to electrospun nanofibrous membranes of chitosan/poly (vinyl alcohol) for Cd (II) and Pb(II) removal. **Applied Clay Science**, v. 220, p. 106460, abr. 2022.

SHU, X.Z.; ZHU, J. Z. Chitosan/gelatin microspheres prepared by modified emulsification and ionotropic gelation. **Journal of Microencapsulation**, v. 18, n. 2, p. 237–245, 29 jan. 2001.

SHUKLA, S. K. et al. Chitosan-based nanomaterials: A state-of-the-art review. **International Journal of Biological Macromolecules**, v. 59, p. 46–58, ago. 2013.

SIKDER, M.D. T. et al. Facile synthesis, characterization, and adsorption properties of Cd (II) from aqueous solution using β-cyclodextrin polymer impregnated in functionalized chitosan beads as a novel adsorbent. **Journal of Environmental Chemical Engineering**, v. 5, n. 4, p. 3395–3404, ago. 2017.

SINHA, V. R. et al. Chitosan microspheres as a potential carrier for drugs. **International Journal of Pharmaceutics**, v. 274, n. 1–2, p. 1–33, abr. 2004.

STAINLOSS, I.; SANKARAN, M. Chitosan–A Versatile Polymer for Targeted Drug Delivery. **IJSART**, v. 2, n. 9, 2016.

SRINATHA, A.; PANDIT, J. K.; SINGH, S. Ionic Cross-linked Chitosan Beads for Extended Release of Ciprofloxacin: In vitro Characterization. **Indian journal of pharmaceutical sciences**, v. 70, n. 1, p. 16–21, jan. 2008.

STREIT, B. Bioaccumulation of contaminants in fish. **Fish ecotoxicology**, 353-387, 1998.

SUTIRMAN, Z. A. et al. Equilibrium, kinetic and mechanism studies of Cu(II) and Cd(II) ions adsorption by modified chitosan beads. **International Journal of Biological Macromolecules**, v. 116, p. 255–263, set. 2018.

SUTIRMAN, Z. A.; SANAGI, M. M.; WAN AINI, W. I. Alginate-based adsorbents for removal of metal ions and radionuclides from aqueous solutions: A review. **International Journal of Biological Macromolecules**, v. 174, p. 216–228, mar. 2021.

TAN, Y. et al. Efficient removal of Cd (II) from aqueous solution by chitosan modified kiwi branch biochar. **Chemosphere**, v. 289, p. 133251, fev. 2022.

TEWARI, N.; VASUDEVAN, P.; GUHA, B. K. Study on biosorption of Cr(VI) by Mucor hiemalis. **Biochemical Engineering Journal**, v. 23, n. 2, p. 185–192, abr. 2005.

TEYMOURI, P. et al. BIOSORPTION STUDIES ON NACL-MODIFIED *CERATOPHYLLUM DEMERSUM* : REMOVAL OF TOXIC CHROMIUM FROM AQUEOUS SOLUTION. **Chemical Engineering Communications**, v. 200, n. 10, p. 1394–1413, 3 out. 2013.

TIPPING, E. et al. Modelling the solid–solution distributions of protons, aluminium, base cations and humic substances in acid soils. **European Journal of Soil Science**, v. 46, n. 1, p. 77–94, mar. 1995.

TORRES, E. Biosorption: A Review of the Latest Advances. **Processes**, v. 8, n. 12, p. 1584, 1 dez. 2020.

UDDIN, MD. N.; DESAI, F.; ASMATULU, E. Engineered nanomaterials in the environment: bioaccumulation, biomagnification and biotransformation. **Environmental Chemistry Letters**, v. 18, n. 4, p. 1073–1083, 4 jul. 2020.

UPADHYAY, U. et al. Recent advances in heavy metal removal by chitosan based adsorbents. **Carbohydrate Polymers**, v. 251, p. 117000, jan. 2021.

URE, A. M.; DAVIDSON, C. M. **Chemical Speciation in the Environment**. [s.l.] Blackie Academic &Professional, Glasgow, 1995.

VARMA, A. J.; DESHPANDE, S. V.; KENNEDY, J. F. Metal complexation by chitosan and its derivatives: a review. **Carbohydrate Polymers**, v. 55, n. 1, p. 77–93, jan. 2004.

VARUN, T. K. et al. Extraction of chitosan and its oligomers from shrimp shell waste, their characterization and antimicrobial effect. **Veterinary world**, v. 10, n. 2, p. 170–175, fev. 2017.

VIJAYARAGHAVAN, K. et al. Assessment of samarium biosorption from aqueous solution by brown macroalga Turbinaria conoides. **Journal of the Taiwan Institute of Chemical Engineers**, v. 74, p. 113–120, maio 2017.

VIJAYARAGHAVAN, K.; YUN, Y.-S. Bacterial biosorbents and biosorption. **Biotechnology Advances**, v. 26, n. 3, p. 266–291, maio 2008.

VOLESKY, B.; MAY, H.; HOLAN, Z. R. Cadmium biosorption bySaccharomyces cerevisiae. **Biotechnology and Bioengineering**, v. 41, n. 8, p. 826–829, 5 abr. 1993.

VON WANDRUSZKA, R. Humic acids: Their detergent qualities and potential uses in pollution remediation. **Geochemical Transactions**, v. 1, n. 1, p. 10, 12 dez. 2000.

WANG, J. et al. Preparation and evaluation of magnetic nanoparticles impregnated chitosan beads for arsenic removal from water. **Chemical Engineering Journal**, v. 251, p. 25–34, set. 2014.

WANG, G. et al. Modeling the source contribution of heavy metals in surficial sediment and analysis of their historical changes in the vertical sediments of a drinking water reservoir. **Journal of Hydrology**, v. 520, p. 37–51, jan. 2015.

WANG, J.; ZHUANG, S. Removal of various pollutants from water and wastewater by modified chitosan adsorbents. **Critical Reviews in Environmental Science and Technology**, v. 47, n. 23, p. 2331–2386, 2 dez. 2017.

WANG, T.; TURHAN, M.; GUNASEKARAN, S. Selected properties of pH-sensitive, biodegradable chitosan–poly(vinyl alcohol) hydrogel. **Polymer International**, v. 53, n. 7, p. 911–918, jul. 2004.

WANG, Y. et al. Ultrasonic assisted microwave synthesis of poly (Chitosan-co-gelatin)/polyvinyl pyrrolidone IPN hydrogel. **Ultrasonics Sonochemistry**, v. 40, p. 714–719, jan. 2018.

WATRAS, C. J. et al. Bioaccumulation of mercury in pelagic freshwater food webs. **Science of The Total Environment**, v. 219, n. 2–3, p. 183–208, ago. 1998.

WEN, Y. et al. Carbonaceous sulfur-containing chitosan–Fe(III): A novel adsorbent for efficient removal of copper (II) from water. **Chemical Engineering Journal**, v. 259, p. 372–380, jan. 2015.

WILSON, O. C.; OMOKANWAYE, T. Biomimetic Lessons for Processing Chitin-Based Composites. In: **Biopolymer Nanocomposites**. Hoboken, NJ, USA: John Wiley & Sons, Inc., 2013. p. 53–81.

WU, F.-C.; TSENG, R.-L.; JUANG, R.-S. Comparative adsorption of metal and dye on flake- and bead-types of chitosans prepared from fishery wastes. **Journal of Hazardous Materials**, v. 73, n. 1, p. 63–75, mar. 2000.

WULANDARI, I. O. et al. Preparation and Characterization of Chitosan-coated Fe $_3$ O $_4$ Nanoparticles using Ex-Situ Co-Precipitation Method and Tripolyphosphate/Sulphate as Dual Crosslinkers. **IOP Conference Series: Materials Science and Engineering**, v. 299, p. 012064, jan. 2018.

YAN, W. L.; BAI, R. Adsorption of lead and humic acid on chitosan hydrogel beads. **Water Research**, v. 39, n. 4, p. 688–698, fev. 2005.

YANG, F.; TANG, C.; ANTONIETTI, M. Natural and artificial humic substances to manage minerals, ions, water, and soil microorganisms. **Chemical Society Reviews**, v. 50, n. 10, p. 6221–6239, 2021.

YANG, W. et al. Adsorption Performance of Cd(II) by Chitosan-Fe_3O_4-Modified Fish Bone Char. **International Journal of Environmental Research and Public Health**, v. 19, n. 3, p. 1260, 23 jan. 2022.

YANG, Y. et al. Adsorption of Pb2+, Cu2+ and Cd2+ by sulfhydryl modified chitosan beads. **Carbohydrate Polymers**, v. 274, p. 118622, nov. 2021.

YONG, S. K. et al. Synthesis and Characterization of Thiolated Chitosan Beads for Removal of Cu(II) and Cd(II) from Wastewater. **Water, Air, & Soil Pollution**, v. 224, n. 12, p. 1720, 20 dez. 2013.

YU, Z. et al. Preparation and characterization of poly(maleic acid)-grafted cross-linked chitosan microspheres for Cd(II) adsorption. **Carbohydrate Polymers**, v. 172, p. 28–39, set. 2017.

YUAN, P. et al. Spatial and seasonal variations and risk assessment for heavy metals in surface sediments of the largest river-embedded reservoir in China. **Environmental Science and Pollution Research**, v. 27, n. 28, p. 35556–35566, 27 out. 2020.

YUWEI, C.; JIANLONG, W. Preparation and characterization of magnetic chitosan nanoparticles and its application for Cu(II) removal. **Chemical Engineering Journal**, v. 168, n. 1, p. 286–292, mar. 2011.

ZARGAR, V.; ASGHARI, M.; DASHTI, A. A Review on Chitin and Chitosan Polymers: Structure, Chemistry, Solubility, Derivatives, and Applications. **ChemBioEng Reviews**, v. 2, n. 3, p. 204–226, jun. 2015.

ZAVARZINA, A. G. et al. Humic Substances: Hypotheses and Reality (a Review). **Eurasian Soil Science**, v. 54, n. 12, p. 1826–1854, 23 dez. 2021.

ZENG, L. et al. Adsorption of Cd(II), Cu(II) and Ni(II) ions by cross-linking chitosan/rectorite nano-hybrid composite microspheres. **Carbohydrate Polymers**, v. 130, p. 333–343, out. 2015.

ZHANG, H. et al. Uptake of Pb(II) and Cd(II) on Chitosan Microsphere Surface Successively Grafted by Methyl Acrylate and Diethylenetriamine. **ACS Applied Materials & Interfaces**, v. 9, n. 12, p. 11144–11155, 29 mar. 2017.

ZHANG, H.; DAVISON, W. Use of diffusive gradients in thin-films for studies of chemical speciation and bioavailability. **Environmental Chemistry**, v. 12, n. 2, p. 85, 2015.

ZHANG, W. et al. Novel pectin based composite hydrogel derived from grapefruit peel for enhanced Cu(II) removal. **Journal of Hazardous Materials**, v. 384, p. 121445, fev. 2020.

ZHAO, B. et al. Spatiotemporal variation and potential risks of seven heavy metals in seawater, sediment, and seafood in Xiangshan Bay, China (2011–2016). **Chemosphere**, v. 212, p. 1163–1171, dez. 2018.

ZHONG, R. et al. Preparation of biocompatible nano-ZnO/chitosan microspheres with multi-functions of antibacterial, UV-shielding and dye photodegradation. **International Journal of Biological Macromolecules**, v. 146, p. 939–945, mar. 2020.

ZHU, K. Y. et al. Biosynthesis, Turnover, and Functions of Chitin in Insects. **Annual Review of Entomology**, v. 61, n. 1, p. 177–196, 11 mar. 2016.